AALBORG UNIVERSITY
DENMARK

Optimization Control of Bidirectional Cascaded DC-AC Converter Systems

Tian, Yanjun

Link to publication from Aalborg University

OPTIMIZATION CONTROL OF BIDIRECTIONAL CASCADED DC-AC CONVERTER SYSTEMS

by

Yanjun Tian

AALBORG UNIVERSITY
DENMARK

Dissertation submitted to
the Faculty of Engineering and Science at Aalborg University

for the degree of
Doctor of Philosophy in Electrical Engineering

Mandatory page in PhD theses:

1.   Thesis title:

Optimization Control of Bidirectional Cascaded DC-AC Converter System

2.   Name of PhD student.

Yanjun Tian

3.   Name and title of supervisor and any other supervisors.

Supervisor: Zhe Chen, Professor;

Co-supervisor: Fujin Deng, Assistant Professor.

4.   List of published papers:

- o   Paper 1: Yanjun Tian, Zhe Chen, Fujin Deng, Xiaofeng Sun, Yanting Hu, "Active Power and DC-link Voltage Coordinative Control for A DC-AC Converter with Bidirectional Power Application." IEEE Transactions on Power Electronics, Vol. 30, NO. 10, October 2015.
- o   Paper 2: Yanjun Tian, Poh Chiang Loh, Fujin Deng, Zhe Chen, Yanting Hu, "DC-Link Voltage Coordinated-Proportional Control for Cascaded Converter with Zero Steady-State Error and Reduced System Type." IEEE Transactions on Power Electronics, Early Access.
- o   Paper 3: Zhanfeng Song, Yanjun Tian, Wei Chen, Zhibin Zou, Zhe Chen, "Predictive Duty Cycle Control of Three-Phase Active-Front-End Rectifiers." IEEE Transactions on Power Electronics, Vol.31, Jan. 2016.
- o   Paper 4: Xiaofeng Sun, Yanjun Tian, Zhe Chen, "Adaptive decoupled power control method for inverter connected DG." IET Renewable Power Generation, Vol. 8, No. 2, 03.2014, p. 171-182.
- o   Paper 5: Yanjun Tian, Fujin Deng, Zhe Chen, Xiaofeng Sun, Yanting Hu, "Coordinative Control of Active Power and DC-link Voltage for Cascaded Dual-Active-Bridge and Inverter in Bidirectional Applications." in proc. of the 2014 IEEE Energy Conversion Congress and Exposition (ECCE). IEEE Press, 2014, p. 2249- 2256.
- o   Paper 6: Yanjun Tian, Fujin Deng, Zhe Chen, Xiaofeng

Sun, Yanting Hu, "Impedance Interaction Modeling and Analysis for the Bidirectional Cascaded Converter in Active Distribution Network." in proc. of the 9th International Conference on Power Electronics – ECCE Asia (ICPE 2015-ECCE Asia), June 1-June 5, Seoul, 2015.

o Paper 7: Yanjun Tian, Fujin Deng, Zhe Chen, Xiaofeng Sun, Yanting Hu, "An Impedance Coordinate Control Method for Cascaded DAB and Inverter in Bidirectional Applications." in proc. of the 9th International Conference on Power Electronics – ECCE Asia (ICPE 2015-ECCE Asia), June 1-June 5, Seoul, 2015.

o Paper 8: Yanjun Tian, Poh Chiang Loh, Fujin Deng, Zhe Chen, Xiaofeng Sun, Yanting Hu "DC-link Voltage Coordinative-Proportional Control in Cascaded Converter Systems." in proc. of IEEE Energy Conversion Congress & Expo ECCE 2015, Montreal Canada September 20-24,2015.

o Paper 9:Yanjun Tian, Poh Chiang Loh, Fujin Deng, Zhe Chen, Yanting Hu, "Impedance Analysis of Control Modes in Cascaded Converter." in proc. of IEEE Industrial Electronics Society 41st Annual Conference, IECON 2015, November 9-12, 2015 Yokohama, Japan.

o Paper 10: Yanjun Tian, Poh Chiang Loh, Fujin Deng, Zhe Chen, Yanting Hu, "Impedance Coordinative Control for Cascaded Converters in Bidirectional Applications." (Planed) IEEE Transactions on Industry Application.

o Paper 11: Yanjun Tian, Poh Chiang Loh, Fujin Deng, Zhe Chen, Yanting Hu, "Impedance Interaction in Bidirectional Cascaded Converter." (Planed) IET Transactions on Power Electronics.

o Paper 12: Yanjun Tian, Poh Chiang Loh, Fujin Deng, Zhe Chen, Yanting Hu, "Front-to-end Impedance Controller in Cascaded Converter System." (Planned) IEEE Transactions on Industrial Electronics.

5. This present report combined with the above listed scientific papers has been submitted for assessment in partial fulfilment of the PhD degree. The scientific papers are not included in this version due to copyright issues. Detailed publication information is provided above and the interested reader is referred to the original published papers. As part of the assessment, co-author statements have been made available to the assessment committee and are also available at the Faculty of Engineering and Science, Aalborg University.

CV

Yanjun Tian received the B.Sc. and M.Sc. degree in electrical engineering from the Yanshan University, Qinhuangdao, China in 2009 and 2012, respectively. He is working toward the PhD degree in the department of Energy Technology, Aalborg University Denmark. His research interest are distributed generation and active distribution network control, focusing on the impedance interaction, cascaded converter control and the parallel connected converter control.

ABSTRACT

For the sustainable development of human utilized energy, and the friendly environment in the future, the renewable energy sources have experienced a constant and rapid growth in recent years, thus the renewable energy based distributed generations (DG) continue to increase in the power system.

The connections of the renewable energy sources to the power system are mostly through the power electronic converters. Moreover, for high controllability and flexibility, power electronic devices are gradually acting as the interface between different networks in power systems, promoting conventional power system to a smarter stage. From a generation plant to transmission and distribution networks, the interconnection of power electronic converters will be widely confronted in the near future. Additionally, the combination of distributed generations, local loads, and storage devices promotes the bidirectional power flow in the distribution level of power systems. Therefore direct contact of converters introduces significant uncertainties to power system, especially for the stability and reliability.

This dissertation studies the optimization control of the two stages directly connected converters, which is the cascaded power converters, with the objective of improving stability, reliability. Conventional control methods for the power converters are built under different control loops, such as the current loop, voltage loop, power loop, and they are mostly implemented in unidirectional power flow. But the bidirectional application is much different from unidirectional condition, and the stability enhancement is thus critical to the grid interface converter. So this research work will develop control methods to adapt the variation of power flow directions and enhance both the stability and reliability in bidirectional cascaded converter.

This research work analyses the control strategies based on the topology of dual active bridges converter cascaded with a three phase inverter. It firstly proposed a dc link voltage and active power coordinative control method for this cascaded topology, and it can reduce dc link voltage fluctuations, enhancing the dc link voltage reliability in case of one sub converter failure. Then the bidirectional power flow effect is analyzed, and an important guide line is proposed for the design of the two stage cascaded converter system. Towards the different stability in different power flow directions, a bidirectional impedance control method is also proposed to unify and improve the system stability. Control system type number is also analyzed in this thesis, then a symmetric proportional control method for the two stage cascaded converter is proposed to reduce the dc link voltage control system type number, which is capable to improve system stability. Afterwards, this dissertation comes up with the concept of front to end impedance control method

for the two stage cascaded converter, and it can greatly improve the system stability. At last the thesis concludes the whole research work and outlook the future development trends.

DANSK RESUME

For en bæredygtig udvikling af menneskelig udnyttet energi og venligt miljø i fremtiden, har de vedvarende energikilder oplevet en konstant og hurtig vækst i de seneste år, og dermed den vedvarende energi baseret distribuerede generationer (GD) fortsætter med at stige i el systemet.

Tilslutningerne for de vedvarende energikilder til el systemet er for det meste gennem effektelektroniske konvertere. Desuden efter høj styrbarhed og fleksibilitet, magt elektroniske enheder gradvist fungerer som grænseflade mellem forskellige netværk i kraftsystemer, fremme konventionelt el systemet til et smartere scene. Fra en generation plante til transmissions- og distributionsnet, vil sammenkobling af magt elektroniske omformere være almindeligt konfronteret i den nærmeste fremtid. Derudover kombinationen af distribuerede generationer, lokale belastninger, og lagringsenheder fremmer tovejs strøm flow i distributionsleddet for el systemer. Derfor direkte kontakt af konvertere introducerer betydelig usikkerhed til el systemet, især for stabilitet og pålidelighed.

Denne afhandling undersøger optimering styring af de to etaper direkte forbundet omformere, som er den kaskadekoblede strøm omformere, med det formål at forbedre stabilitet, pålidelighed. Konventionelle metoder til strøm omformere kontrol er bygget under forskellige reguleringskredse, såsom den aktuelle løkke, spænding loop, magt loop, og de er for det meste gennemført i ensrettet strøm flow. Men den bidirektionale ansøgning er meget forskellig fra ensrettet tilstand og forbedring stabilitet er dermed afgørende for nettet grænseflade konverter. Så dette forskningsarbejde vil udvikle kontrolmetoder for at tilpasse variationen af magt flow retninger og forbedre både stabilitet og pålidelighed i tovejs kaskader konverter.

Denne forskning analyserer kontrol strategier baseret på topologi dobbelt aktive broer konverter kaskader med en trefaset inverter. Det første foreslog en DC link spænding og aktiv effekt koordinater kontrol metode til dette kaskader topologi, og det kan reducere dc link spændingsudsving, styrke DC link spænding pålidelighed i tilfælde af en sub-konverter fiasko. Derefter tovejs strøm flow effekt analyseres, og der foreslås en vigtig guide linje for udformningen af to trins kaskader konverter system. Mod forskellige stabilitet i forskellige power flow retninger, er en tovejs impedans kontrolmetode også foreslået at ensrette og forbedre systemets stabilitet. Kontrolsystem typenummer er også analyseret i denne afhandling, så en symmetrisk proportional metode til to-trins kontrol kaskader konverter foreslås at reducere DC link spænding kontrolsystem typenummer, som er i stand til at forbedre systemets stabilitet. Bagefter afhandlingen kommer op med begrebet front til ende impedans kontrol fremgangsmåde til to trins kaskader konverter, og det kan

i høj grad forbedre systemets stabilitet. Omsider konkluderer afhandlingen hele forskningsarbejdet og udsigterne de fremtidige udviklingstendenser.

ACKNOWLEDGEMENTS

Firstly, I would like to express my thanks to my supervisor Professor Zhe Chen. Thank you for offering me this precious opportunity to do the Ph.D. study, as well as the great help to encourage my research. Your advices on the research and career are priceless. All these concerns help me grow as a young motivating researcher.

I would also like to express my thank my committee members, professor Braham Ferreira, professor Fred Wang, professor Francesco Iannuzzo for serving as the committee members even at hardship.

I also want to thank Professor Poh Chiang Loh, who helped me express ideas through a deeply technical and professional way. Also thank my co-supervisor Dr. Fujin Deng, who gave me many practical advices and technical views. I would also send my special thanks to Mr Kiwoo Park, who showed great patient and interaction on the academic discussions and lab activities. Dr Rongwu Zhu is thanked here, and you make the office time more enjoyable. Then I want to thank the researchers in our group, associate professor Weihao Hu, assistant professor Chi Su, Jiakun Fang and Xiao Liu, Dr Chengxi Liu and Hongzhi Liu, Ph.D fellow Jie Tian and Yanbo Wang, thanks you all for the help on my research work. I am also going to thank assistant professor Xiongfei Wang, post doctor Yongheng Yang and Yi Tang. Thank you guys for helping me expand my technical views. All you guys make the Ph.D time with great enrichment.

Special thanks to my parents and sister, who spare no effort to support me. I love you all so much just as you do all the time.

Then I want to specially thank my beloved girlfriend, Li Wan, who supports me and motivates me, then I can enjoy the research and life in a better way, as well as being a better man.

Finally but significantly, I want to thank my colleagues and all my best friends here. I can not list your names one by one, but will write them in my heart. Thank you all for making our life so wonderful in this peaceful place. I will cherish the golden time we are together in my life.

LIST OF ACRONYMS

ADN   Active Distribution Network

CHP   Combined Heat and Power

CPL   Constant Power Load

DAB   Dual-Active-Bridge converter

DER   Distributed Energy Resources

DG   Distributed Generation

DQ   Direct Quadrature

DR   Distributed Resource

DSO   Distribution System Operator

GM   Gain Margin

HVDC   High Voltage Direct Current

MMC   Multi Modular Converter

MPPT   Maximum Power Point Track

PCC   Point of Common Coupling

PI   Proportional Integral

PM   Phase Margin

PV   Photovoltaic

PWM   Pulse Width Modulation

ZVS   Zero Voltage Switching

LIST OF SYMBOLS

C DC link capacitor

C_1 Capacitor on DAB input side

C_2 Capacitor on DAB output side

D_{abc} Three phase duty ratio of inverter

D_d Inverter duty ratio on D axis

D_q Inverter duty ratio on Q axis

E Energy on the dc link capacitor

E_{DAB} Energy output of DAB converter

$E_{Inverter}$ Energy output of inverter

f Switching frequency of DAB converter

g Gain of voltage PI controller

$G(s)$ Interference transfer function on dc link

$G_A(s)$ Transfer function of converter A

$G_B(s)$ Transfer function of converter B

$G_{AB}(s)$ Transfer function of Cascaded converter A and B

$G_{DAB}(s)$ Closed loop transfer function of DAB power control

$G_{DAB-I}(s)$ Closed loop transfer function of DAB current control

$G_i(s)$ Transfer function of current controller

$G_{i-open}(s)$ Open loop transfer function of current loop

$G_{i-plant}(s)$ Transfer function of current functioning loop

$G_{INV}(s)$ Closed loop transfer function of DAB power control

$G_{open}(s)$ Open loop transfer function

$G_{PI}(s)$ Transfer functions of PI controller

$G_V(s)$ Transfer function of voltage controller

$G_{V_{dc}-I_d}(s)$ Transfer function from input of dc voltage to the current on D axis.

$G_{V-open}(s)$ Open loop transfer function of voltage loop

$G_{V-plant}(s)$ Transfer function of voltage functioning loop

$G_Z(s)$ Transfer function of impedance controller

I_{abc} Current output in three phase inverter

I_{abc}^* Reference current output in three phase inverter

I_{abc} Small signal of current output in three phase inverter

I_a Inverter current of phase A

I_1 Average value of DAB input current.

I_{10} Initial value of DAB average input current.

I_2	Average value of DAB capacitor feeding current
I_d	Inverter current on the D axis
I_d^*	Inverter current reference on the D axis
ΔI_d	Current variation on the D axis
I_{dq0}	Inverter output AC current in DQ0 frame.
I_{DAB}	DAB output current.
I_{in}	Input current.
I_{in}^*	Input current reference.
ΔI_{in}	Input current variation.
I_o	Output current
ΔI_o	Output current variation
I_q	Inverter current on the Q axis
I_q^*	Current reference on the Q axis
ΔI_q	Current variation on the Q axis
$i_t(t)$	Transformer primary side current
ΔV_{in}	Input voltage variation
k	Transformer turn ratio between secondary side and primary side
K	Gain of PI controller

K_i	Integral parameter in PI controller
K_{i-DAB}	Integral parameter in DAB PI controller
K_{i-i}	Integral parameter in current PI controller
K_{i-inv}	Integral parameter in inverter PI controller
K_{i-V}	Integral parameter in voltage PI controller
K_P	Proportional parameter in PI controller
K_{P-DAB}	Proportional parameter in DAB PI controller
K_{P-i}	Proportional parameter in current PI controller
K_{P-inv}	Proportional parameter in inverter PI controller
K_{P-V}	Proportional parameter in voltage PI controller
K_Z	Proportional impedance controller
K_{Z-F}	Front proportional impedance controller
K_{Z-E}	End proportional impedance controller
L	Inductor filter
L_l	Leakage inductor of DAB transformer
M_I	Magnitude of current
M_V	Magnitude of voltage
P^*	Active power reference

P_{DAB}	Power output of DAB
P_{DAB}^*	Reference power of DAB
ΔP_{DAB}	DAB power output variation
P_{in}	Input power
P_{INV}	Power output of inverter
P_{INV}^*	Reference power of inverter
ΔP_{INV}	Inverter power output variation
P_o	Output power
Q^*	Reactive power reference
r	Parasitic resistance of inductor filter
R_1	Parasitic resistance of DAB transformer
$s_1(t)$	Primary side switching functions
$s_2(t)$	Secondary side switching functions
T	DAB switching period
T_m	Impedance minor loop gain in forward power flow
T_{m-R}	Impedance minor loop gain in reversed power flow
T_P	PARK transformation matrix
U_{dq0}	Inverter output AC voltage under DQ0 frame

V_1	DAB input voltage
V_{abc}^*	Voltage reference of three phase inverter
V_{abc1}	Inverter three phase voltage between bridges and inductor filter
V_a	Inverter voltage of phase A
V_{abc}	Inverter three phase voltage between inductor filter and grid
V_{dc}	Inverter DC side voltage on inverter or DC link voltage
V_{dc}^*	Reference DC voltage on inverter or DC link
V_{dc0}	Initial value of DC voltage on inverter or DC link
V_{dc}^*	Reference of DC voltage on inverter or DC link
V_{grid}	AC Grid voltage
V_{gd}	AC Grid voltage on D axis
V_{gq}	AC Grid voltage on Q axis
V_{in}	Input voltage
V_o	Output voltage
ΔV_o	Output voltage variation
v_p	Primary side voltage of DAB transformer
V_{PWM}	Amplitude of the triangular carrier wave
v_s	Secondary side voltage of DAB transformer

Z_{DAB}	DAB impedance towards dc link voltage
Z^*_{DABo}	DAB output impedance in proposed control
Z_{in}	Input impedance in forward power flow
Z^*_{in}	Input impedance in forward power flow with proposed control.
Z_{in-B}	Input impedance of converter B
Z_{in-R}	Input impedance in reverse power flow
Z_{out}	Output impedance in forward power flow
Z_{out-A}	Output impedance of converter A
Z_{o-R}	Output impedance in reverse power flow
Z^*_{o-R}	Output impedance in reverse power flow with proposed control
θ	Phase
φ	DAB phase shift
τ	Time constant of PI controller
θ_o	Phase of output impedance
θ_{in}	Phase of input impedance
θ_T	Phase of impedance minor loop gain

TABLE OF CONTENTS

LIST OF FIGURES

CHAPTER 1. INTRODUCTION

This chapter firstly introduces the motivation and background of the research project, coming with the brief history of the renewable energy generations. Then the objective and contributions of this research work are presented, lighting the spirit of this research work. At last this chapter gives the chapter overview and the publication list.

1.1. BACKGROUND AND MOTIVATION

In the past decades, to support the growing industry, transportation and human residence, the demand for electricity energy is kept increasing, from 7000TWh in 1980 to 20,000 T in 2015. As shown in Fig. 1-1[1], the increasing of energy consumption continues in a higher speed in the future, indicating the fast developing prosperity and civilization of the future.

There are also concerns towards future energy, and they are mainly focused on two aspects: one is that the reservation of fossil energy is finite, not be available all the time; the other is that the fossil energies are not environment friendly, because the emission of greenhouse gases CO_2 and other harmful gases increase the global temperature and brings huge damage to human health.
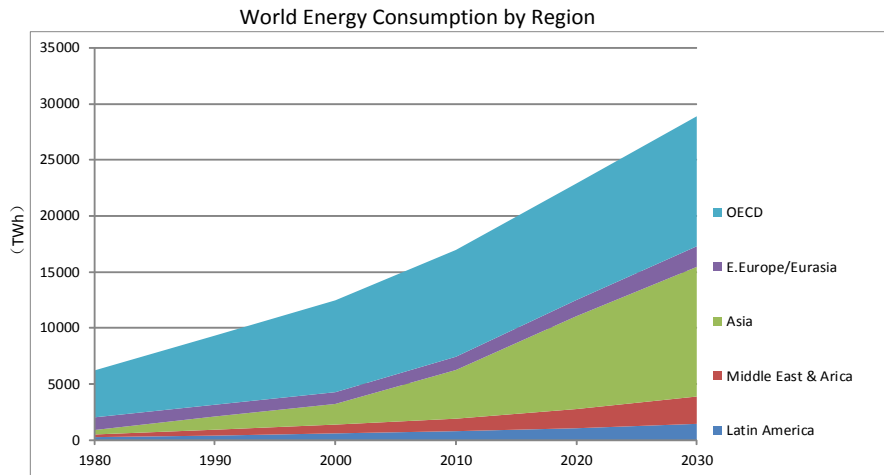
Fig. 1-1 Global electricity consumption by region.

World Energy Deman-Long-Term Energy Sources
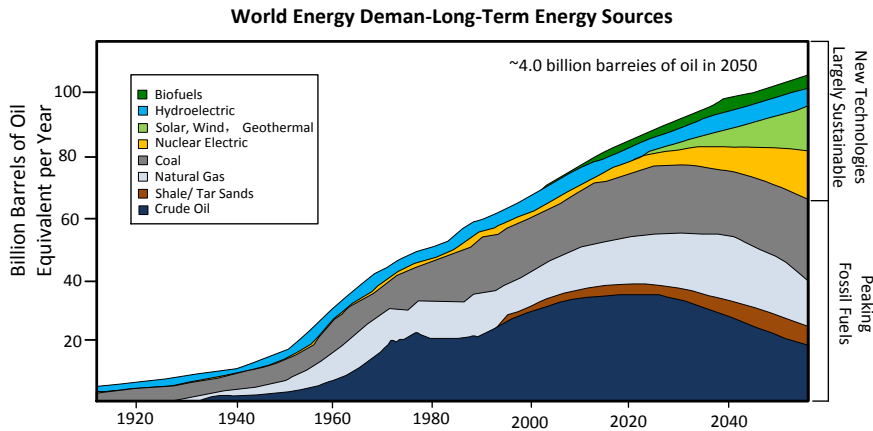
Fig. 1-2 Global energy demand-Long term energy Sources.

So societies are required to reshape not only the way that they use energy, but the energy sources as well. Governments strive to reduce the consumption of low efficiency, high-polluting fossil energy, such as the coal. In USA from 1920 to 1973, the coal contribution to the whole energy consumption shrank from 78% to 18 % [2]. As shown in Fig. 1-2, at the meantime, the technology of renewable energy based generations develops fast in the past few years, which contributes to the growth of renewable energy consumption[3]. In the future, renewable energies will play a more important role in the power system.

1.1.1. RENEWABLE ENERGY GENERATIONS

Renewable energy is generally defined as energy that comes from resources which are naturally replenished on a human timescale, such as the sunlight, wind, rain, tides waves and geothermal heat [4]. One distinct area that renewable energy replaces conventional fuels is the electricity generation. Solar power and wind power are significant parts among them.

1.1.1.1 Solar power plants

Solar power is recognized as a pure clean and sustainable power. In 1876, the first solar cell was demonstrated by William Adams and Richard Day, afterwards the research of photovoltaic cells started [5]. In 1905, Albert Einstein explained the photoelectric effect, and rewarded by the Nobel Prize. After 40 years accumulation of the research, the first industrial product crystalline silicon solar cells were produced in the Bell Laboratories [6]. Afterwards the solar cells began to be implemented on the satellite [7].

Solar Demand by Country
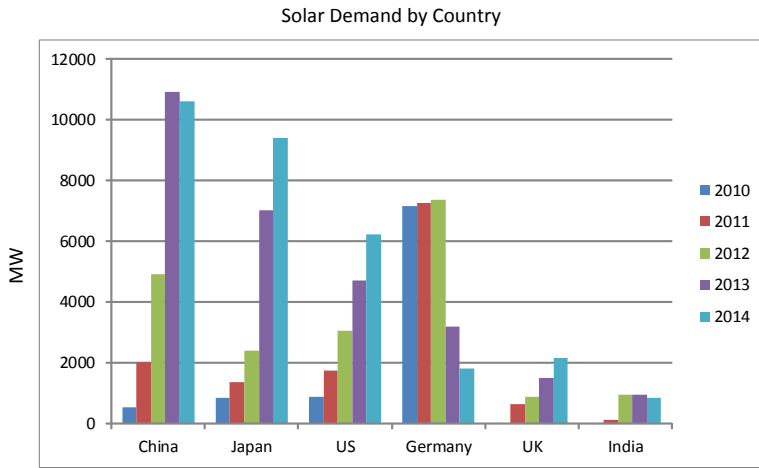
Source: Mercom Capital Group, llc

Fig. 1-3 Solar demand in recent years

In the following years, the efficiency of solar cell was increased up to near 15%, therefore solar power based power plants started to be installed, and the boom of solar power plant first stared in Europe, such as in Spain and Germany in early 21th [8]. The prosperity of solar power plants soon spread to China, Japan, US, UK and India, becoming the global trend [9], as shown in Fig. 1-3 [10].

In 2015, the global solar new installations reach up to 57.4 GW. China, Japan, and US are the main growth counties, counting for the 60% global new installations. Germany hold the maximum installation capacity, which is 38,754 megawatts (MW) by the end of May 2015, accounting for approximately 6.2 to 6.9 percent of the total electricity generation in 2014, ahead of China, Japan, Italy, and the United States [11].

The capacity of newly installed individual solar power plant is also increasing rapidly, now over 500MW, therefore the solar power plants becomes more competitive to conventional power generations. Although its availability significantly affected with alternating day and night, as well as the weather, these evidences indicate that solar power in the future would occupy a significant part in the energy landscape.

1.1.1.2 Wind power farms

Addition to solar power, wind power also has extremely important impact in both the past and future. From the sailing on the sea, to water pumping on the land, wind

power has been used since thousands years ago. It is in 1887 that the windmill was firstly used to produce electricity power [12].

Nowadays the capacity of single wind turbine can reach 8MW, with single blade of 80 meters long. Such huge wind turbines are grouped physical together to form a wind farm. The grouped wind turbine can be several hundred, constituting a wind power plant with the power capacity of hundreds of MW. By 2014, over 240,000 wind turbines are rotating on the earth, contributing 4% of the whole world's electricity power. As shown in Fig. 1-4 [13], the increasing tendency of wind power will continue to up limit, which the power system can hold utmost.

The physical location of wind farm is gradually moving from the land to the sea, that is the offshore wind farm. On the offshore wind farm, the wind harvesting is superior than the one on the land, as well as no disturbance to human residence. Consequently, long distance power transmission devices are necessary to deliver the electricity power from offshore to onshore and meanwhile guarantee the power quality and acting friendly to the utility grid.

So in the future, wind power relevant facility and devices will be deeply involved in the power system, which need to be accommodated.

Global cumulative instanlled wind capacity
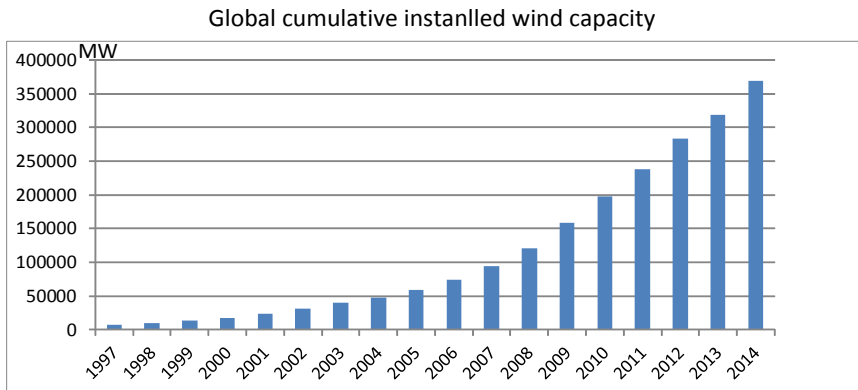
Fig. 1-4 Global cumulative installed wind capacity

1.1.2. ACTIVE DISTRIBUTION NETWORK

It is an effective way to form a sub-network that integrates the renewable energy based generations, PV plants or wind turbines, as well as storage devices and local load, and then connect with the electric power system. This sub network can also be described as active distribution network or microgrid [14,15].

Traditionally, electrical power is produced in bulk size in remote locations, usually near resource centers, then the effective transmission system is necessary to transmit the power. Recently, things get harder and harder to open a new transmission line. Added that the customer side needs more and more power with a higher reliability level, the consequences in the future may be the increase of congestion in some crowed power transmission lines, as well as the decline of the efficiency and reliability of the whole power system [16].

The renewable energy is dispersed widely, so the distributed generation (DG) is an effective way to take advantage of the green renewable energy. So in the future, electricity power will be produced everywhere and transported in all direction in power system. This trend will intensify in the coming years, and then the consumers will not only use electricity but also generate this energy, becoming the producer as well. So if the renewable energy is integrated in large amount in the power system in an efficient and social economic way, the power system are necessary to be reconfigured. However, for the difference from the operational characteristic of conventional utility grid, the universal application of renewable energy is severely limited [17].

Conventionally, the passive distribution network is designed to receive power from transmission network and distribute to loads. Real time control problems are predicted and solved in the planning stage. Then distributed energy resources are limited on their capacity. Therefore it hampered the widely use of renewable energy sources.

Active distribution network (ADN) refers to the distribution network with the capability to control the combination of the active distributed generators, loads and storage devices [18]. At the meantime, the distribution system operator (DSO) is able to manage the power flow of this network [19], and the distributed energy resources (DERs) share the responsibility of system support [20].In the active distribution network, distributed generations and energy storage devices enable the network with the capability of self-support, or output power to the utility grid. The concept of active distribution network may be characterised by words like flexible, intelligent, integration and cooperation.

Besides conventional AC system, DC distribution network is attracting great attention and it is becoming an effective solution for the modern energy distribution challenges, since it has significant advantages, such as reduced power losses, simplified regulation. In the past century, after the "war of currents", ac has been the standard choice for the electric power system. With the rapid development of power electronics, dc systems show great potential of reduced losses, higher reliability and increased power capacity. The success of HVDC system and the advanced power electronics promote the feasibility of dc system to be implemented in active distribution networks[21]. Moreover, some renewable power based

generations are naturally dc power based system on their prime side. For photovoltaic systems, fuel cell systems and battery based energy storage system, their prime side energies are in the form of dc, afterwards a DC/DC converter cascaded with an DC/AC inverter is needed to converter the energy from DC to AC. Therefore DC distribution system can reduce the number of power conversion stages, which can substantially increase the efficiency.

Another aspect of advantage of dc system is the omission of synchronous problem. In ac active distribution system, when transferring from self-support modes to grid-connected mode, the DG needs to adjust the output voltage, frequency and phase to avoid the obvious impact caused by the asynchronous voltage. The normal solution is to use synchronization control before reconnect to the main grid [22]. While the dc system is easier to reconnect without the synchronization issues. So dc active distribution system is becoming more and more attractive.

Therefore the connection of DC and AC networks will be necessary and inevitable. So this research will focus on the interface converter between DC and AC bidirectional flow application.

1.1.3. INTERFACE CONVERTER APPLICATIONS

Mostly, the renewable power generations are connected to the ADN through the power electronic devices. Then the power electric devices have a significant effect on the characteristic that the renewable power plant presents to the power system.

For the photovoltaic (PV) system, the interface converters have the responsibility to convert the dc voltage from PV array side into an acceptable ac current for the grid, and at the same time, it is needed to control the terminal voltage of the PV module(s) to achieve the Maximum Power Point Track (MPPT)[23]. Fig. 1-5 shows the configuration of PV modules' interface converter.

PV interface converters have different configurations, and Fig. 1-5 shows the single stage DC/AC inverter, two stages DC/DC-DC/AC converter, and the string two stages DC/DC-DC/AC topology[24]. So the direct contact of the individual power electronic converters will be widely encountered in the PV system.

For the wind power, from wind farm to the utility grid, power electronic converters also hold the mission of energy conversion. Fig. 1-6 shows the wind farm interface converter arrangement. An AC/DC converter is cascaded with a DC/AC converter to transfer the energy from the wind farm to the utility grid . Normally, one sub converter regulates the power, and the other one controls the DC link voltage [25].So in the wind farm transmission system, power converters also constitute the main part of the system.

(a)Singal stage   *(b)Two stages*
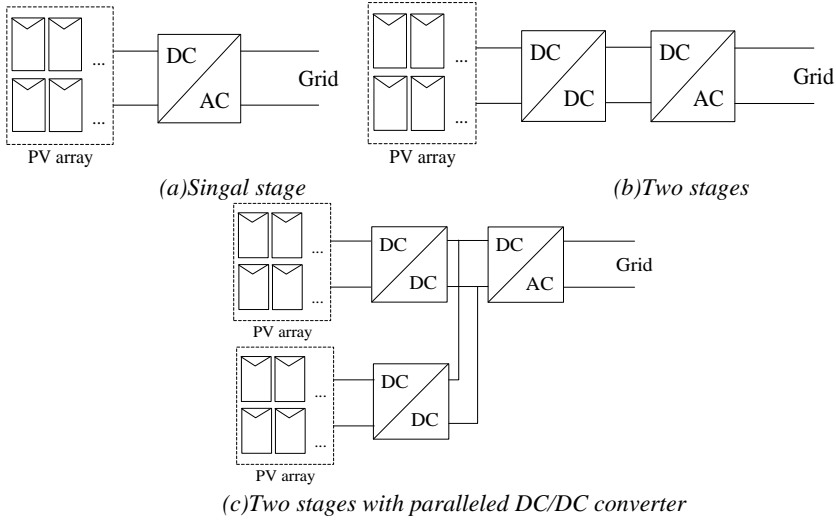
(c)Two stages with paralleled DC/DC converter
Fig. 1-5 Configurations of PV modules interface converter.
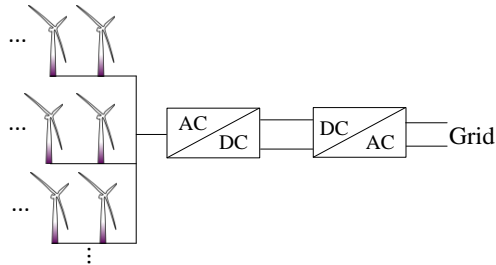
(a)VSC based HVDC transmission
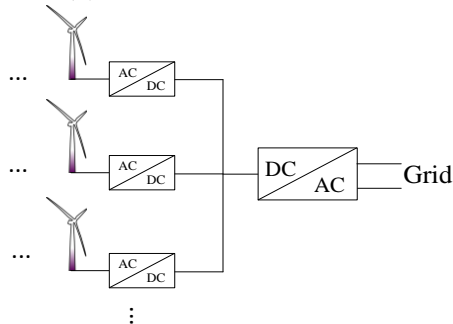
(b)Internal dc network and individual power control
Fig. 1-6 Wind farm interface converter configurations

Besides the PV system and the wind power system, there are still some other distributed generations, such as the fuel cell system, where the chemical reaction generate electricity energy in the form of dc, but still their interface elements with the utility grid are also power electronic converters.

1.1.4. FUTURE INTERFACE CONVERTER BETWEEN GRID AND DISTRIBUTION NETWORK

When distributed generations cooperate with local loads, storage devices, as well as combined heat and power (CHP), they will form an active distribution network, or called micro-grid. The distribution network needs effective control, protection and system expansion schemes to achieve high reliability and capability, as well as become friendly to the utility grid [26]. The upper layer interface converter would become the key element to accommodate the distributed generation with utility power grid. Then the interface converter will reshape the energy through bidirectional power flow direction, as shown in Fig. 1-7.
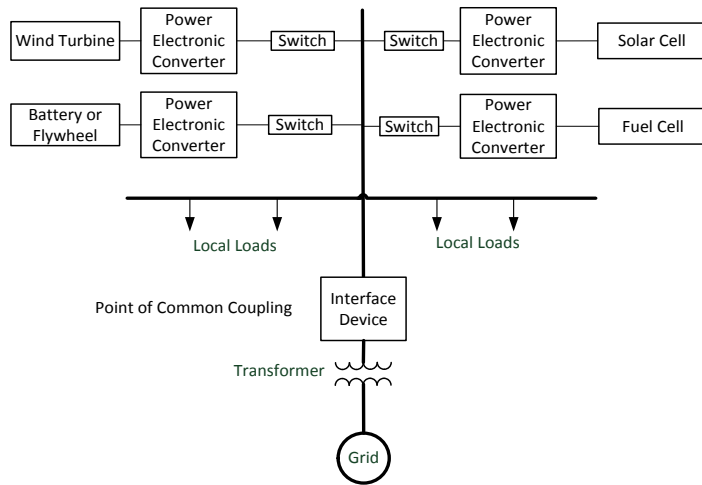
Fig. 1-7 Schematic of an active distribution network

1.2. OBJECTIVES AND NEW CONTRIBUTION OF THE WORK

In the future, power converters will be widely used in the distribution network, and the directly contact of them introduces significant change to both the power system and itself. So this work will analyze the interaction between converters in series connection, where the widely used two-stage cascaded converter system is studied.

The objective of the research is to develop optimized control strategies for the bidirectional cascaded interface converter, and it aims to ensure the stability of the interface converter under the bidirectional occasion.

The contribution of this research work includes that:

- A symmetric dc link voltage and active power control method is proposed, which can increase the stability and reliability of the dc link voltage, therefore the stability of the cascaded converter can be enhanced，and the stress on the switching devices can also be reduced.
- The power flow effect on the interface converter is studied, and which is helpful to design the interface converter with enhanced stability.
- An impedance coordinate control method is proposed, and it is able to modify the impedance of constant power controlled converter, and then the negative impedance can be avoided, therefore the system stability of the cascaded interface converter can be improved.
- An control system type number reduced control method is also proposed in this research work, in which the dc bus voltage control system type can be reduced, hereby the system is more easier to control and controllers are easier to tune
- The front to end impedance control method is proposed. It can modify the output impedance of the source converter and input impedance of the load converter, and both of them present resistive low frequency impedance to dc link connection and accordingly contribute a more decoupled cascaded system.

1.3. CHAPTER OVERVIEW

This research work is organized with 7 chapters. Chapter 1 and 2 are the first part. Chapter 3, 4, 5 and 6 offer the optimized control for the two stage cascaded converters. At last, chapter 7 concludes all the research work and outlook further research work. The contents of each chapter are as following:

Chapter 1 shows the motivation and background of this research work.

Chapter 2 introduces the interface converter topology and control issues of the dual active bridges converter cascaded with a three phase inverter.

Chapter 3 proposes a symmetric control method to improve the reliability and stability of the dc link voltage in the two stages cascaded converter system.

Chapter 4 analyzes the power flow effect, and concludes an important guide line for the design of two cascaded converter system, and proposes an impedance

coordinate control for the constant power converter in two-stage cascaded system. It can improve the system stability and reliability by adjusting the impedance of constant power converter.

Chapter 5 proposes a symmetric proportional control method for the two stage cascaded converter. This method can reduce the DC-link voltage control system type number, and drive the low frequency impedance of source converter and load converter becomes resistive, which is capable to improve system stability.

Chapter 6 proposes the front to end impedance controller concept, and it can modify the converter impedance presented to the dc link, and make them behave resistive in the low frequency range, improving the system stability.

Chapter 7 concludes the whole dissertation and presents the future potential research direction.

1.4. LIST OF PUBLICATIONS

Journal papers:

J1 **Y. Tian**, Z. Chen, F. Deng, X. Sun, Y. Hu, "Active Power and DC-link Voltage Coordinative Control for A DC-AC Converter with Bidirectional Power Application." *IEEE Transactions on Power Electronics*, Vol. 30, NO. 10, October 2015.

J2 **Y. Tian**, P. C. Loh, F. Deng, Z. Chen, Y. Hu, "DC-Link Voltage Coordinated-Proportional Control for Cascaded Converter with Zero Steady-State Error and Reduced System Type." *IEEE Transactions on Power Electronics*, Early Access.

J3 Z. Song, **Y. Tian**, W. Chen, Z. Zhou, Z. Chen, "Predictive Duty Cycle Control of Three-Phase Active-Front-End Rectifiers." *IEEE Transactions on Power Electronics*, Vol.31, Jan. 2016.

J4 X. Sun, **Y. Tian**, Z. Chen, "Adaptive decoupled power control method for inverter connected DG." *IET Renewable Power Generation*, Vol. 8, No. 2, 03.2014, p. 171-182.

Paper Submitted & Under review:

S1 **Y. Tian**, P. C. Loh, F. Deng, Z. Chen, Y. Hu, "Impedance Coordinative Control for Cascaded Converters in Bidirectional Applications." *IEEE Transactions on Industry Application*.

S2 **Y. Tian**, P. C. Loh, F. Deng, Z. Chen, Y. Hu, "Impedance Interaction in Bidirectional Cascaded Converter." *IET Transactions on Power Electronics*.

S3 **Y. Tian**, P. C. Loh, F. Deng, Z. Chen, Y. Hu, "Front-to-end Impedance Controller in Cascaded Converter System." *IEEE Transactions on Industrial Electronics.*

S4 X. Sun, Z. Chen, **Y. Tian**, "Study of a Novel Equivalent Model and a Long Feeder Simulator Based Active Power Filter in a Closed-Loop Distribution Feeder." *IEEE Transactions on Industrial Electronics.*

S5 Z. Song, **Y. Tian**, W. Chen, Z. Zou, Z. Chen, "Predictive Direct Power Control for Three-Phase Grid-Connected Converters Based on Extended-State Observation.*" IEEE Transactions on Power Electronics*, Vol.31, Jan. 2016.

Conference presentations:

C1 **Y. Tian**, F. Deng, Z. Chen, X. Sun, Y. Hu, "Coordinative Control of Active Power and DC-link Voltage for Cascaded Dual-Active-Bridge and Inverter in Bidirectional Applications." *in proc. of the 2014 IEEE Energy Conversion Congress and Exposition (ECCE).* IEEE Press, 2014, p. 2249- 2256.

C2 **Y. Tian**, F. Deng, Z. Chen, X. Sun, Y. Hu, "Impedance Interaction Modeling and Analysis for the Bidirectional Cascaded Converter in Active Distribution Network." *in proc. of the 9th International Conference on Power Electronics – ECCE Asia (ICPE 2015-ECCE Asia)*, June 1-June 5, Seoul, 2015.

C3 Y. Tian, F. Deng, Z. Chen, X. Sun, Y. Hu, "An Impedance Coordinate Control Method for Cascaded DAB and Inverter in Bidirectional Applications." *in proc. of the 9th International Conference on Power Electronics – ECCE Asia (ICPE 2015-ECCE Asia)*, June 1-June 5, Seoul, 2015.

C4 Y. Tian, P. C. Loh, F. Deng, Z. Chen, X. Sun, Y. Hu "DC-link Voltage Coordinative-Proportional Control in Cascaded Converter Systems." *in proc. of IEEE Energy Conversion Congress & Expo ECCE 2015*, Montreal Canada September 20-24,2015.

C5 **Y. Tian**, P. C. Loh, F. Deng, Z. Chen, Y. Hu, "Impedance Analysis of Control Modes in Cascaded Converter." *in proc. of IEEE Industrial Electronics Society 41st Annual Conference, IECON 2015,* November 9-12, 2015 Yokohama, Japan.

CHAPTER 2. BIDIRECTIONAL DC-AC CASCADED INTERFACE CONVERTERS

This chapter will analyze the function and requirement for the interface converter of dc active distribution network. Then the topology of the interface converter is selected. Finally a brief introduction about the operating principle of the selected topology is presented.

2.1. FUNCTION ANALYSIS OF INTERFACE CONVERTER

Distributed resource (DR) or distributed energy resources (DER) refer to the sources of electric power that are not directly connected to a power transmission system. DR includes both generator and energy storage technologies. The energy that DR or DER produced is called distributed or decentralized energy [27].

The renewable energy sources belong to the DER systems, such as the solar power, wind power, biomass, and biogas. Aided by interface devices, the distributed energy can be converted to the electric energy that can be accepted by the load or the electric power system and this is the distributed generations. Distributed generations (DG) storage enable collection of energy from many sources and may lower environmental impacts. Fig. 2-1 shows the scheme of distributed generation.

Owing to the sustainability and environmental friendliness, the renewable energy based DG becomes more and more involved in the distribution level of electric power system. In addition, DER systems are widely spread with flexible technologies, located closer to their served loads, although even their capacities are only tens megawatts (MW) or less [28].

But conventional utility power systems are built to delivery and distribute electricity power from central power plant to consumers, so the power host and consumer are fully decoupled. Their dynamics are pretty slow, because the generator is rotating at constant frequency with great inertia, so dynamic reaction time is within electro-mechanics domain, which is the seconds or minute level. The response of interface converter of the distributed generations is much faster than that of the rotating generator, which can be the millisecond level (ms). Therefore the conventional central generator, transmission and distribution equipment can not timely respond to the dynamics of the distributed generations, consequently the stability and reliability of power system will be degraded [29]. So it is necessary to
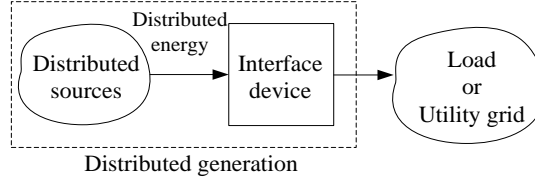
Fig. 2-1 Distributed generations

buffer the two kinds of different dynamic behaviors.

Moreover, conventional power system is designed for unidirectional power flow, not planned to accommodate active facilities, such as the distributed generations and storage devices. Therefore, there are barriers for the coherent transition from conventional utility grid to deeply integrating distributed power resources. The engagement of power electronics interface converter with advanced control in distribution level of power system provides inspiring solving methods on the above mentioned issues.

2.2. REQUIREMENT FOR NETWORK INTERFACE CONVERTER

Fig 2-2 shows a schematic diagram of a DC active distribution network with the implementation of bidirectional DC/AC interface converter.

As previously mentioned, the renewable energy based DGs have significant intermittent dynamics, and it can be decoupled by the power electronic interface converter with the grid. Through advanced control methods, the transient stability problems can be avoided [30]. With the interface converter, the faults of sub-connected system can be decoupled and isolated from the utility grid, which effectively prevent the negative effect on the distribution network in the power system.

The basic function of the interface converter in distribution network can be summarized as [31, 32]:

1) Bidirectional power flow capability: In the active distribution network, when the energy production of DGs is higher than the local load and energy storage capability, the excess power can be fed to the utility grid, and this can reduce the stress and power loss on the electric power transmission system, increasing the system efficiency of the power system. Moreover, the consumption of fossil resources in central power plants can
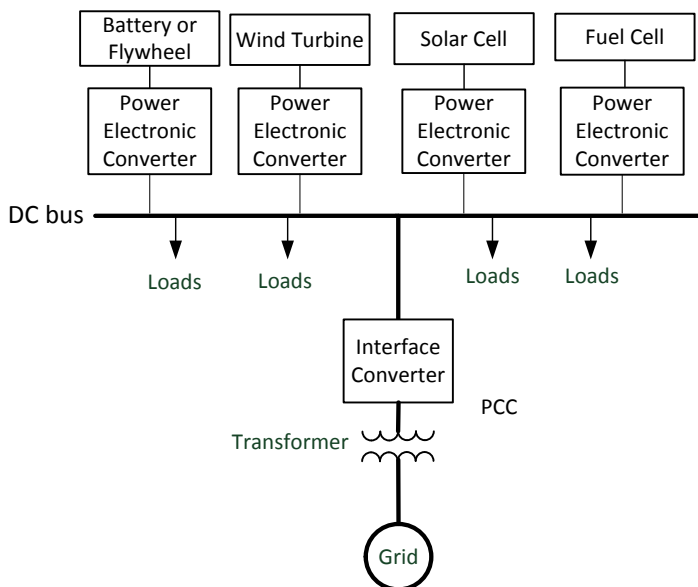
Fig. 2-2 Distributed Schematic Diagram of an active distribution network

also be reduced. When there is fault in the utility grid, with enough DG capacity, the dc active distribution network can achieve self support, which is the islanding mode. By controlling the power flow, the interface converter can perform the transition between grid connected mode and islanding mode.

2) Dynamic decoupling and isolation of interconnected systems: The interface converter can support the DC bus of connected sub network and also it can ride through the transient dynamics happened on both sides, and the transient dynamics can not be felt or reflected by the other side of the interface converter, so the interface converter is acting as the decoupled or isolation shield.

3) Bidirectional fault current interrupt capability: The interface converter can act as the mechanical protection equipment. When there is fault current, the interface converter output current will be controlled within the limitation, such as the short circuit voltage support.

4) Smart metering and communication function: The interface converter can measure the voltage and current on its both sides. With communication capability, the power system can not only monitor the operation of the interface converter, but also can send orders to the interface converter. Meanwhile, the interface converter of the active distribution network will correspondingly support the power system.

Based on practical requirements, the interface converter has to be capable with:

1) High power density. The high power density can reduce the physical volume of the interface converter, and provide high power flow capability, which is benefit to system expansion and widely installation.
2) Voltage buck-boost capability: Voltage buck-boost conversion capability is necessary for the interface converter to connect between DC and AC networks with different voltage levels.
3) High efficiency: In terms of long run, high efficiency will be benefit for the economic operation. Moreover with less power loss, the life time of the device will also be prolonged.
4) High cost-effectiveness. It can reduce the investment in initial stage, and promote the spread of industrial application.
5) High safeness with galvanic isolation. This is significant for the safety requirement, and more significant for residential or building application of the DC sub network.

2.3. TOPOLOGY SELECTION FOR THE GRID INTERFACE CONVERTER

The interface converter between AC and DC system should have the previously mentioned features. Single stage buck-boost converter is difficult to satisfy these requirements, so the interface converter normally adopts two stages cascaded topology. In the analysis of two stages cascaded converter system, the directly contact of power electronic converters is helpful to review the stability issue in multi-power converter system.

The two stage cascaded interface converter includes DC/DC and DC/AC power conversion stage. For the consideration of DC/DC converter, the dual-active-bridge converter (DAB) has significant advantages: The high frequency transformer can fulfil the requirements of galvanic isolation and high power density [33]; Voltage buck-boost control can be realized by phase difference between the primary side and the second side [34]; Symmetric structure can achieve bidirectional power control, and the configuration of H-bridge with transformer can easily be operating in zero voltage switching [35-3637]. So the DAB converter is an ideal choice for the first stage DC/DC converter. For the DC/AC inversion stage, the widely used two level three phase inverter is qualified for this requirement. Fig. 2-3 shows the topology. The similar topology can also be used in the HVDC application, with Multi Modular Converter (MMC) [38].

This section will show the basic operating principle of DAB converter and inverter.
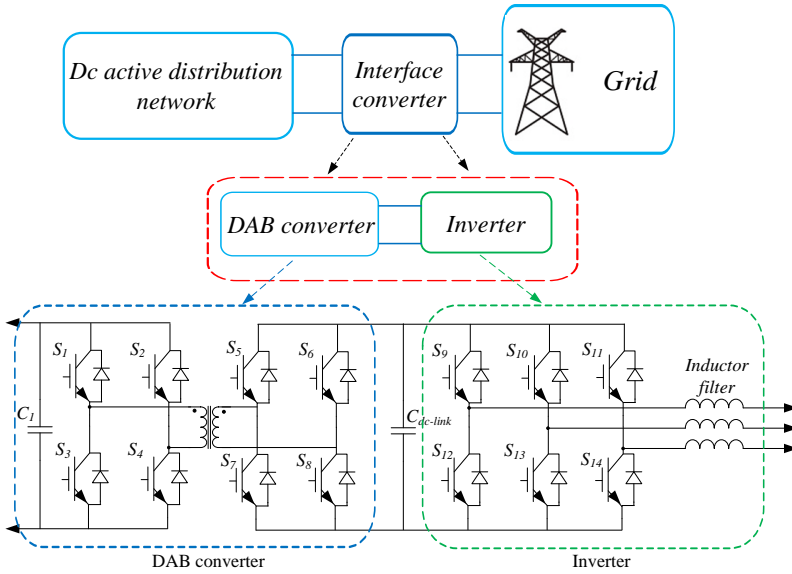
Fig. 2-3 The topology of the grid interface converter

2.4. CONTROL ISSUES OF DAB AND INVERTER

2.4.1. DAB CONVERTER

DAB converter consists of two H-bridges, and they are connected by a high frequency transformer. Its topology is totally symmetric, which facilitates the bidirectional power flow. With the existence of transformer leakage inductance or with external inductor, the switches of DAB converter can operated in zero voltage switching (ZVS), which can substantially increase the efficiency.

In DAB converter, bidirectional power flow can be realized by phase shift control [39,40].

The main working wave forms of DAB converter under phase shift control is shown in Fig. 2-5 [41].

As shown in, Fig. 2-5 (a), the switches are modulated by the PWM signal with 50% duty ratio. When the transformer primary side voltage leads the secondary side, the power will flow from the primary side to the secondary side, and the current can be regulated by the phase difference between the two sides of the transformer [42].
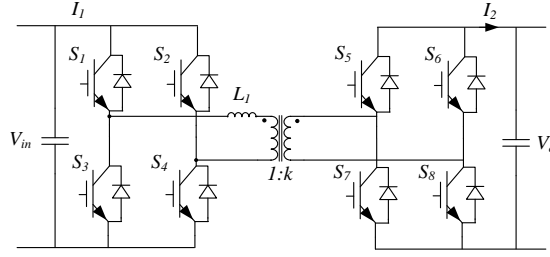
Fig. 2-4 DAB converter topology
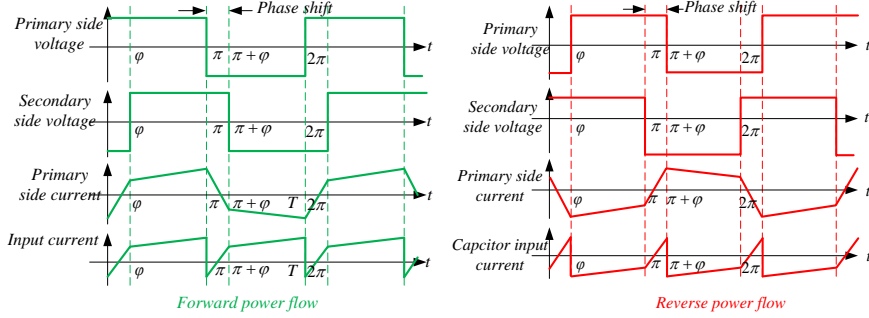
(a) Forward power flow.	(b) Reverse power flow

Fig. 2-5 DAB operating waveforms of the transformer and capacitor current.
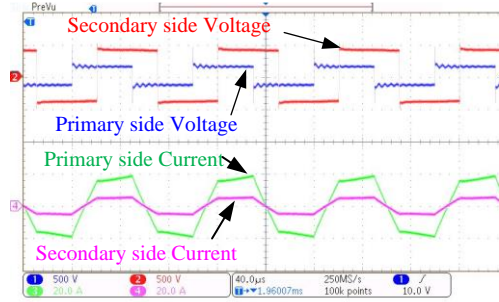
Fig. 2-6 Experimental waveforms of transformer in DAB converter

Fig. 2-6 shows the experimental waveforms of DAB transformer.

In one switching period, the input current of I_1, which is marked in Fig 2-4, can be expressed as (2.1). In (2.1), I_{10} is the initial value of the input current, when t is zero in Fig. 2-5 (a), and L_l is the leakage inductance of DAB transformer. Then the average input current I_1 can be obtained by (2.2).

$$I_1 = \frac{1}{\pi}\int_0^\pi I_{in}(\theta)d\theta = \frac{V_o}{2k\pi^2 fL_l}\varphi(\pi - |\varphi|) \tag{2.1}$$

$$I_1(\theta) = \begin{cases} I_{10} + \dfrac{V_{in} + \dfrac{1}{K}V_o}{2\pi fL_l}\theta, & \theta \in (0,\varphi) \\[4mm] I_{10} + \dfrac{V_{in} + \dfrac{1}{K}V_o}{2\pi fL_l}\varphi + \dfrac{V_{in} - \dfrac{1}{k}V_o}{2\pi fL_l}(\theta - \varphi), & \theta \in (\varphi,\pi) \\[4mm] -\left(I_{10} + \dfrac{V_{in} + \dfrac{1}{k}V_o}{2\pi fL_l}\varphi + \dfrac{V_{in} - \dfrac{1}{k}V_o}{2\pi fL_l}(\pi - \varphi)\right) + \dfrac{V_{in} + \dfrac{1}{k}V_o}{2\pi fL_l}(\theta - \pi), & \theta \in (\pi, \pi + \varphi) \\[4mm] -\left(I_{10} + \dfrac{V_{in} - \dfrac{1}{k}V_o}{2\pi fL_l}(\pi - \varphi)\right) + \dfrac{V_{in} - \dfrac{1}{k}V_o}{2\pi fL_l}[\theta - (\pi + \varphi)], & \theta \in (\pi + \varphi, 2\pi) \end{cases} \tag{2.2}$$

Then the input power of DAB converter can be obtained as:

$$P_{in} = V_{in}I_1 = \frac{V_{in}V_o}{2k\pi^2 fL_l}\varphi(\pi - |\varphi|) \tag{2.3}$$

Neglecting the converter losses, the input power P_{in} equals the output power P_o, as $P_{in} = P_o$. Therefore the current feeding capacitor filer can be obtained as:

$$I_2 = \frac{V_{in}}{2k\pi^2 fL_l}\varphi(\pi - |\varphi|) \tag{2.4}$$

So by controlling the phase shift angle φ, the capacitor feeding current can be controlled. Through inner current loop control, the outer voltage and power can also be regulated. Additionally, to increase the power capacity, the switching frequency or the leakage inductance need to be reduced, and the maximum power happens when the phase shift is $\pi/2$.

2.4.2. INVERTER

Fig. 2-7 shows the main circuit of two levels three phase inverter [43]. It consists of three phase H-bridges and the inductor filters, where r is the parasitic resistance. D_{abc} is the three phase duty ratio of the inverter. V_{PWM} is the amplitude of the triangular carrier. V_{grid} is the grid voltage.
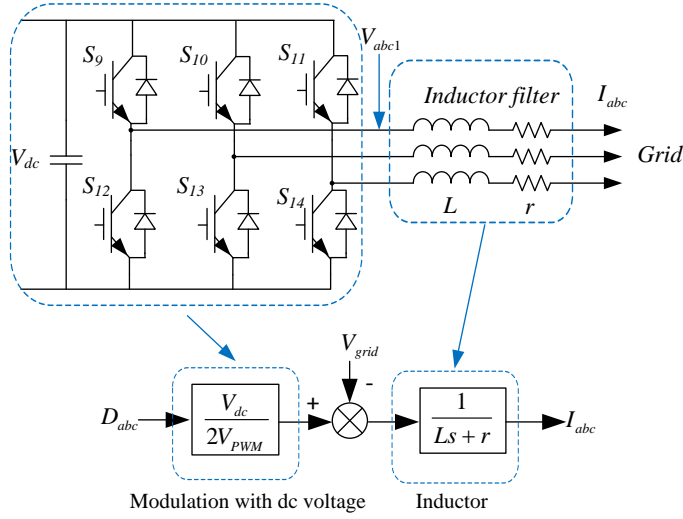
Fig. 2-7 Topology and systematic model of inverter

According to the PWM modulation [44], the three phase duty ratio can be obtained as:

$$D_{abc} = \frac{1}{2}\left(1 + \frac{V_{abc1}^*}{V_{PWM}}\right) \tag{2.5}$$

V_{abc1}^* is the voltage reference. When the modulation is bipolar, as in Fig. 2-7, the average voltage (V_{abc1}) in front of the inductor filter in each switching cycle is:

$$V_{abc1} = V_{dc}\left(2D_{abc} - 1\right) \tag{2.6}$$

Based on (2.5) and (2.6), the transfer function from the input of PWM modulation to the voltage output of the bridges circuits can be expressed as:

$$\frac{V_{abc1}}{V_{abc}^*} = \frac{V_{dc}}{2V_{PWM}} \tag{2.7}$$

Therefore the current output of the three phase inverter can be expressed as:

$$I_{abc}(s) = D_{abc}^* \frac{V_{dc}}{2V_{PWM}} \frac{1}{Ls+r} - V_{grid} \frac{1}{Ls+r} \tag{2.8}$$

The power output of inverter can be calculated in the DQ rotation frame through PARK transformation [45], and the transformation matrix is:

$$T_P = \frac{2}{3} \begin{bmatrix} \cos(\omega t) & \cos\left(\omega t - \frac{2}{3}\pi\right) & \cos\left(\omega t + \frac{2}{3}\pi\right) \\ -\sin(\omega t) & -\sin\left(\omega t - \frac{2}{3}\pi\right) & -\sin\left(\omega t - \frac{2}{3}\pi\right) \\ \frac{1}{2} & \frac{1}{2} & \frac{1}{2} \end{bmatrix} \tag{2.9}$$

Under DQ rotation frame, the inverter current and voltage in can be obtained as:

$$I_{dq0} = I_{abc} T_P \tag{2.10}$$

$$V_{dq0} = V_{abc} T_P \tag{2.11}$$

I_{abc} V_{abc} are the inverter voltage and current outputs, respectively. I_{dq0} U_{dq0} are respectively the current and voltage in DQ frame.

According to the power calculation under three-phase stationary coordinates, and with the consideration of PARK transformation T_P, the power output under the synchronous rotation frame can be obtained as[46]:

$$P = \frac{3}{2}(U_d I_d + U_q I_q) \tag{2.12}$$

$$Q = -\frac{3}{2}(U_d I_q - U_q I_d) \tag{2.13}$$

According to (2.5)~(2.13), the power output of the inverter can be regulated. Fig. 2-8 shows the experimental results of inverter under step response from 0 to 1kW. As shown, the power output can be maintained at reference value.
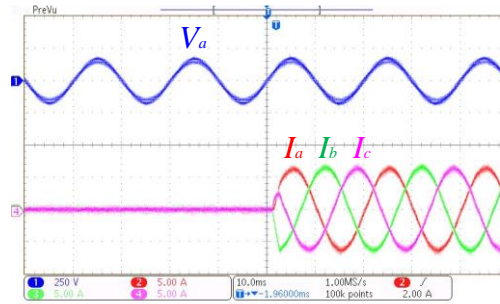
Fig. 2-8 Experimental waveforms of inverter under1kW step response

2.5. CONCLUSION

This chapter mainly introduces the application of grid interface converter for the dc active distribution network. The significance of the interface converter is to buffer the characteristic difference between distributed generations and the electric power grid. The selected topology is the Dual Active Bridges (DAB) converter cascaded with a three phase two level inverter, contributing to the bidirectional power flow galvanic isolation, high power density and high efficiency. The basic operation principle of the DAB and inverter is also presented.

CHAPTER 3. SHARING CONTROL FOR CASCADED DC-AC CONVERTERS

This chapter analyzes control methods for the cascaded interface converter, and also proposes a coordinative control method. The proposed control can effectively reduce the voltage fluctuation on the dc-link in the interface converter, therefore the stress on switching devices can be reduced and system performance also can be improved.

3.1. CONTROL OF THE INTERFACE CONVERTER

Fig. 3-1 shows conventional control scheme of the cascaded converter system. As shown, one sub-converter maintains the dc-link voltage V_{dc}, and the other one controls the power output [47]. For instance in the selected topology, DAB maintains the dc-link voltage and the inverter controls the power output. In order to improve the dynamic behavior, a feed forward loop is often implemented to the control loop. The following parts will show the detail analysis of DAB and inverter.
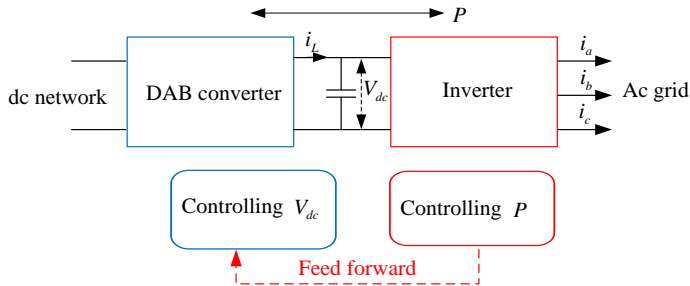
Fig. 3-1 Control scheme of the interface converter.

3.1.1. DAB CONTROL SCHEMES

For the control of DAB converter, the phase-shift control is used to regulate the output variable at the reference value [48]. The basic operation of phase shift is introduced in the previous 2.4.1.

DAB voltage control strategies can be classified into two types: Single voltage loop control [49] and voltage current double loop control [50].Fig. 3-2 shows the block diagram of DAB under voltage control.

(a)Single loop voltage control

(b) Double loop voltage control

(c)Double loop with feed forward control
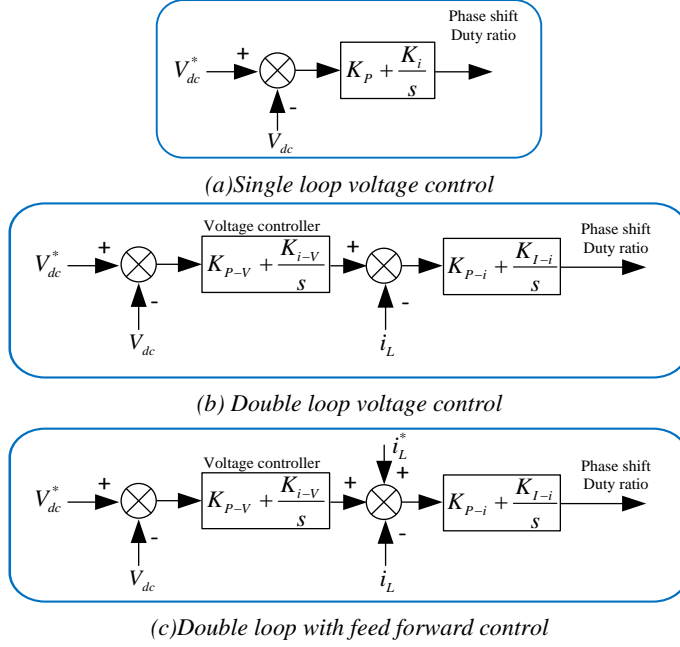
Fig. 3-2 Control block diagram of DAB

As in Fig. 3-2, in the single loop control scheme, the output voltage and the reference voltage is compared, and then, the phase-shift angle is adjusted by the proportional-integral (PI) controller. Only one control loop is involved, so it is a single loop voltage control [51].

Double loop control methods nest an inner current loop to the single loop control structure. DAB converter is a current source converter [52], and as afore mentioned, DAB inner loop current can be expressed as:

$$I_2 = \frac{V_{in}}{2k\pi^2 fL_1} \varphi(\pi - |\varphi|)$$ (3.1)

where k is transformer turn ratio between secondary side and primary side, f is the frequency of the square waves. $\Delta\varphi$ is phase shift between two bridges. Therefore an inner current loop can be implemented to improve dynamic performance.

Feed-ford control strategies share the reference or real time signals of one sub converter to the other. For instance in Fig. 3-2, the power reference of inverter is fed to DAB converter. Dynamic power difference between DAB and inverter will be further decreased, because the power feed-forward path shares the power output

signal between DAB and inverter, then DAB converter is more easier and faster to track inverter power output. Then the dc link voltage will be more stable.

3.1.2. MODELLING OF VOLTAGE CONTROLLED DAB.

Assume v_P and v_s are the transformer primary and secondary side voltage, respectively, which can be expressed as:

$$v_p = s_1(t)V_1(t) \tag{3.2}$$

$$v_s = s_2(t)V_2(t) \tag{3.3}$$

where $s_1(t)$ and $s_2(t)$ are respectively the primary and secondary side switching functions, which can be expressed as (3.4) and (3.5).

$$s_1(t) = \begin{cases} 1, & 0 < t \leq \dfrac{T}{2} \\ -1, & \dfrac{T}{2} < t \leq T \end{cases} \tag{3.4}$$

$$s_2(t) = \begin{cases} 1, & \dfrac{\varphi T}{2\pi} < t \leq \dfrac{T}{2} + \dfrac{\varphi T}{2\pi} \\ -1, & 0 < t \leq \dfrac{\varphi T}{2\pi} \ OR \ \dfrac{T}{2} + \dfrac{\varphi T}{2\pi} < t \leq T + \dfrac{\varphi T}{2\pi} \end{cases} \tag{3.5}$$

T is the period of the square wave. Recognizing the transformer primary side current $i_t(t)$ and output capacitor voltage V_o as the state variables, state equations of DAB converter are as following:

$$\frac{di_t(t)}{dt} = -\frac{R_1 i_t(t)}{L_1} + \frac{s_1(t)V_{in}(t)}{L_1} - \frac{s_2(t)V_o(t)}{kL_1} \tag{3.6}$$

$$\frac{dV_o(t)}{dt} = \frac{s_2(t)\dfrac{i_t(t)}{k}}{C_2} - \frac{i_o(t)}{C_2} \tag{3.7}$$

Through Fourier analysis [53], state equations can be derived as:

$$\frac{dx}{dt} = Ax + B\phi \tag{3.8}$$

$$y = Cx \tag{3.9}$$

$$x = \left[\Delta V_2\ \Delta i_{t1R}\ \Delta i_{t1I} \right] \tag{3.10}$$

$$y = \Delta V_2 \tag{3.11}$$

$$A = \begin{bmatrix} -\dfrac{1}{RC_2} & \dfrac{-4\sin(\phi)}{\pi C_2} & \dfrac{-4\cos(\phi)}{\pi C_2} \\[2ex] \dfrac{2\sin(\phi)}{\pi L_1} & -\dfrac{R_1}{L_1} & w_s \\[2ex] \dfrac{2\cos(\phi)}{\pi L_1} & -w_s & -\dfrac{R_1}{L_1} \end{bmatrix} \tag{3.12}$$

$$B = \begin{bmatrix} \dfrac{4}{C_2}\left(I_{0I}\sin(\phi) - I_{OR}\cos(\phi)\right) \\[2ex] \dfrac{2V_2}{L_1}\cos(\phi) \\[2ex] \dfrac{-2V_2}{L_1}\sin(\phi) \end{bmatrix} \tag{3.13}$$

$$C = \begin{bmatrix} 1 & 0 & 0 \end{bmatrix} \tag{3.14}$$

i_{t1R} and i_{t1I} are the real and imaginary part of the transformer primary side current.

$$w_s = 2\pi f \tag{3.15}$$

Then DAB voltage control transfer function (G) can be obtained by:

$$G = C(sI - A)^{-1} B \tag{3.16}$$

Based on above modeling, the power controller can be designed.

Fig. 3-3 shows the bode plots of the DAB under voltage control, including compensated and uncompensated results. The controller parameters are shown in the Appendix. As shown, after the compensation of PI controller, the performance of DAB converter can be maintained within a stable area and the steady stage error in the voltage output can also be eliminated.
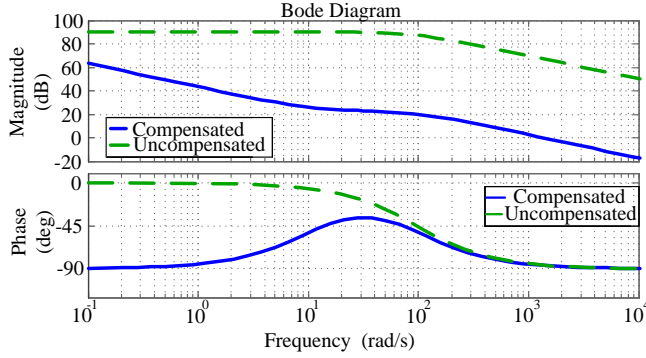
Fig. 3-3 Bode diagram of DAB converter under voltage control

3.1.3. INVERTER CONTROL SCHEME

Inverter controls power output through current loop, and Fig. 3-4 shows the control scheme. As shown, the current control loop is performed under DQ rotation reference frame. The sampled three phase current signals have been processed through Park transformation, and represented by the variables of (I_d, I_q), so two control paths are laid in the control unit as d- and q-path. Two PI controllers are used to track the current references (I_d^*, I_q^*). Then the generated the three phase duty ratio D_{abc} is used to generate the PWM singles driving the main circuit switches.

The current references can be generated by the power reference and sampled voltage signal. The angle in rotation frames is oriented with the grid side voltage, therefore the voltage on the quadrature (Q) axis is zero, and direct (D) axis voltage is the amplitude of grid voltage. Then according to the power calculation (2.12) and (2.13), the current references can be expressed as (3.17) and (3.18).
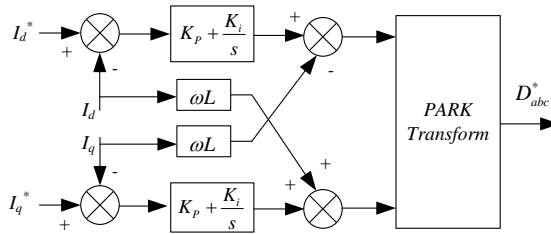
Fig. 3-4 Control block diagram of inverter under current control
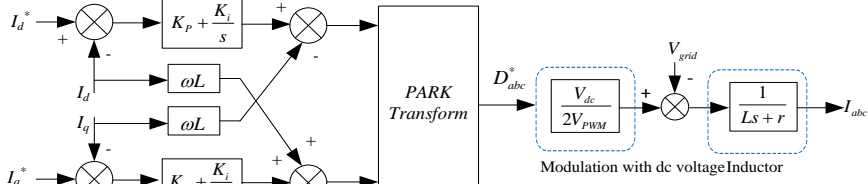
Fig. 3-5 Systematic model of inverter under current control

$$I_d^* = \frac{2}{3}\frac{P^*}{U_d} \tag{3.17}$$

$$I_q^* = -\frac{2}{3}\frac{Q^*}{U_d} \tag{3.18}$$

where P^* and Q^* are the active and reactive power references. I_d^*, I_q^* are the current reference on the D, Q axis respectively, U_d is the voltage on the D axis.

Involving the main circuit, the whole inverter block diagram is shown as Fig. 3-5. Then the plant transfer function of current control can be expressed as:

$$I_{abc}(\mathrm{s}) = \frac{1}{Ls+1+r}\frac{V_{dc}}{2V_{PWM}}I^*(\mathrm{s}) + \frac{1}{(Ls+1+r)}V_{grid}(s) \tag{3.19}$$

where L is the inductance and r is the parasitic resistance of the inductor filter. As shown in Fig. 3-5. V_{dc} is the voltage on the inverter dc side.

As shown in (3.19), the inverter output current is determined by the current reference $I^*(\mathrm{s})$ and the ac side grid voltage $V_{grid}(s)$. The current reference $I^*(\mathrm{s})$ refers to (3.17) (3.18). In order to damp the response to the switching noises, the current loop control bandwidth is much less than the switching frequency [54]. The ratio of K_P and K_i equals to the ratio of L and the parasitic resistance r, as in (3.20), then the zero of PI controller and the pole of inductor filter can be cancelled, which can reduce the order of the open loop transfer function of the current loop, that is to say system is more easily controlled [55].

$$\frac{K_P}{K_i} = \frac{L}{r} \tag{3.20}$$
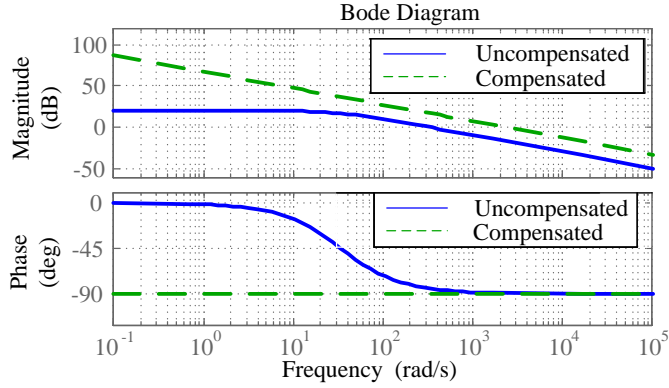
Fig. 3-6 The bode plots of the current controlled inverter

Based on the control bandwidth requirement, the magnitude of PI controller can be figured out. Fig. 3-6 shows the bode diagram of the current open loop transfer function, and it is a typical type 1 control system [56]. Controller parameters are shown in the appendix.

3.1.4. ANALYSIS OF DC LINK VOLTAGE IN CONVENTIONAL CONTROL

Conventionally dc link capacitors are designed with two kinds of consideration: one is to minimize the steady state voltage ripple[57], and maintain dc link voltage at a desirable quality; the other one is to reduce the output impedance of source converter, and decouple the source converter with load converter to certain extent, which can ensure the stability [58], because the stability of the cascaded converter system not only depends on well designing of individual converter, but also the impedance issues of sub-converters [59].

For the control methods of cascaded converter systems, the responsibility of power control and dc-link voltage control are respectively assigned to two individual converters, then one sub converter is used to control dc-link voltage and the other to control power. Under steady state, these control strategies can maintain system stable and satisfy the requirement of power control. In dynamics, under power output variations, the dc link voltage controlling converter has to track the power output variations, and its control bandwidth needs to be wide enough to track the power variations timely.

For the selected topology, DAB converter and inverter have different dynamic behaviors, because of the different topology and control scheme parameters, so for the dynamic performance, power unbalance between DAB and inverter will occur, which will alter voltage on the dc link.
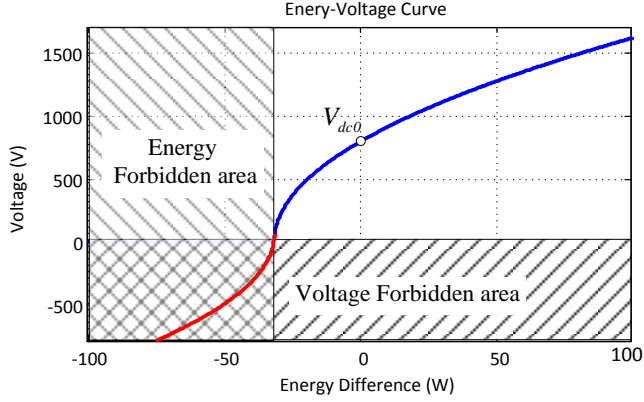
Fig. 3-7 The curve between energy difference and voltage on the dc-link capacitor

The relation between power unbalance and dc-link voltage variation can be obtained as:

$$V_{dc} = \sqrt{V_{dc0}^2 + \frac{2(E_{DAB} - E_{Inverter})}{C}} \tag{3.21}$$

where V_{dc} is the dc link voltage, and it is also the inverter dc side voltage. V_{dc0} is the initial value of dc link voltage. E_{DAB} and $E_{Inverter}$ are respectively the output energy of DAB and inverter. These energies can be obtained by integrating converter power output. C is the dc link capacitor.

The relationship between energy difference and voltage is shown in Fig. 3-7. As shown, when the energy difference occurs, the dc-link voltage will shift away from nominal value(V_{dc0}), and when the energy difference is below -32W, the dc link capacitor will be reverse charging, and this is vital for the electrolytic capacitors, since it will damage the capacitor. When the energy difference is above 0, the plus energy will promote the dc link voltage and potential extra high voltage. The oscillation will reduce the reliability of dc link capacitor [60], as well as increase the stress on the switching devices. In the perspective of the small signal modelling, inverter output current is:

$$I_{abc}(s) = \frac{1}{Ls + 1 + r} \frac{V_{dc}}{2K_{PWM}} I_{abc}^*(s) + \frac{1}{Ls + 1 + r} \frac{I^*(s)}{2K_{PWM}} V_{dc} \tag{3.22}$$

The superscript $\wedge$ represents the relevant small signal. So it can be seen that the variation of dc link voltage will disturb the output inverter current. Therefore a
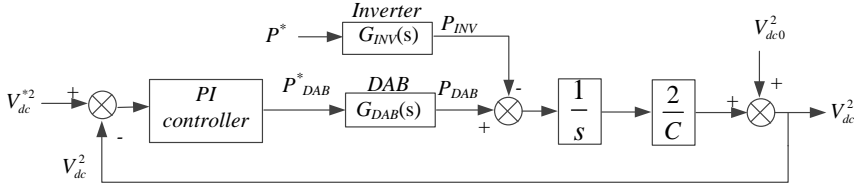
Fig. 3-8 The Block diagram of the DAB converter with voltage control

stable dc-link voltage is mandatory for improving the performance of inverter and the reliability of the system.

Normally, for the dc-link voltage controlling converter, it is designed by its own feature [61].In the cascaded DAB and inverter topology, the voltage controller is designed based on DAB model, and the block diagram is shown in Fig. 3-8, where the block diagram is illustrated from the perspective of energy[62], so V_{dc}^2 is used.

Around a specific operation point, the small signal of dc-link voltage V_{dc} is linear with the small signal of voltage square V_{dc}^2, because high order and smaller items can be omitted, as:

$$V_{dc}^2 = \left(V_{dc}^* + V_{dc}\right)^2 - V_{dc}^{*2} \approx 2V_{dc}^* V_{dc} = kV_{dc} \qquad (3.23)$$

Therefore the energy model can be implemented to analysis the voltage model.

In Fig. 3-8, the total energy stored on a capacitor is $CV_{dc}^2/2$, and the integration of power difference between DAB and inverter is the energy variation on the dc link capacitor, which causes the voltage fluctuations. Power output of DAB and inverter can be calculated by multiplying power references (P_{DAB}^* , P_{INV}^*) with the transfer function of power control ($G_{DAB}(s)$, $G_{INV}(s)$).

Based on Fig. 3-8, the voltage controller can be designed. The uncompensated open loop transfer function for the voltage control loop is:

$$G(s) = \frac{2G_{DAB}(s)}{Cs} \qquad (3.24)$$

As shown in Fig. 3-8, the power reference (P^*) is an interference item to the dc link voltage control.
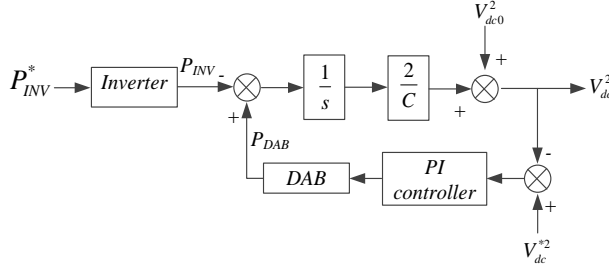
Fig. 3-9 Small signal blocks of the interference effect on the DC voltage
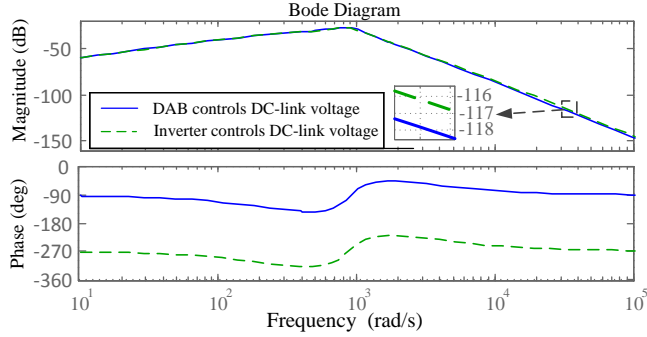
Fig. 3-10 Bode plots of the DC-link voltage fluctuations in cascaded system

Fig. 3-9 shows the interference model, and it is actually the same as Fig. 3-8, but it is from the view of interference. As shown, the DAB control loop is feed-back loop, while the inverter is a forward path in the dc-link voltage control.

$$G_1(s) = \frac{dc-link\ voltage}{Power\ reference} = \frac{-\dfrac{2}{Cs}G_{INV}(s)}{1+G_{DAB}(s)G_{PI}(s)\dfrac{2}{Cs}} \tag{3.25}$$

Equation (3.25) is the transfer function of interference, from the input of transmitted power reference to the output of dc-link voltage, in which $G_{PI}(s)$ represents the transfer function of the PI controller. The bode plots of the interference is shown in Fig. 3-10. DAB and inverter might exchange their responsibility, that is DAB controlling the power flow and inverter controlling the dc-link voltage, and the control block diagram can be obtained by exchanging the position of DAB and inverter in Fig. 3-9. The corresponding bode plot of the interference is also shown in Fig. 3-10. As shown in Fig. 3-10, for the blue curves, DAB maintaining dc-link voltage. In high frequency range, the amplitude gain of interference is smaller than

that when inverter controlling the dc-link voltage, meaning that the power reference variations caused interference can be damped more effectively.

By comparing Fig. 3-3 and Fig. 3-6, it can be observed that control bandwidth of DAB is wider than inverter, so when the dc-link voltage is controlled by DAB, the equivalent feed-back loop in Fig. 3-9 will be faster, therefore the variation of

inverter power output is tracked more quickly, which helps reduce the fluctuations on the dc-link voltage.

3.1.5. ANALYSIS OF FEED FORWARD CONTROL

The PI voltage controller maintains dc link voltage based on the offset from the nominal value, therefore dynamic transient fluctuations on the dc link voltage still exist. Therefore a feed forward solution is usually implemented to improve the performance of the cascaded converter.

Fig. 3-11 is the dc link voltage control diagram of the feed forward control, and the interference transfer function from the power reference P^* is shown in (3.26).
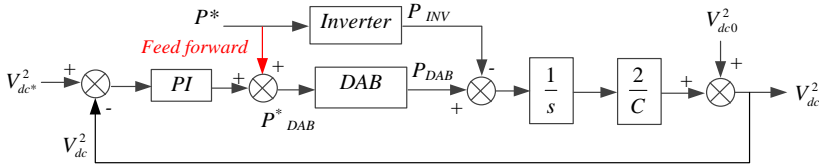
Fig. 3-11 Control block of the cascaded system added with feed forward.
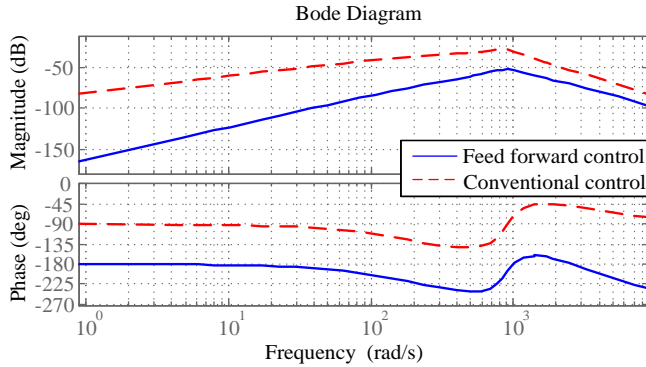
Fig. 3-12 The compared bode plots conventional control with feed forward control

$$G(s) = \frac{DC-link\,voltage}{Power\,Reference} = \frac{(G_{DAB}(s) - G_{INV}(s))\dfrac{2}{Cs}}{1 + G_{DAB}(s)G_{PI}(s)\dfrac{2}{Cs}} \qquad (3.26)$$

Fig. 3-12 depicts the interference bode plot with feed forward control, compared with conventional control. As shown, interference gain of the feed forward control is much smaller than the conventional control, meaning that under same power reference variations, the feed forward control can maintain the dc-link voltage with smaller fluctuations.

3.2. DC LINK VOLTAGE AND ACTIVE POWER COORDINATIVE CONTROL FOR CASCADED CONVERTER

Conventional control methods only use one sub converter to control the dc link voltage. For instance, the DAB converter controls the dc-link voltage, and then the inverter current will be interference for the dc link voltage control. Feed-forward control shares the current reference with DAB and inverter, and it can improve the dynamic performance of the cascaded converter, but when the power reference stays the same, under dynamics such as voltage sag or flickers, the responsibility of the dc-link voltage maintenance and power regulation are still individually assigned. Its control scheme is not symmetric, so still the cooperation of sub-converters needs to be improved. This chapter proposed a coordinative control for the cascaded interface converter.

3.2.1. PROPOSED CONTROL SCHEME

Fig. 3-13 shows the proposed control scheme. As shown, DAB and inverter equally share the responsibilities of dc link voltage control and power control. Power references for the DAB (P_{DAB}^*) and inverter (P_{INV}^*) are generated by the tasks sharing block. DAB power reference (P_{DAB}^*) is the sum of the power reference P^* with the output of the dc link voltage controller. Inverter power reference (P_{INV}^*) is that P^* subtracts the output of dc-link voltage controller.

As the interface converter of dc active distribution network, when the power flows from DAB to inverter, meaning that the dc active distribution network outputs energy to the grid DAB and inverter regulate the dc link voltage by their own power output, but they work in opposite way, because DAB locates the upstream and inverter sits on downstream of the dc link, respectively. For instance, to increase the dc-link voltage, DAB needs to increase power output and the inverter needs to decrease power output. So the output of voltage controller is positively fed to the DAB and negatively fed to inverter.
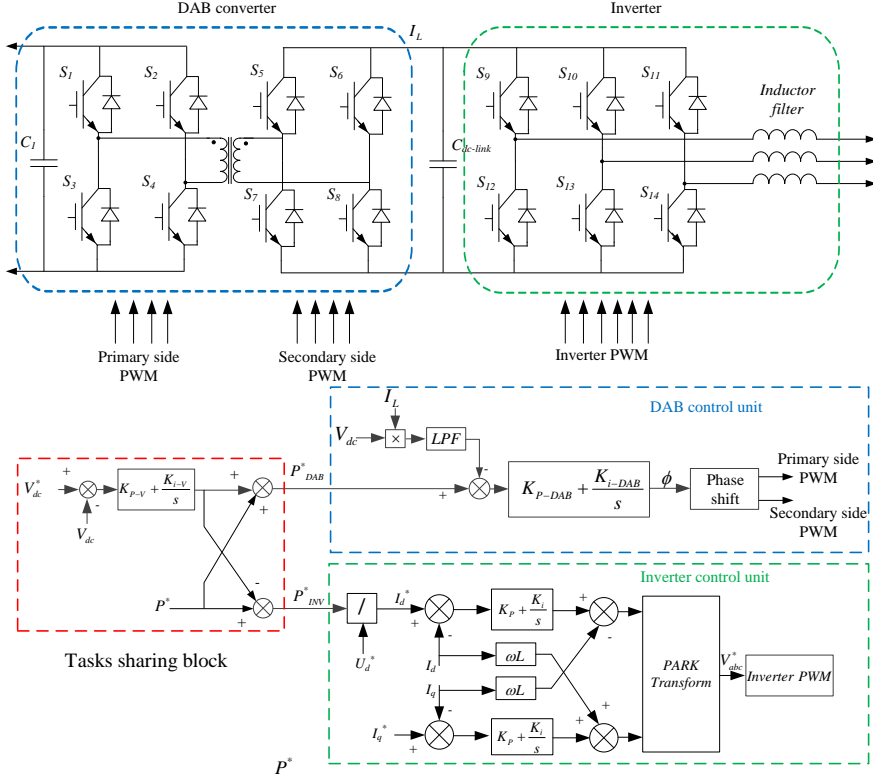
Fig. 3-13 The scheme of the proposed coordinative control

In the proposed control, every single sub converter has its own dc link voltage controller. If the voltage controllers are designed differently, the two sub converter will compete with each other, so the proposed control uses the same voltage controller for DAB and inverter, which can be recognized as the synchronization in dc link connection. With the same controller, DAB and inverter cooperatively control the dc-link voltage, and act in the same direction. For instance, to reduce the dc-link voltage, the DAB converter will reduce power output, and inverter needs to increase power output, so the inverter helps the DAB control the DC link voltage, not compete, and this can avoid the cross regulation issue.

For the DAB converter, conventional voltage control is replaced by the power control, I_L is the output current of DAB, which is determined by the load. The PI controller also is divided by reference value of current output, and then DAB voltage control block diagram can be modified as power control scheme.

3.2.2. DC-LINK VOLTAGE ANALYSIS

Fig. 3-14 is the interference block diagram of the proposed control method, from the input of power reference to the output of the dc-link voltage. It is also shown in energy perspective, so V_{dc}^2 is used. Compared with conventional control in Fig. 3-9, it can be observed that loop 2 and the power reference feed-forward loop are added in the proposed control. The interference transfer function is:

$$G(s) = \frac{V_{dc}(s)}{P^*(s)} = \frac{(G_{DAB}(s) - G_{INV}(s))\dfrac{2}{Cs}}{1 + G_{DAB}(s)G_{PI}(s)\dfrac{2}{Cs} + G_{INV}(s)G_{PI}(s)\dfrac{2}{Cs}} \quad (3.27)$$

So compared with interference transfer function in feed forward control (3.26), in (3.27), the item of $2G_{INV}(s)G_{PI}(s)/Cs$ is added to the dominator, indicating the proposed control introduces the inverter feed-back loop to the dc link voltage control, so the dominator is larger than the one in feed-forward control, indicating the gain of dc link voltage fluctuation is smaller than in feed forward control.

Fig. 3-15 is the bode plot of interference transfer function, including the proposed control and the feed-forward control, and the controller parameters are shared between the two control methods. As illustrated, with the proposed control method, the magnitude is always smaller than feed forward control, which is almost 6.9dB less, meaning that under the same power reference variation, the dc-link voltage fluctuation of the proposed control is almost a half of the feed forward control, much smaller than conventional control.
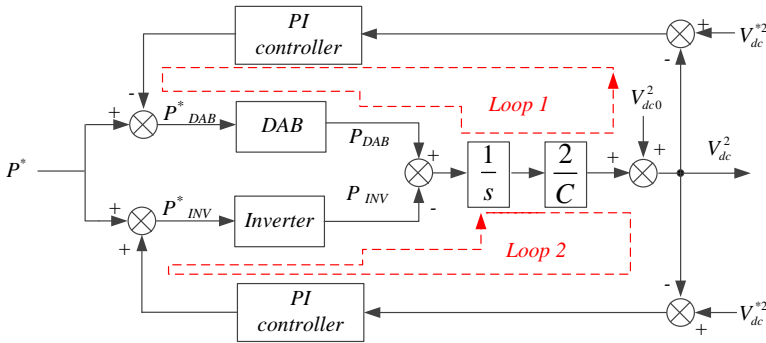
Fig. 3-14 The block diagram of the proposed coordinative control
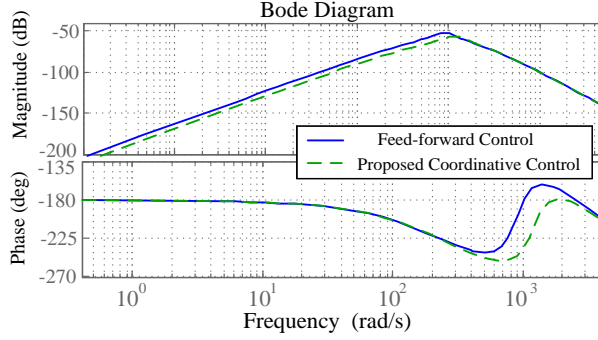
Fig. 3-15 The Compared interference bode plots of the coordinative control with feed forward control

(a) The proposed control

(b) Feed-forward control
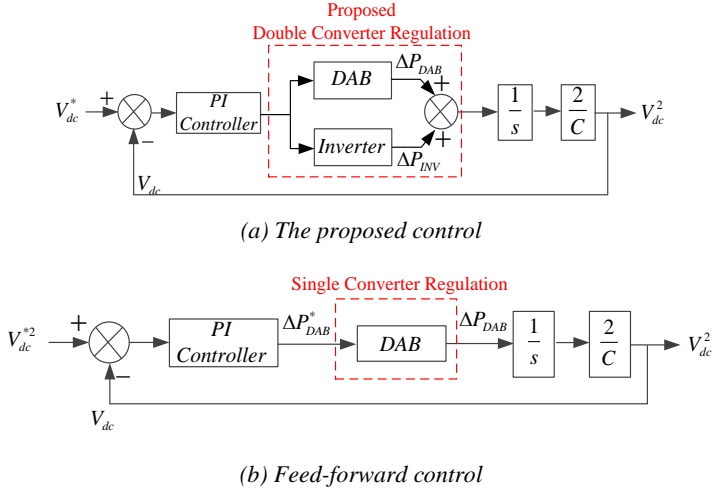
Fig. 3-16 DC link votlage control block diagram

With two sub converters controlling the dc-link voltage, the dc-link voltage control block diagram is shown in Fig. 3-16, including the comparison of feed forward control. As shown in Fig. 3-16 (a), in the proposed control, both DAB and inverter are the plant transfer function; while in Fig. 3-16 (b), for feed forward control and conventional control, only one sub converter is used to control the dc-link voltage, so the proposed control method has a larger gain than the conventional single converter regulation. In the proposed control, the gain parameter is adjustable, and then the single converter may have a smaller gain to achieve the same performance with conventional control.
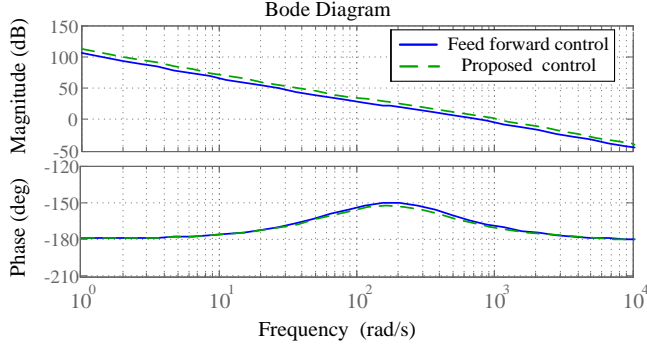
Fig. 3-17 Bode plots of the feed forward control and the proposed control

Fig. 3-17 is the bode plot of dc-link voltage control loop. As shown, the proposed control enlarges the control bandwidth than feed forward control. For a reasonable comparison between different control methods, the voltage controller parameters varied from 0.1 pu to 10 pu of the selected value. Correspondingly, the voltage controller here is the PI controller with the responsibility of regulating the dc link voltage, which is involved in Fig. 3-9, Fig. 3-11, Fig. 3-17 and Fig. 3-18. PI controller is expressed as:

$$G_{PI}(s) = K \frac{\tau s + 1}{\tau s} \tag{3.28}$$

Here K is the gain of the controller, τ is the integral time. K directly affects the dc-link voltage performance. With the increment of K, the dc-link voltage control loop will be faster, and under the decrement of K, it will become slower, but the increment of K will reduce the system stability margin. Therefore the dc link voltage interference in feed-forward control and the proposed control can be compared in the damping performance on dc-link voltage fluctuations.

Fig. 3-18 is the interference bode plots with the variation of voltage controller gain-K, including the condition of 10 times enlarged and one tenth shrunk. As depicted, when K is 10 times enlarged, dc-link voltage interference gains, caused by power reference, are decreased by 15dB compared with Fig. 3-17, meaning that dc link voltage fluctuations will be suppressed more deeply. When K decreases to 0.1 pu, interference gains increase by 7.3dB, indicating the dc-link voltage fluctuations becomes larger. In any cases that the voltage controller changes, the interference gain in the proposed control is always 6dB smaller than feed forward control. Therefore conclusion can be drawn that the proposed control can damps the dc link voltage fluctuations more effectively than the feed forward control.
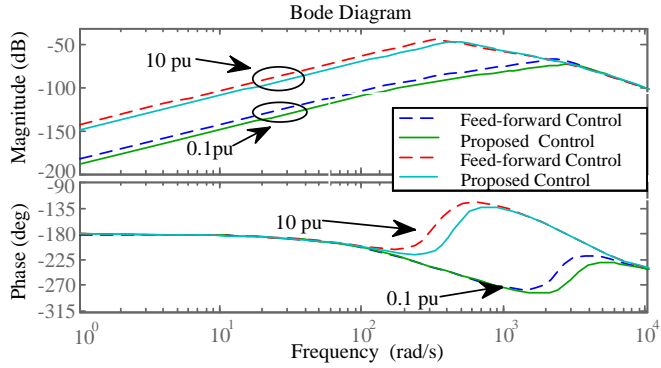
Fig. 3-18 The interference bode plots of the proposed control with feed forward control
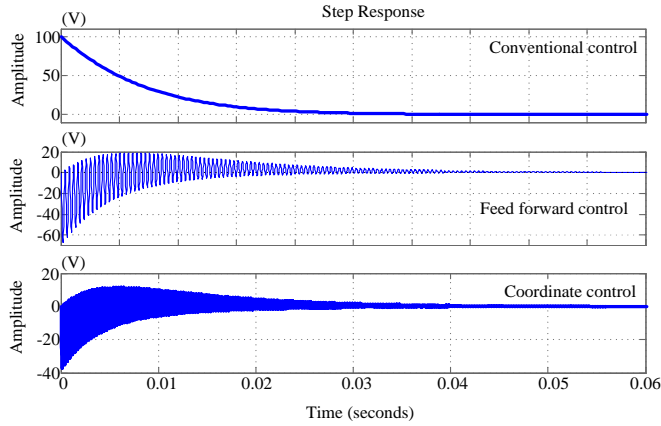
Fig. 3-19 The Compared -10kW Step response of the voltage fluctuation

It can be summarized that: if the inner power (current) loop has a high gain, converter will be faster, and the faster converter can damp the dc link voltage fluctuations more effectively; within the stability area, for the voltage controller, if the voltage controller gain is larger, the dc link voltage fluctuations caused by the power reference will be damped more effectively.

The voltage step response under the -10kW power reference variation (from 5kW to -5kW) is shown in Fig. 3-19, which is based on the model in Fig. 3-9,Fig. 3-11 and Fig. 3-14, the parameters in the Appendix. The 10 kW response figure will be symmetric with the zero axis with Fig. 3-19.
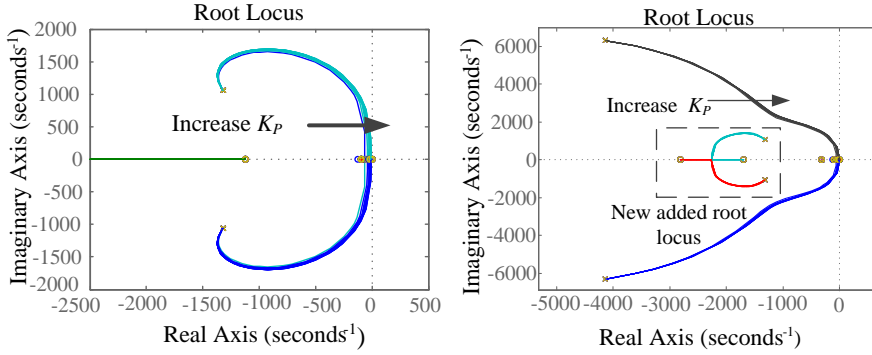
Fig. 3-20 The Root locus of conventional control   Fig. 3-21 Root locus of proposed control

So under the power reference stepping between -5kW and 5kW repeatedly, the voltage fluctuation is 198V in conventional control, 136V in feed forward control and 74V in the proposed control. Afterwards these data will be compared with simulation results.

System stability can be analyzed by the root locus, which can be obtained by the model of (3.25)(3.26). In the root locus, the proportional parameter K_P in the PI controller increases from 40 to 400. Fig. 3-20 and Fig. 3-21are respectively the root locus of conventional control and the proposed control. As shown, the roots moves towards the imaginary axis with the increasing of K_P,   meaning that the bigger the proportional value is, the less stable the system behaves.

As in (3.25) and (3.26), the characteristic equation of the feed forward control is the same as the conventional control, so the stability in feed forward control is the same as conventional control. By comparing, Fig. 3-20 and Fig. 3-21, it can be observed that two pairs of zero-poles are added in the proposed control, but they not only locate on the left side of the plane, but also further away from the imaginary axis, so the system is stable with the proposed control method.

3.3. SIMULATION AND EXPERIMENT

3.3.1. SIMULATION EVALUATION

Simulation evaluation is performed with the software of PLECS. Simulation parameters are shown in the appendix. Conventional control and feed forward control methods are also evaluated by the simulations to compare with the proposed control. The same voltage controllers and inner loop controllers are used for all the control strategies.
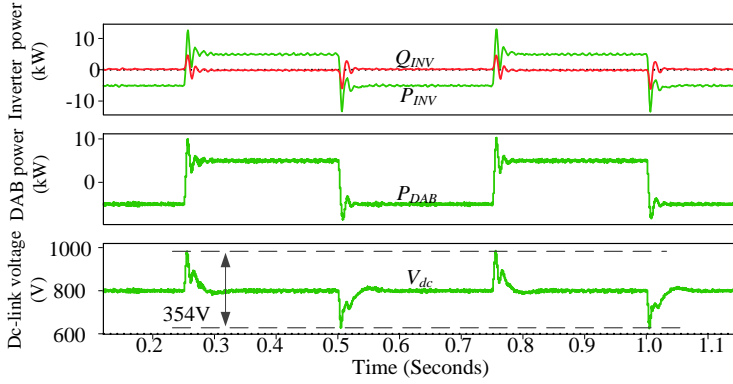
Fig. 3-22 DAB controls power output and inverter maintains DC voltage
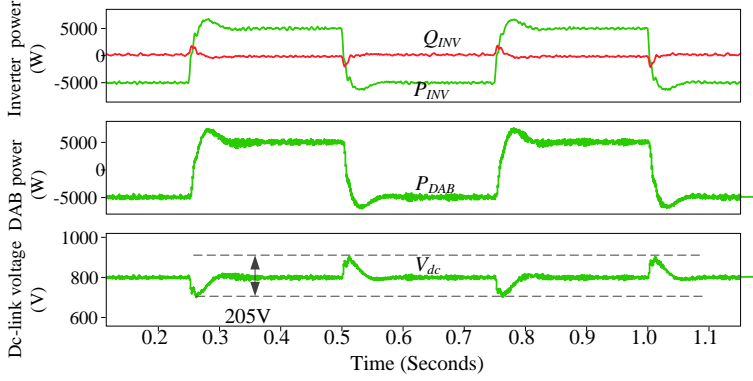
Fig. 3-23 DAB maintains DC voltage and inverter control power output

Fig. 3-22 and Fig. 3-23 show the simulation results of conventional control, with exchanging the responsibilities of dc link voltage control and power control between DAB and inverter. In Fig. 3-22, DAB controls power flow and inverter regulates dc link voltage, while in Fig. 3-23, inverter controls the power flow and DAB controls the dc link voltage. The simulation scenario is the power reference stepping between +5kW and -5kW periodically.

As shown, in Fig. 3-22 the dc link voltage fluctuates with the magnitude of 354V from peak to peak, and needs 0.055s to recover stable at nominal value. While in Fig. 3-23, under the same circumstance, the peak value of dc link voltage fluctuation is 205V, smaller than in Fig. 3-22. The recovering time of dc link voltage is 0.038s, also faster than the 0.055s in Fig. 3-22.

DAB control band width is wider than inverter, meaning that DAB converter is faster than inverter, so if inverter regulates dc-link voltage, its slower dynamics can
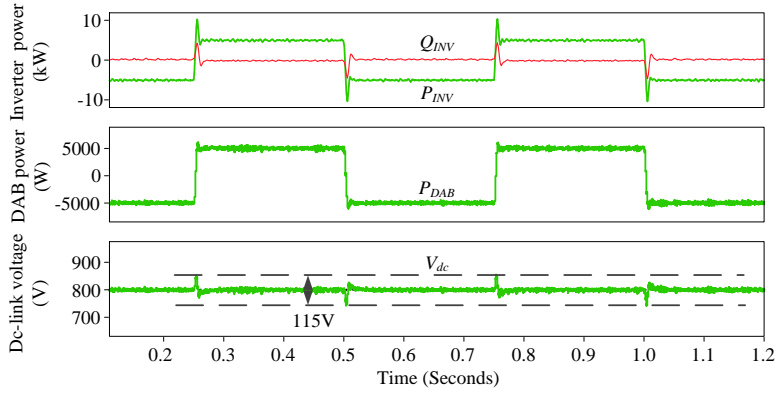
Fig. 3-24 Active power and DC voltage coordinative control for the cascaded system

not follow the rapid changing of DAB power flow timely, therefore the dc link voltage fluctuations are enlarged.

Fig. 3-24 shows the simulation wave forms of the proposed control method. Under the same conditions, the magnitude of dc link voltage fluctuation reduces to 115V, and significantly improvement can be verified by comparing with Fig. 3-22 and Fig. 3-23. The adjusting time of dc link voltage is 0.012s, much shorter than conventional control in Fig. 3-23.

So conclusion can be drawn that when the responsibilities of dc link voltage control and power control are shared between DAB and inverter, power references variations caused dc link voltage fluctuations can be better suppressed.

In Fig. 3-25, the proposed control is compared with feed forward control. The cascaded system is running with feed forward control before the vertical dash line, and after the dash line the proposed control is activated.

As in Fig. 3-25 (a), under the same power reference variations, in the feed forward control, dc link voltage fluctuations are 132V. In the proposed control method, fluctuations reduce to 115V, behaving with improved steady state performance.

In Fig. 3-25 (b), a sinusoidal power reference is introduced with the frequency of 16Hz and amplitude of 5000W. As shown, in the feed-forward control, amplitude of voltage fluctuation is 60V; it is reduced to 38V in the proposed control. The power output of DAB and inverter have phase and amplitude error in feed-forward control, but these errors are much less in the proposed control.
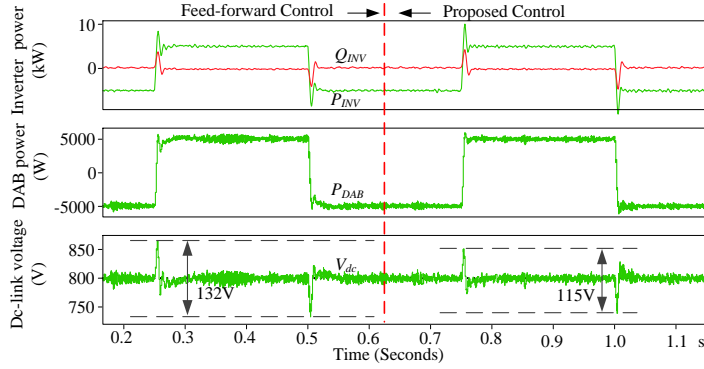
(a)   Simulation results in the square reference wave
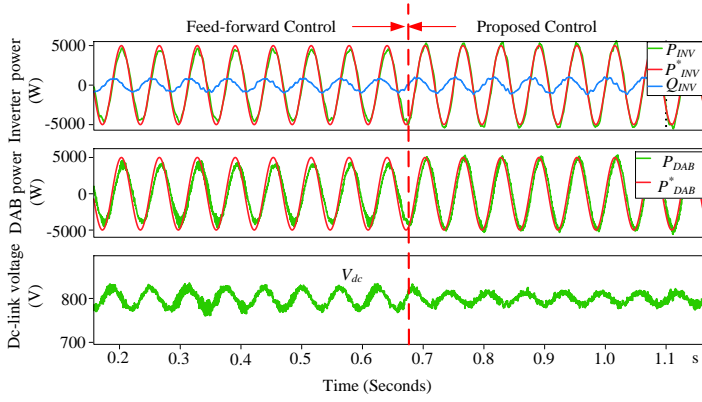
(b)   Simulation results in the sinusoidal reference wave
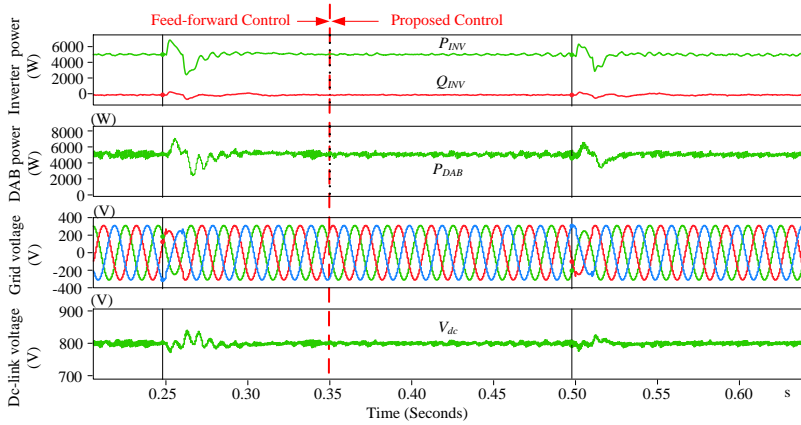
(c)   Simulation results in grid voltage sag
Fig. 3-25 Feed forward control with active power and DC voltage coordinative
control

In Fig. 3-25 (c), 0.2 pu voltage sags happen in the grid voltage at the time of 0.25s and 0.5s. The simulation results show that in feed forward control, the voltage fluctuation is 65V; in the proposed control, it reduces 49V.

So the simulations indicate that the proposed control can damp the power reference caused interference more effectively than feed-forward control method, and at the same time it improves the performance of the dc link voltage and the power flow regulation.

Table 3-1 shows the comparison of simulation with the modeling step responses in Fig. 3-19. As shown, the relevant of dc link voltage fluctuations are approximately similar, although small errors exist, which are caused by the parasitic parameter and modelling accuracy. So the simulation results can support the analysis.

Table 3-1

SIMULATION RESULTS AND MODELING STEP RESPONSE COMPARISON

Control method	Value	Simulation results
Conventional control	198V	205V
Feed forward control	136V	132V
Proposed coordinative control	74V	115V

3.3.2. EXPERIMENT VERIFICATIONS

The experiment setup is a scaled-down laboratory prototype. The topology is shown in Fig. 3-26. The parameters are shown in Appendix. The inverter is connected with grid through a transformer, and the dc active distributed network is constituted by a dc voltage source with local load. The power waves are captured from the DA output block DS2101 of dSPACE 1006. In the experiment, the power reference of
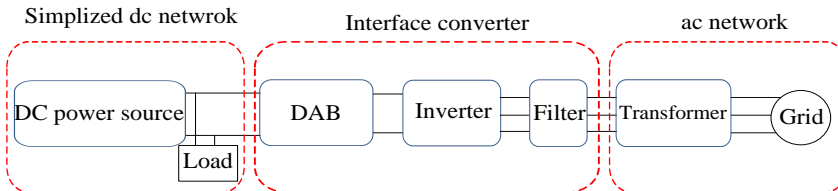
Fig. 3-26 Experiment setup
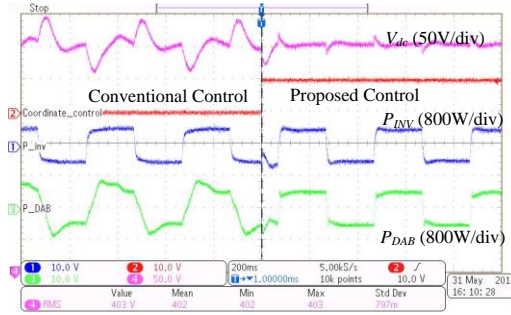
(a) Switching from conventional control to proposed control
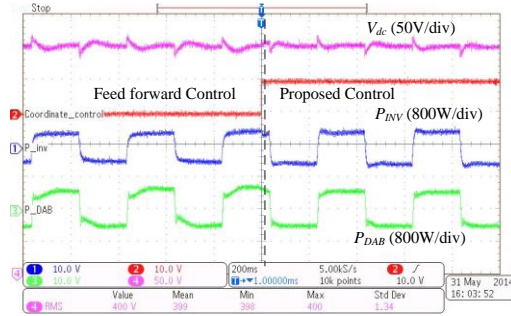
(b) Switching from feed forward control to proposed control

Fig. 3-27 Experiment results of the power output and DC-link voltage

the interface converter is a square periodic wave, changing between 400 W and -400 W, with the frequency of 2.5Hz. Conventional control employs DAB to maintain DC voltage, and inverter to control power output. The feed-forward control introduces a reference feed forward signal to DAB.

Fig. 3-27 (a) is the experiment results of inverter power output and dc link voltage, in which the control method transfers from conventional control to the proposed control at the time of dashed line. In conventional control, when the power output step changes between 400W and -400W, the dc link voltage fluctuation is 84V, and recovering time is 0.115s. In the proposed control, under the same conditions, the dc link voltage fluctuation is 28V and needs 0.04s to be stable. Inverter dynamic performance of the proposed control is also much better than conventional control. Fig. 3-27 (b) compares inverter detail waveforms between feed forward control and the proposed control. Feed forward control is activated before 0.1 s, and dc link voltage fluctuations are 40V, and recovering time is 0.08s. The proposed control is adopted after 0.1s, and then dc link voltage fluctuations reduce to 30V, and
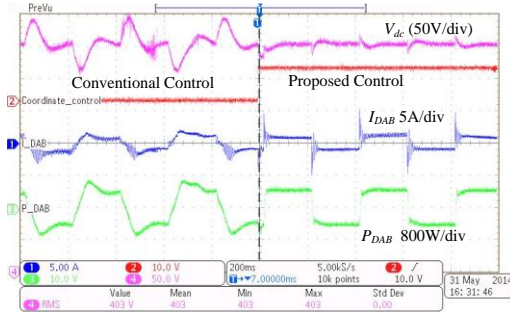
(a)   Switching from conventional control to the proposed control
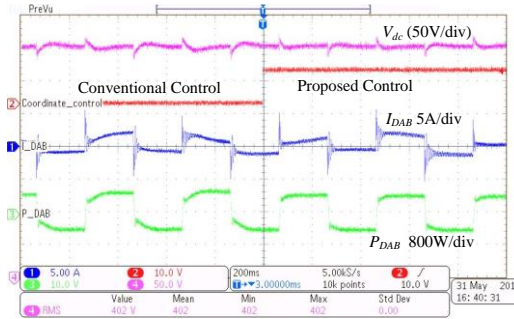
(b)Switching from feed forward control to the proposed control

Fig. 3-28 Experiment results of DAB output current, active power and dc link voltage

adjusting time is 0.04s. The proposed control can maintain dc link voltage with smaller voltage fluctuations and faster recovering speed. So both steady state and dynamic performances of inverter are improved.

Fig. 3-28 (a) shows the detail waveforms of the DAB converter under the transition from conventional control to the proposed one, including the output voltage, active power, as well as the current. As illustrated, after switching from conventional control to the proposed coordinative control, both the power and current output become faster than conventional control. Fig. 3-28 (b) shows the detail waveforms of DAB converter switching from feed forward control to the proposed control. As shown, dynamic performance of DAB power and current output become faster in the proposed control, and because in the proposed control, the dc link voltage more stable so the power between DAB and inverter becomes more decoupled.
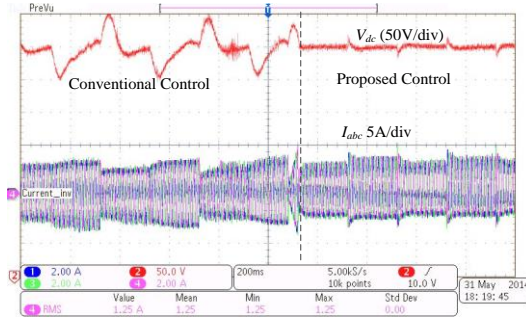
(a) Switching from conventional control to the proposed control
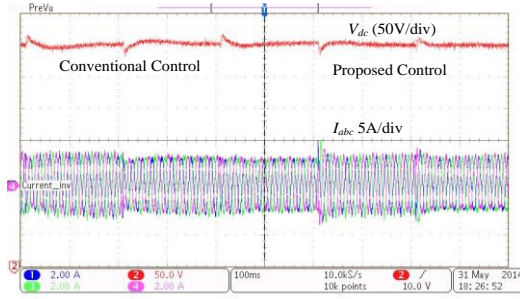
(b)Switching from feed forward control to the proposed control

Fig. 3-29 Experiment results of inverter output current and DC-link voltage

Fig. 3-29 shows the inverter detail waveforms, including three phase current, and the dc side voltage, which is the dc link voltage.

As shown in Fig. 3-29 (a), in the proposed control, inverter maintains the dc link voltage at the instant time when power reference changes, so dc link voltage is more stable, therefore the dynamic performance of current is much faster than in conventional control.

Fig. 3-29 (b) compares the feed forward control with the proposed control. The proposed control presents faster dynamic response in inverter output current, because of the more stable dc link voltage, created by the sharing control of dc link voltage.
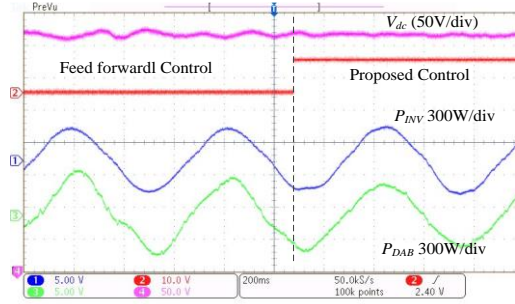
(a)With sinusoidal power reference wave
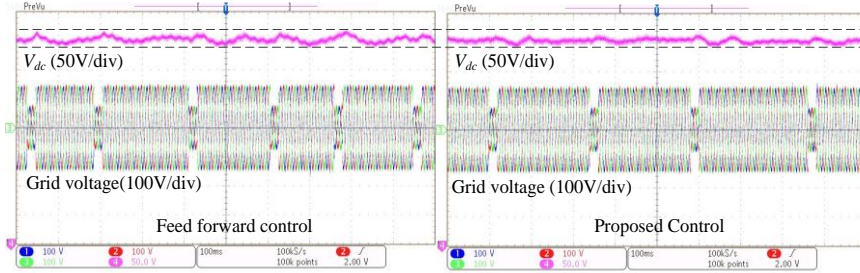
(b) Feed-forward control and the proposed control under voltage sag

Fig. 3-30 Experiment results of feed forward control and the proposed control

Fig. 3-30 shows experiment comparison between the proposed control and the feed forward control, under the sinusoidal power reference at 1.8 Hz and 300 W.

Fig. 3-30 (a) indicates that in the feed forward control, the dc link voltage has certain oscillation. Under the same condition, the proposed control can maintain dc link voltage more stable, and the power output more sinusoidal. So in feed forward control, power output of the DAB and inverter can not match each other satisfactorily. In the proposed control, good agreement of power output can be achieved between DAB and inverter. So the proposed control strategy can maintain dc link voltage more stable with better stability.

Fig. 3-30 (b) shows the experiment results under grid voltage sag, including the proposed control and feed forward control. The grid voltage sags happen with 0.5 p.u. and last for 0.02 s. The results show that in the proposed control, the dc link voltage is more stable than that in the feed forward control. The grid voltage is emulated by a programmable AC power source and it has less inductance than the transformer, which means damping in the AC net becomes much smaller, so the dc-

link voltage behaves with bigger oscillations than that with transformer, but in the proposed control, with the exactly same condition, the dc link voltage is more stable.

Based on the experiment results, it can be seen that during the transitions of power reference variations, the proposed control maintain the dc link voltage by varying power output of the sub converter, the effect of this phenomenon needs to be evaluated. The stored energy (E) on dc-link capacitor can be calculated by the voltage and its capacitance, as:

$$E = \frac{1}{2}CV^2 \qquad\qquad (3.29)$$

In the experiment C =300uF, $V = 400V$; so $E = 24W$, which is a small value compared with power reference. On the other side, a more stable dc link voltage can improve the dynamic behavior of the cascaded converter system. So the power assigned to maintain dc-link voltage will not slow the power output of the cascaded converter, but can accelerate the power response to the reference variations.

3.4. CONCLUSION

This chapter firstly showed the conventional control methods for the cascaded interface converter between dc active distribution network and the grid, and then proposed a coordinated control methods. The proposed control method employs inverter and DAB to share the control of dc link voltage and power flow, which manages to present a more stable dc-link voltage with improved dynamic performance.

The derived system model shows that the proposed control method can reduce the dc link voltage fluctuations, and provide more effectively damping with better stability. Then the volume of dc link capacitors can be reduced, so is the stress on the switching devices. Then the responsibility can be evenly shared between the cascaded converters. In the proposed control, to maintain the same voltage performance, the dc link voltage controller can also be smaller than conventional control.

CHAPTER 4. POWER FLOW EFFECT AND COMPENSATION CONTROL FOR CASCADED CONVERTER

Cascaded converter refers that two converters are directly connected in series. Based on the power flow, the upstream converter is the source converter, and the downstream converter is the load converter. The relation between power supply of source converter and demand of load converter can be analyzed by the impedance interaction, which involves the output impedance of the source converter and the input impedance of load converter. Without proper design, the impedance interaction will introduce instability to the cascaded system. In addition, between different power flow directions, forward and reverse, impedance interactions are prominently different in terms of dynamics and stability, even if the cascaded converter control remains unchanged.

This chapter will firstly show the impedance based stability assessment, and then analysis the impedance behavior of the selected DAB converter and inverter. Afterwards the bidirectional stability of the interface converter is assessed and an important guide line is formulated for the cascaded bidirectional interface converter. At last, an impedance control method is proposed, which can make the cascaded converter more bidirectional stable than before.

4.1. IMPEDANCE BASED STABILITY ASSESSMENT

The input impedance refers to the equivalent impedance viewed from the power source [63], and the output impedance is the impedance viewed by its output terminals [64]. The output and input impedance for converter can be obtained as:

$$Z_{out} = -\frac{\Delta V_o}{\Delta I_o} \tag{4.1}$$

$$Z_{in} = \frac{\Delta V_{in}}{\Delta I_{in}} \tag{4.2}$$

where ΔV_o and ΔI_o are respectively the output voltage and current variations, ΔV_{in} and ΔI_{in} are the input voltage and input current variations.
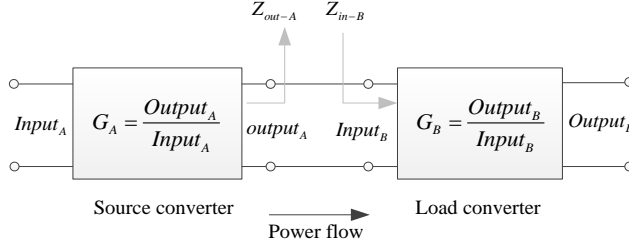
Fig. 4-1 Cascaded connection with source and load sub system
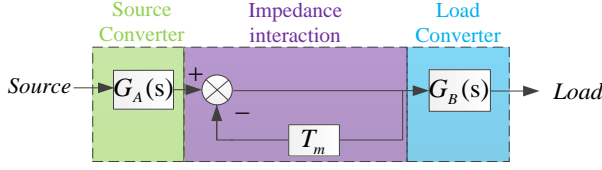
Fig. 4-2 Block diagram of cascaded system

In Fig. 4-1, two converters are connected in series. $G_A(s)$ and $G_B(s)$ are the individual transfer function of source converter and load converter, respectively.

Fig. 4-2 shows the block diagram of the cascaded converter, in the view of impedance. The total transfer function from the input of source converter to the output of load converter can be expressed as [65]:

$$G_{AB}(s) = \frac{output_B}{Input_A} = G_A(s)G_B(s)\frac{1}{1+T_m} \tag{4.3}$$

$G_{AB}(s)$ is the total transfer function, and it constitutes not only the individual transfer functions $G_A(s)$ $G_B(s)$, but also the impedance interaction term ($\frac{1}{1+T_m}$). So the stability of cascaded system not only relies on the well designing of individual converter, but also the impedance interaction. T_m is the open loop transfer function of the impedance interaction, and it is also recognized as the minor loop gain. Based on the type of source converter, voltage source or current source, T_m has different manifestations [66], which are expressed in (4.4). In (4.4), Z_{out-A} is the output impedance of source converter A, and Z_{in-B} is the input impedance of load converter B.

$$\begin{cases} T_m = \dfrac{Z_{out-A}}{Z_{in-B}} \text{ Voltage source converter} \\[3mm] T_m = \dfrac{Z_{in-B}}{Z_{out-A}} \text{ Current source converter} \end{cases} \qquad (4.4)$$

So for the minor loop gain: if the source converter is voltage source converter, then the numerator has to be the internal impedance of the source converter, and the denominator has to be the input impedance of the load sub system; when the source converter is current source converter, the dominator has to be the output impedance of the source converter, and the numerator has to be input impedance of the load converter.

In the year of 1979, Middlebrook firstly noticed the impedance interaction，and proposed the stability criterion, known as the Middlebrook criterion. He pointed that if the output impedance of source converter is much smaller than the load converter, the system stability can be guaranteed. As expected, the Middlebrook criterion has become the base for comparison with other developed criteria [67 68]. The impedance-based stability criterions have been used in more and more occasions [69].

Without proper design, the impedance interaction will give rise to stability degradation. This phenomenon can be explained by the interpretations that [70]-[71]: the interaction among the feedback loops between the interconnected converters. Typically, converters are regulated under various feedback loops, such as the voltage loop, current loop or the instantaneous power loop, but the common dc link voltage combines two individual feed-back loops together. For the constant power loads (CPL), they are under constant instantaneous power control, and they behave as negative impedance [72]. The negative impedance tends to destabilize the power system [73]-[74], because the negative impedance directly change the sign of impedance interaction loops, from negative to positive feed-back, which is unstable for the system.

4.2. IMPEDANCE INTERACTION IN UNIDIRECTIONAL POWER FLOW

In this part, the impedance interaction in conventional unidirectional power flow will be modelled and analyzed. DAB and inverter impedance modelling are as followings.

4.2.1. DAB OUTPUT IMPEDANCE IN VOLTAGE CONTROL
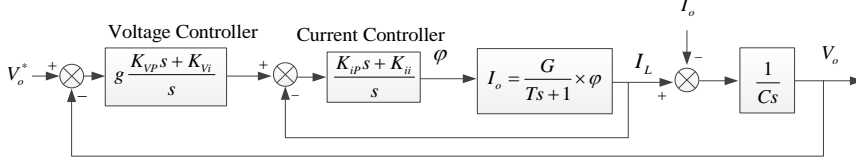
Fig. 4-3 Block diagram of DAB converter under voltage control

As described in chapter 3, conventionally DAB converter is voltage-controlled, and an inner current loop might be implemented for improve the dynamic performance. The responsibility of DAB is to maintain the dc link voltage constant. Then transfer function of DAB output impedance can be derived by firstly analyzing the inner current loop for controlling the average output current I_2 of the DAB converter.

DAB current can be controlled by varying the phase-shift φ as:

$$I_2 = \frac{V_{in}}{2k\pi^2 L_1 f} \varphi(\pi - \varphi) \tag{4.5}$$

where V_{in} and L_1 are respectively the input dc voltage and leakage inductance of the high frequency transformer. f and k are respectively representing switching frequency and turns ratio of the DAB converter.

Strictly, the current is nonlinear with the phase shift, but when confined to a narrow operating frequency, which is lower than the PWM switching frequency, the current can be linearized as:

$$I_2 = m\frac{KV_{in}}{2\pi^2 L_1 f} \varphi \tag{4.6}$$

Here m is the linearization coefficient, equal to the mean differential value in the same narrow range [75]. Besides the linearization, this equation also provides the mean value in each switching period, without including the dynamics. Therefore a low pass filter is implemented with the time constant T, which represents as the average period. I_2 is the average current in each PWM switching period, so T is related to this switching period. Then the inner loop current is expressed as:

$$I_2 = \frac{1}{Ts+1} m\frac{kV_{in}}{2\pi^2 L_1 f} \varphi = \frac{G}{Ts+1} \varphi \tag{4.7}$$

With the obtained "plant" model, the block diagram of DAB converter under voltage control can be shown as Fig. 4-3. V_o is the voltage output of DAB converter, I_2 is the DAB inside current output. Based on the diagram, the current control loop transfer function (G_{DAB-I}) is expressed as (4.8).

$$G_{DAB-I} = \frac{G\left(K_{iP}s + K_{ii}\right)}{Ts^2 + \left(1 + K_{iP}G\right)s + GK_{ii}} \tag{4.8}$$

where K_{iP} and K_{ii} are proportional and integral parameter in the current controller. Transfer function of the output voltage can then be expressed as:

$$V_o = \frac{g\left(K_{VP}s + K_{Vi}\right)G_{DAB-I}}{Cs^2 + g\left(K_{VP}s + K_{Vi}\right)G_{DAB-I}}V^* - \frac{s}{Cs^2 + g\left(K_{VP}s + K_{Vi}\right)G_{DAB-I}}I_{DAB} \tag{4.9}$$

where K_{VP} and K_{Vi} are the proportional and integral parameter in the voltage controller. g is used for the tuning of K_{VP} and K_{VP} simultaneously, used for following analysis. The output impedance DAB expressed as (4.10). Fig. 4-4 shows the bode plots of DAB output impedance.

$$Z_o = \frac{s}{Cs^2 + g\left(K_{VP}s + K_{Vi}\right)G_{DAB-I}} \tag{4.10}$$
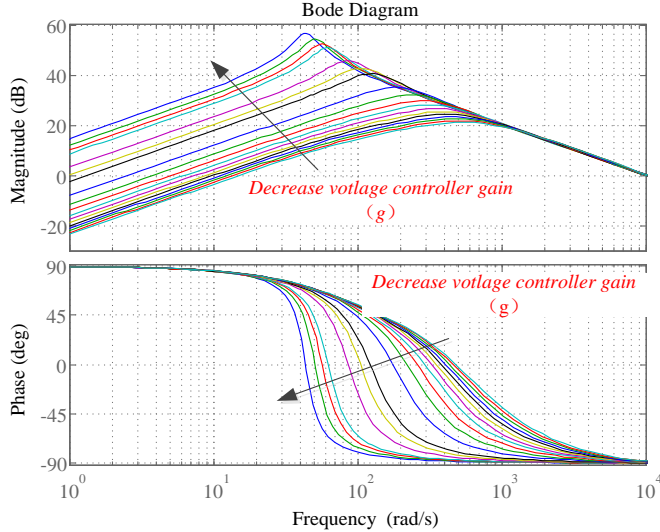
Fig. 4-4 Bode plots of DAB output impedance

In Fig. 4-4, g varies within certain range. As shown Z_o is inductive in low frequency range and capacitive in high frequency range. The magnitude of low-frequency output impedance is also increasing when the voltage controller gain (g) decreases. According to Middlebrook criterion, larger output impedance for the voltage source converter will make the system more unstable, because the bigger output impedance means slow and weak dynamics of the source converter.

4.2.2. INPUT IMPEDANCE OF CONSTANT POWER INVERTER

In conventional control, inverter controls the power flow as a constant power load and it is commonly implemented the control in synchronous d-q frame, rotating at the grid angular frequency ω. Fig. 4-5 shows the block diagram of grid connected inverter under constant power control. As shown, inverter active power and reactive power are respectively controlled through d- and q- channels. The state equations in d-q frame are commonly given as:

$$L\frac{dI_d}{dt} = D_d\frac{V_{dc}}{2} - V_{gd} + I_d r + \omega L I_q \tag{4.11}$$

$$L\frac{dI_q}{dt} = D_q\frac{V_{dc}}{2} - V_{gq} - I_q r - \omega L I_d \tag{4.12}$$

$I_d\ I_q$ are respectively the current on d and q axis; $D_d\ D_q$ represent the inverter duty ratios under d and q channel. The duty ratios are multiplied with half of dc-link voltage, then gives the inverter initial voltage on d and q axis. Here V_{dc} is divided by 2, because the maximum utilization is 0.5 in conventional two level inverter. V_{gd} V_{gq} are the grid voltage on d and q axis respectively. As shown in Fig. 4-5, the cross-coupling between the d- and q-paths can clearly be seen. This cross-coupling, especially at high frequency or large inductance, prevents the d- and q-paths from
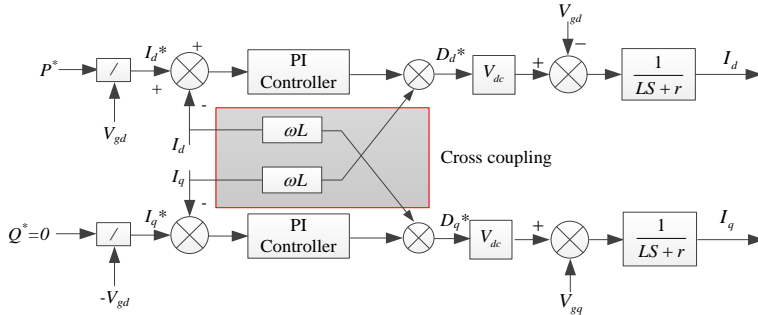
Fig. 4-5 System model of grid connected inverter under constant power control
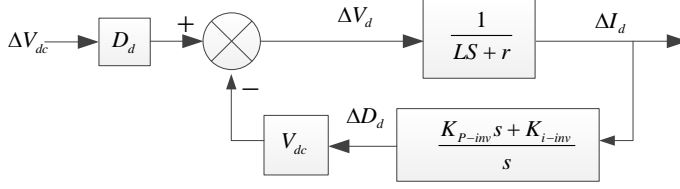
Fig. 4-6 Small signal block diagram from dc link voltage to d-axis current

being analyzed independently. Decoupling may therefore be necessary [76, 77, 78, 79], where the simplest solution is to omit the cross item in the grey block in Fig. 4-5. Actually, the d-axis is aligned with stiff grid voltage, so $V_{gq} = 0$ and $\Delta V_{gd} = 0$. Then power balance between inverter ac and dc side can be expressed as:

$$P = V_{dc}I_{in} = \frac{3}{2}V_{gd}I_d \qquad (4.13)$$

Accordingly, small signal of power balance between dc and ac side is:

$$\Delta P = \frac{3}{2}\Delta I_d V_{gd} = \Delta V_{dc}I_{in} + \Delta I_{in}V_{dc} \qquad (4.14)$$

Around specific operation point, ΔI_d can be expressed through ΔV_{dc}, and the block diagram is shown in Fig. 4-6, which can be obtained from Fig. 4-5 and (4.11) (4.12). In Fig. 4-6, K_{P-inv} and K_{i-inv} are respectively the proportional and integral parameter of the PI controller in inverter current loop. The transfer function in Fig. 4-6 can be written as:

$$G_{V_{dc}-I_d}(s) = \frac{D_d s}{Ls^2 + (r + K_{P-inv})s + V_{dc}K_{i-inv}} \qquad (4.15)$$

Therefore the small signal power balance can be expressed as:

$$\Delta P = \frac{3}{2}\Delta V_{dc}V_{gd}G_{V_{dc}-I_d}(s) = \Delta V_{dc}I_{in} + \Delta I_{in}V_{dc} \qquad (4.16)$$

The inverter input impedance can be obtained by (4.16), and Fig. 4-7 shows the bode plot.

$$Z_{in} = \frac{\Delta V_{dc}}{\Delta I_{in}} = -\frac{V_{dc}}{I_{in} - 1.5V_{gd}G_{V_{dc}-I_d}(s)} \qquad (4.17)$$
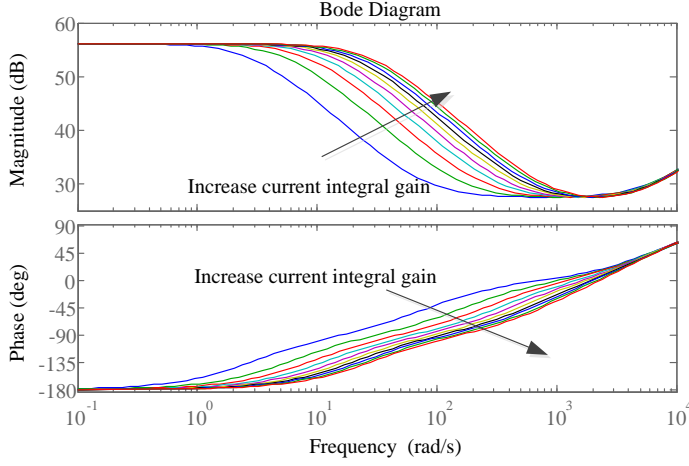
Fig. 4-7 Bode plots of inverter input impedance

As shown in Fig. 4-7, the integrator gain of the PI controller varies from 0.2 pu to 2 pu. As shown, for the constant power inverter, the input impedance is clearly negative in the low frequency range, because the phase is -180°. In the high frequency range, it goes to inductive, so the phase turns to 90°. The corner frequency increases with the increasing of current integral gain, then the negative impedance occupies wider band on the spectrum.

4.2.3. IMPEDANCE INTERACTION ANALYSIS.

Based on DAB output impedance in (4.10) and inverter input impedance in (4.16), the impedance interaction in conventional control can be obtained. DAB is operating in the voltage source mode, and inverter controls the power flow through current control, so the minor loop gain can be written as:

$$T_m = \frac{Z_o}{Z_{in}} \tag{4.18}$$

Z_o is DAB converter output impedance, and Z_{in} is the input impedance of inverter.. The impedance can be analysed through Nyquist plots. Fig. 4-8 shows the example of Nyquist plots. Phase margin (PM) in the Nyquist plot is defined as the angle measured from the negative real axis when the Nyquist curve crosses the unit circle [80]. Gain margin (GM) is the reciprocal value of the distance measured from the origin to the point, where the Nyquist curve crosses the negative real axis. With this understanding, Nyquist plots of the minor loop gain T_m are shown in Fig. 4-9. As shown, the *GM* read is 2.8, and *PM* is stable.
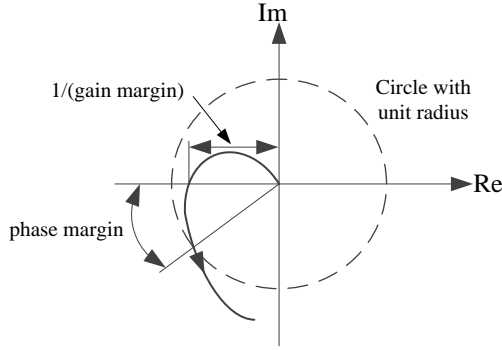
Fig. 4-8 Definitions of phase and gain margins in forward power flow.
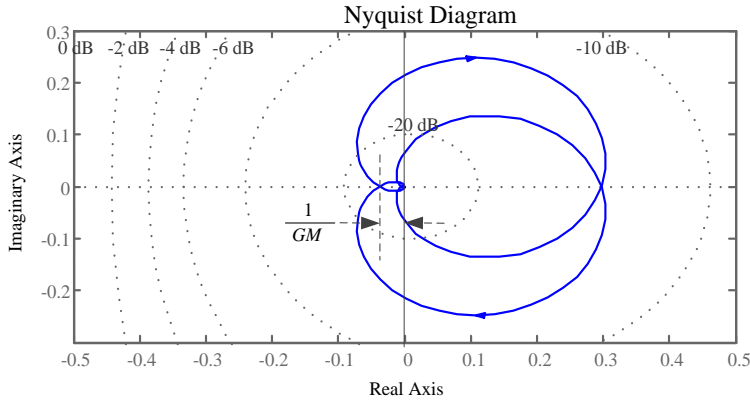
Fig. 4-9 Nyquist plot the minor loop gain T_m in conventional control

To see the stability difference more clearly, DAB output impedance (Z_o) is intentionally increased, and this is achieved by reducing the voltage controller gain in DAB, as illustrated in Fig. 4-4. Then the obtained Nyqusit plots are drawn as Fig. 4-10. In Fig. 4-10 , the gain of the DAB voltage controller (g) subsequently changes from 1pu to 0.03pu, the observations noted are an increase of $1/GM$ and a decrease of PM , and the system tends to cross the unstable point (-1,0). The cascaded converter is hence harder to stabilize. It can be saying that the stability of cascaded converter is gradually becoming unstable under the condition when the voltage source converter increasing output impedance. Comparatively, when the input impedance of load converter is reducing, it will be the same with this condition.
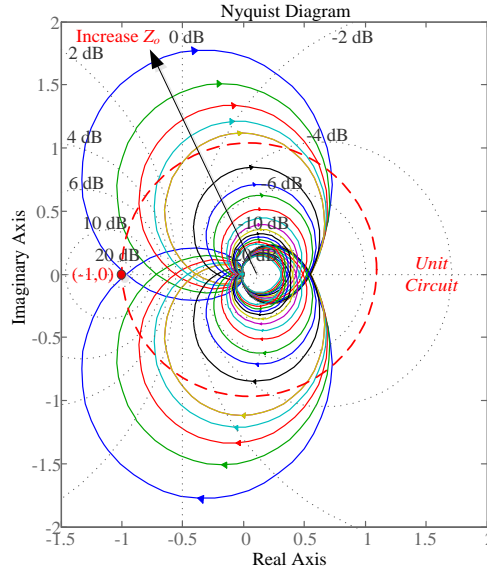
Fig. 4-10 Nyquist plots of impedance minor loop gain with DAB impedance variation

4.3. IMPEDANCE ANALYSIS IN REVERSED POWER FLOW

Under practical operations, for the interface converter between dc active distribution network and grid, it will face the bidirectional power flow. When the power flow reverses, the impedance interaction will also change. Therefore, an investigation is performed here for showing that forward and reverse impedance interactions are prominently different in terms of dynamics and stability, even the cascaded converter control remains unchanged.

When the power flow reverses, DAB converter becomes the load converter, and inverter turns to be the source converter. The following part will analysis the impedance interaction in reversed power flow, and the control scheme remains the same with forward power flow.

4.3.1. DAB AND INVERTER IMPEDANCE IN REVERSE POWER FLOW

When power flow reverses, DAB still controls the dc link voltage, DAB output current in forward power flow becomes the input current in opposite direction, the reference direction of DAB current loop also becomes opposite. Fig. 4-11 shows the block diagram of DAB converter in reversed power flow.
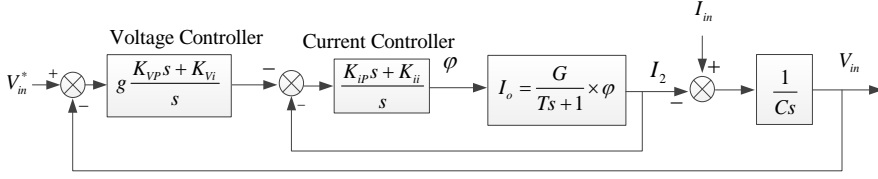
Fig. 4-11 Block diagram of DAB converter under voltage control in reversed power flow

Under the control of DAB converter, dc link voltage can be expressed as:

$$V_{in} = \frac{g\left(K_{VP}s + K_{Vi}\right)G_{DAB-I}(s)}{Cs^2 + g\left(K_{VP}s + K_{Vi}\right)G_{DAB-I}(s)}V_{in}^* + \frac{s}{Cs^2 + g\left(K_{VP}s + K_{Vi}\right)G_{DAB-I}(s)}I_{in} \text{ (4.19)}$$

Then the input impedance in reversed power flow can be obtained as:

$$Z_{in-R} = \frac{V_{in}}{I_{in}} = \frac{s}{Cs^2 + g\left(K_{VP}s + K_{Vi}\right)G_{DAB-I}(s)} \tag{4.20}$$

Compared with the output impedance (4.10) in forward power flow, DAB input impedance in reversed power is the same as the output impedance in forward power flow.

For the inverter, when power flow is reversed, it works in the rectifier mode, and previous input dc current becomes the output current. As for the reference direction, the output current is opposite with the previous input current:

The power balance between dc and ac side still exist and becomes:

$$P + \Delta P = V_{gd}(I_d + \Delta I_d) = (V_{dc} + \Delta V_{dc})(I_o + \Delta I_o) \tag{4.21}$$

The small signal power balance is obtained as:

$$\Delta P = \Delta I_d V_{gd} = \Delta V_{dc}I_o + \Delta I_o V_{dc} \tag{4.22}$$

The reference directions of d- and q-axis current also change. The rectifier output impedance can be obtained by:

$$Z_{o-R} = -\frac{\Delta V_{dc}}{\Delta I_o} = \frac{V_{dc}}{I_o - 1.5V_d G_{V_{dc}-I_d-R}} \tag{4.23}$$
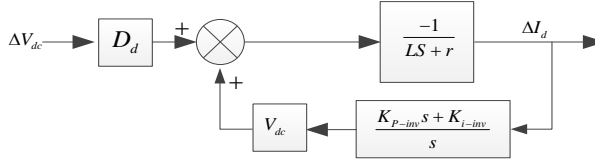
Fig. 4-12 Small signal block diagram from dc voltage to d-axis current
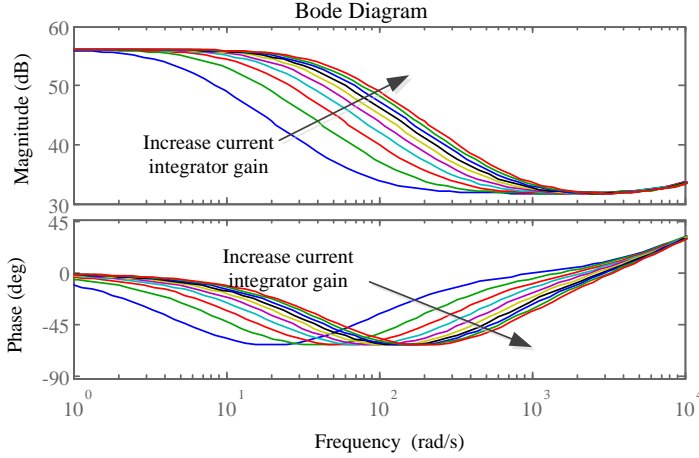
Fig. 4-13 Bode plots of inverter output impedance in rectifier mode with the variation of K_i from 0 to 2 pu

$G_{V_{dc}-I_d-R}$ is the transfer function from the input of dc link voltage to the output of d-axis current, and Fig. 4-12 shows the block diagram, which can be obtained by Fig. 4-5 and (4.11) and (4.12). $G_{V_{dc}-I_d-R}$ can be obtained, as:

$$G_{V_{dc}-I_d-R} = \frac{-D_d s}{Ls^2 + (r + V_{dc}K_{P-inv})s + V_{dc}K_{I-inv}} \tag{4.24}$$

Fig. 4-13 shows the output impedance of inverter in reverse power flow. The phase shift is generally 0 in the low frequency, therefore the output impedance is generally resistive in low frequency range, different from the input impedance in forward power flow, and the impedance goes to inductive in the high frequency range. With the increase of integrator gain, the resistive impedance covers wider frequency spectrum. So for the constant power converter, when transmit the same amount power, the output impedance in reversed power flow has an opposite sign to the input impedance in forward power flow. Then impedance minor loop gain can be obtained by (4.25). The Nyquist plots of the minor loop gain T_{m-R} are shown in Fig. 4-14, which is compared with the forward power flow.
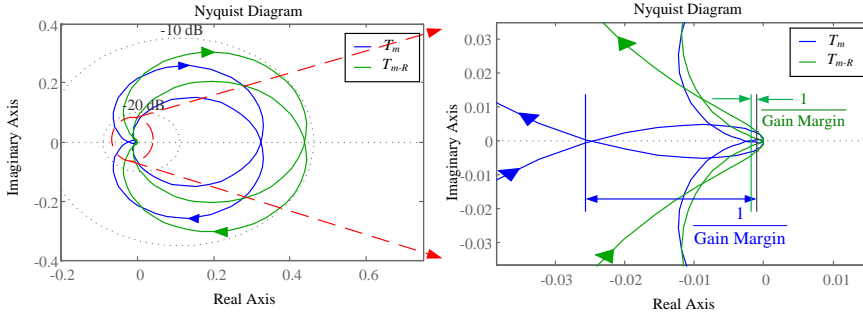
Fig. 4-14. Reversed power flow Nyquist plot
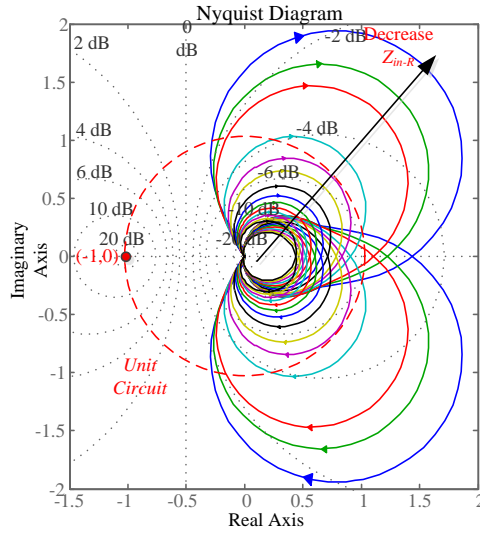
Fig. 4-15 Reversed power flow Nyquist plots of impedance minor loop gain with DAB impedance variation

$$T_{m-R} = \frac{Z_{in-R}}{Z_{o-R}} \tag{4.25}$$

In Fig. 4-14, it can be seen that the gain margin in the reversed power flow is much larger than that in conventional control, meaning that under the same condition, system is more stable in reversed power flow. Because the impedance of constant power converter toward dc link is resistive in the low frequency range, and it is negative in the forward power flow.

Fig. 4-15 shows the Nyquist plots of impedance minor loop gain (T_{m-R}) in reverse power flow, which is also under the variation of DAB impedance, the same

condition as in Fig. 4-10. In Fig. 4-15, it is clear that with the increasing of DAB impedance, the Nyquist plots still stay away from the unstable point (-1, 0), meaning that the system remains stable. But in forward power flow, the Nyquist plots tends to across the point of (-1, 0), indicating system tends to be unstable. So under the same condition, when DAB converter regulates dc link voltage and inverter controls the power, system is more stable in reversed power flow than the forward power flow.

So conclusion can be drawn that to the direction of power flow, system will be more stable if the source converter controls the power and the load converter controls the dc link voltage. Because under this condition, the constant power converter presents resistive impedance to the dc link, and the impedance interaction will introduce less phase shift to the overall system.

4.3.2. SIMULATION VEFIRICATION

The derived input and output impedances at the common dc link are measured in this part. For the DAB converter, the output impedance is measured by replacing the rear three-phase inverter with a controlled ripple current source. Frequency and peak-to-peak magnitude M_I of this current source can be changed, which will, in turn, give rise to the peak-to-peak ripple voltage M_V measured across the current source and shown in Fig. 4-16. Then DAB output impedance at different frequencies, including the magnitude and phase, can then be computed by the following expressions (4.24), (4.25).

At the frequency of 10 rad/s, the measured impedance magnitude and phase are respectively 1.23dB and 84.55°. This data, together with others measured at other frequencies, is plotted in Fig. 4-17. The measured results are compared with the predicted values, and it is found to match well with its theoretical precedence.
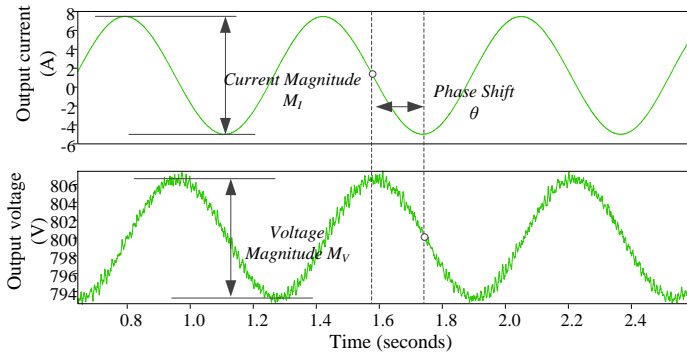
Fig. 4-16 DAB output voltage and current at 10rad/s.
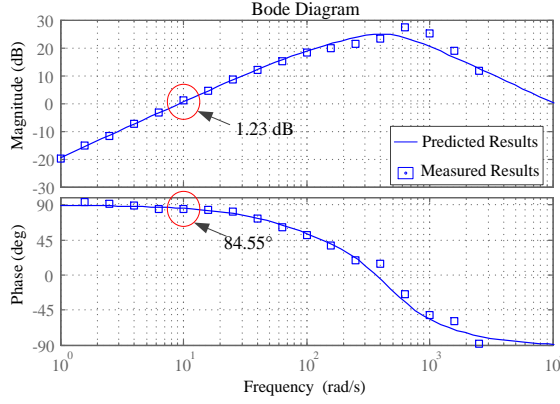
Fig. 4-17 The measurement of DAB impedance under voltage control

$$Magnitude = \frac{M_V}{M_I} \tag{4.26}$$

$$Phase = \theta \tag{4.27}$$

It should also be emphasized that the DAB forward and reverse impedances are not measured separately, since for a voltage-controlled converter, they are the same. Corresponding measurements for the three-phase inverter are plotted in Fig. 4-18 (a) for its forward input impedance and Fig. 4-18 (b) for its reverse output impedance.

As shown, for the constant power inverter when as the load, the input impedance is negative in the low frequency range. When it works as the source, its low frequency output impedance is resistive. The measured results match the predicted results well, verifying the correctness of the inverter input impedance modelling.

Fig. 4-19 shows the simulation results with variations of power flow. Inverter power reference P^* has been periodically switched between forward (5kW) and reverse (-5kW) power flows. DAB impedance is intentionally increased by reducing the voltage controller gain, and it can deteriorate the system stability, which highlights the stability difference.

As anticipated, oscillation in forward power flow is generally larger than that in the reverse power flow, because of its weaker impedance interaction, resulted from the negative input resistance of the constant power inverter. Under the same condition, the reverse power flow is well-damped, because it presents resistive impedance to the dc link voltage in the low frequency part. Stabilities in different power flow directions are different, therefore, in bidirectional cascaded applications, control schemes for the elementary converters should be designed with optimal stability, which needs to consider the most sensitive impedance minor loop gain.

(a)

(b)
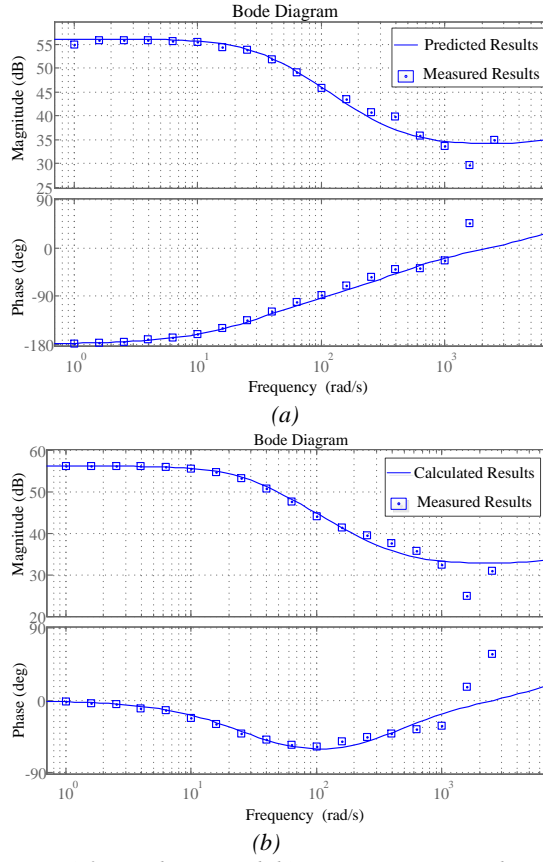
Fig. 4-18 Inverter (a) forward input and (b) reverse output impedance measurements.
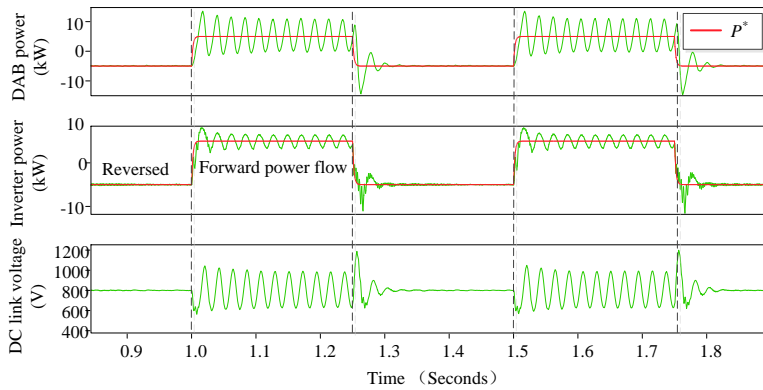
Fig. 4-19 Simulation results of transition between forward and reversed power flow.

4.3.3. EXPERIMENT VERIFICATION
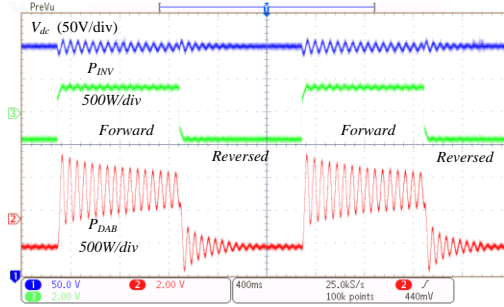
Fig. 4-20 Experimental dc-link voltage (V_{dc}), power through inverter (P_{INV}) and power through DAB converter (P_{DAB}).
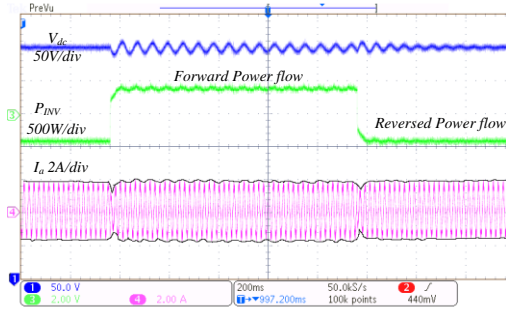
(a) dc-link voltage V_{DC}, actual power flow P_{INV} and ac output current I_a
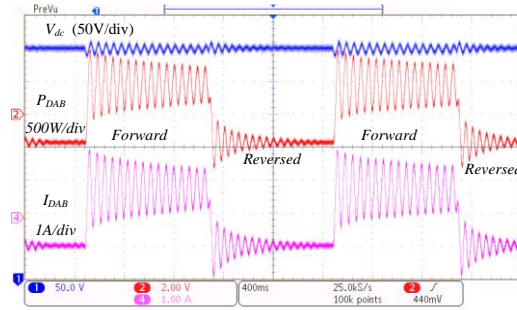
(b) dc-link voltage V_{dc}, actual power flow PDAB and dc output current IDAB

Fig. 4-21 Experimental waveforms of (a) inverter and (b) DAB converter.

The experimental prototype has been operated under a periodic power reference, stepping between −400W and 400W, and the parameters are shown in the appendix.

The DAB impedance is also enlarged to deteriorate the stability, which facilitates to show stability difference between different power flows.

Fig. 4-20 depicts the power flow waveforms through the sub converter and the dc link voltage. More oscillations in forward power flow can be observed.

The waveforms of converter output current and power are illustrated in Fig. 4-21(a) and (b). As shown, both the DAB and inverter currents are more oscillatory in the forward power flow, and for the inverter, the oscillation is reflected in the envelope of the ac current. The oscillations are introduced by the negative impedance of the rear constant power-controlled inverter in the forward direction. The destabilizing negative impedance is however not present when power reverses. The reversed power waveforms are thus more stable than the forward power flow.

4.4. IMPEDANCE COORDINATIVE CONTROL

As previously analyzed, the impedance interaction significantly affects the system dynamics and stability. The constant power sub-converter has different impedance behaviors between different power flow directions, which introduce more instability and uncertainties to the bidirectional system. Then the following part of this chapter will propose a method to coordinate the impedance behavior of the constant power converter in bidirectional application, and it can make the bidirectional converter impedance alike each other, greatly stabilizing the cascaded converter system.

4.4.1. ANALYSIS OF IMPEDANCE COORDINATIVE CONTROL

As analyzed, in the cascaded interface converter system, conventional control methods use DAB converter working at voltage mode to maintain common dc link voltage，and implement the inverter to control the power flow as a constant power converter. The impedance of voltage controlled converter stays the same between forward and reversed power flow, but for the constant power converter, its impedance to the common dc link is different between forward and reversed power flow, which causes the stability difference between different power flow directions. So the proposed control modifies the impedance of constant power converter to have similar performance between forward and reversed power flow. The control scheme of the proposed control is shown in Fig. 4-22.

An impedance controller is implemented in the power loop. The common dc link voltage is sampled and fed back to the inverter control unit. Then the dc link voltage is compared with the reference, hereby the error is used to modify the power reference. Since the impedance controller is implemented in the outer loop, so the time scale is second, then the conventional low frequency negative impedance can be eliminated, and at the same time, the constant power flow can
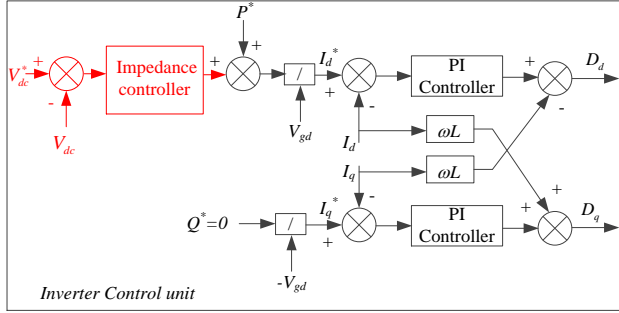
Fig. 4-22 Control scheme of impedance control

still be achieved, because the output of impedance controller is 0 in steady state.

4.4.2. IMPEDANCE MODELLING

In forward power flow, inverter input impedance can also be obtained by the power balance equations, as:

$$\Delta P = \Delta I_d V_{gd} = \Delta V_{dc} I_o + \Delta I_o V_{dc} \tag{4.28}$$

Under the impedance control, inverter input impedance can be written as:

$$Z_{INV-in} = \frac{\Delta V_{dc}}{\Delta I_{in}} = \frac{V_{dc}}{1.5 V_{gd} G^*_{V_{dc}-I_d}(s) - I_{in}} \tag{4.29}$$

Here $G^*_{V_{dc}-I_d}(s)$ is the transfer function from the inverter dc side voltage to the ac side output current on d-axis, and Fig. 4-23 shows the block diagram of $G^*_{V_{dc}-I_d}(s)$.

As depicted in Fig. 4-23, the red lines represent the new added impedance controller function path. The corresponding transfer function of $G^*_{V_{dc}-I_d}(s)$ can be written as:

$$
\begin{aligned}
G^*_{V_{dc}-I_d}(s) &= \frac{D_d s}{Ls^2 + \left(r + V_{dc} K_{P-inv}\right)s + V_{dc} K_{i-inv}} + \frac{G_Z(s)}{V_{gd}} \\
&= G_{V_{dc}-I_d} + \frac{G_Z(s)}{V_{gd}}
\end{aligned}
\tag{4.30}
$$
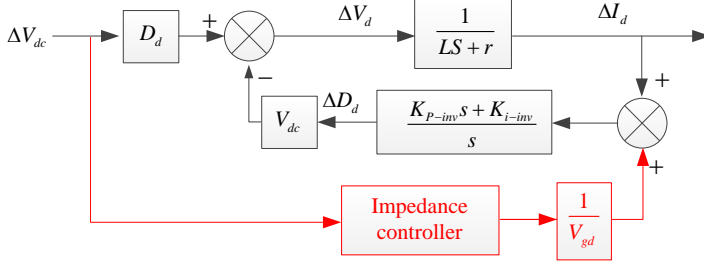
Fig. 4-23 Block diagram of $G^*_{V_{dc}-I_d}(s)$ (*Forward* power flow)
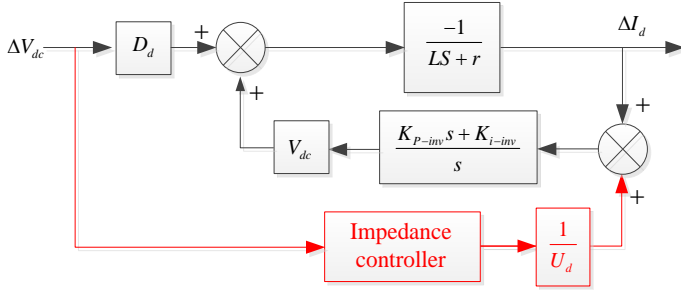
Fig. 4-24 Block diagram of $G^*_{V_{dc}-I_d-R}(s)$ (*Reversed power flow*)

In the impedance control, the relationship between dc side voltage and ac side current is constituted by conventional constant power schemes and the newly joined impedance controller path $\dfrac{G_Z(s)}{V_{gd}}$.

Therefore the impedance of inverter in the proposed control can be obtained as:

$$Z^*_{in} = \frac{\Delta V_{dc}}{\Delta I_{in}} = \frac{V_{dc}}{1.5 G_Z(s) \cdot I_{in} + 1.5 V_{gd} G_{V_{dc}-I_d}(s)} \tag{4.31}$$

In reversed power flow, inverter operates in the rectifier mode, and its output impedance can also be obtained by the power balance equation as (4.26). Correspondingly, $G^*_{V_{dc}-I_d-R}(s)$ is the transfer function from dc side voltage to ac side current on d-axis, and its block diagram is shown in Fig. 4-24.

The transfer function of $G^*_{V_{dc}-I_d-R}$ can be expressed as:

$$G_{V_{dc}-I_d-R}^*(s) = \frac{-D_d s}{Ls^2 + (r + V_{dc}K_{P-inv})s + V_{dc}K_{i-inv}} + G_Z(s)$$

$$= G_{V_{dc}-I_d-R}(s) + \frac{G_Z(s)}{V_{gd}}$$

(4.32)

Similar with forward power flow, $G_{V_{dc}-I_d-R}^*(s)$ constitutes the conventional $G_{V_{dc}-I_d-R}(s)$ and the impedance controller path $G_Z(s)/V_{gd}$.

Correspondingly, in reverse power flow, inverter output impedance to the common dc link voltage can be obtained as:

$$Z_{o-R}^* = -\frac{\Delta V_{dc}}{\Delta I_o} = \frac{V_{dc}}{1.5G_Z(s) + I_o - 1.5V_{gd}G_{V_{dc}-I_d-R}^*(s)}$$

(4.33)

$G_Z(s)$ is the impedance controller transfer function.

For the optional requirement of stability, it is needed to increase the input impedance of current controlled converter, as well as get rid of the negative impedance. To present resistive impedance to the dc link voltage, the impedance controller is designed with a proportional value.

As in (4.29), if $1.5G_Z(s) > I_o$ and $1.5G_Z(s) > I_{in}$, the low frequency negative input impedance can be avoided. But $G_Z(s)$ is not the larger the better, because excessive increasing the value will reduce the inverter impedance towards the common dc link, which will introduce instability to the cascaded system. Thus make the system impedance unaffected by the reference current, $G_Z(s)$ can be designed with a proportional values two or 3 times of the maximum inverter dc current, and also the value should be within the stability area of inverter control block diagram.

Fig. 4-25 shows inverter bidirectional impedance towards the common dc link, which are the input impedance in forward power flow and output impedance in reversed power flow.

As shown to the common dc link voltage, the inverter impedances towards the dc link are both resistive in the low frequency range, and the bidirectional impedances are more similar with each other, compared with conventional control. In the proposed control, the negative impedance in conventional CPL is successfully turned to resistive impedance.
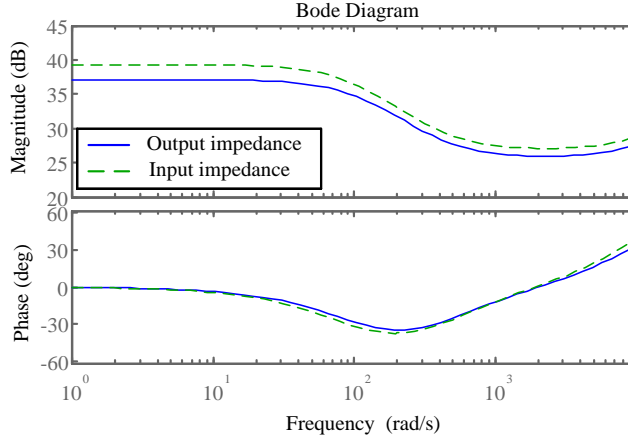
Fig. 4-25 Inverter Input and output impedance with the impedance controller

4.4.3. ANALYSIS OF MINOR LOOP GAIN

Based on previous impedance modelling, the bidirectional impedance minor loop gain in the proposed control can be written as:

$$\begin{cases} T_m = \dfrac{Z_{in}}{Z_o} \text{ forward power flow} \\ T_{m-R} = \dfrac{Z_{in-R}}{Z_{o-R}^{\;*}} \text{ reversed power flow} \end{cases} \tag{4.34}$$

The bode plots of T_m and T_{m-R} are shown in Fig. 4-26.
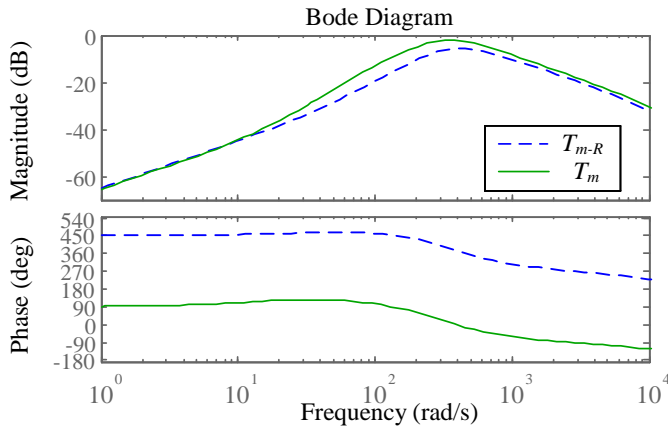
Fig. 4-26 Bode plots of bidirectional minor loop gain in the proposed control

(a) T_m in forward power flow   *(b) $T_{m\text{-}R}$ in reversed power flow*
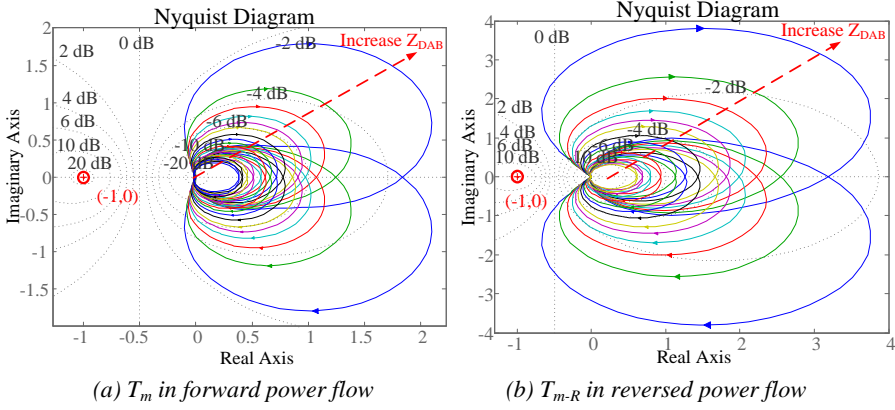
Fig. 4-27 Bidirectional Nyquist plots of the minor loop gain in the impedance control

As shown in , T_m in the forward power flow is almost the same as T_{m-R} in reversed power flow. The phase shift of the bidirectional impedance minor loop gain ranges from 90° in the low frequency part to -90° in the high frequency part.

Fig. 4-27 shows the bidirectional Nyquist plots of the impedance minor loop gain. As shown in Fig. 4-27, the DAB impedance (Z_{DAB}) is intentionally increased to deteriorate the stability, and it is the same condition with conventional control in Fig. 4-10 and Fig. 4-15. As depicted in Fig. 4-27 (a), in the forward power flow, with the increase of DAB impedance, T_m always stays away from the unstable point (-1,0), meaning that the system is stable with the increasing of DAB impedance. Fig. 4-27 (b) shows the minor loop gain in reversed power flow, and the T_{m-R} also keeps away from the unstable point, representing that the system stability can be maintained. Therefore the impedance interaction in the proposed control is more bidirectional stable.

4.4.4. SIMULATION AND EXPERIMENT VERIFICATION

4.4.4.1 Simulations

The simulation parameters are shown in the appendix.

Fig. 4-28 illustrates the simulation measured inverter bidirectional impedance under the impedance control, with 1kW transmitted power. As shown, towards the dc link, the measured inverter impedances behave similar between forward and reversed power flow, both resistive in the low frequency range and goes to inductive in the high frequency range. The measured results match the predicted value in Fig. 4-25.
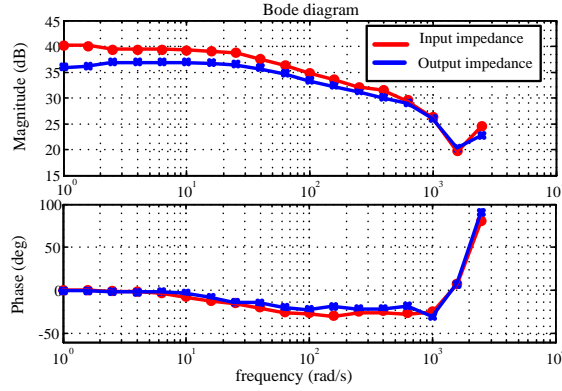
Fig. 4-28 Impedance measurement of the proposed control
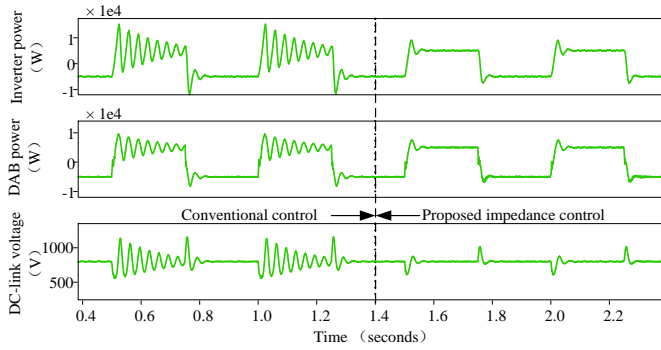
Fig. 4-29 Simulation results of conventional control and the impedance control

Fig. 4-29 shows the compared simulation esults between conventinoal control and the proposed impedance control. The DAB voltage controller gain is intentionally reduced to show the stability differentce. Power reference is also periodic square wave, with the frequency of 1Hz, steping between -5kW and 5kW.

As shown in Fig. 4-29, betfore 1.4 s, conventional control is activated, and it is clearly that osscillations in reversed power flow are better damped than in the forward power flow, because, in reversed power flow, inverter presents resistive impedance to dc link votlage, while it presntes negative impedance in forward power flow. After 1.4s, in the proposed impedance control, the osscillations in both forward and reversed power flow are effectively damped. Since in the proposed impedance control, the negative impedance is avoided, and the system becomes bidirectional stable.

4.4.4.2 Experiments

Experiment parameters are shown in the appendix. Fig. 4-30, Fig. 4-31 and Fig. 4-32 are the experiment results, in which the DAB impedance is intentionally reduced to deteriorate the system stability. In the experiment, the power reference changes between 400W and -400W, and the period is 2s. Also the DAB voltage controller is intentionally reduced to highlight the stability difference.

Fig. 4-30 shows the comparing experimental waveforms. As shown before the dash line control method is conventional control, and after dash line, it transfers to the proposed impedance control. In conventional control, dynamic oscillations in forward power flow are much bigger than in the reversed power flow. But in the proposed impedance control, oscillations become effectively damped in both forward and reversed power flow. Therefore the proposed control manages to improve the bidirectional stability, and then the system has similar stability between forward and reversed power flow.

 Fig. 4-31depicts the detail curves of inverter, including the dc side voltage, inverter power and current output.
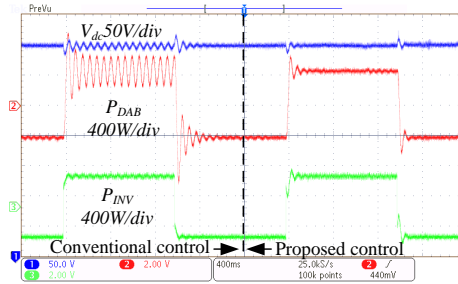
Fig. 4-30 Experiment results of the DC-link voltage and DAB inverter power output

(a)Conventional control   *(b) Proposed Impedance control*
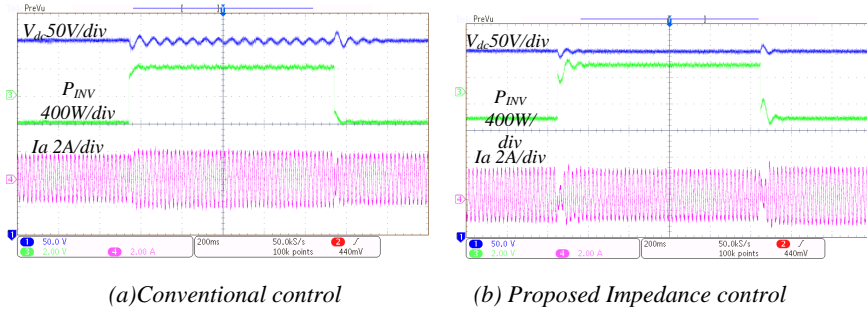
Fig. 4-31 Experiment results of the DC-link voltage, inverter power and current output
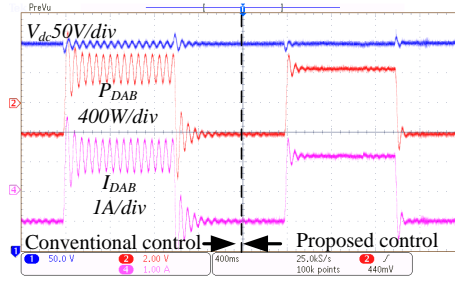
Fig. 4-32 Experiment results of the DC-link voltage, DAB power and current output

As in Fig. 4-31 (a), under conventional control, inverter ac side current and power has apparent oscillations when the power output is 400W in forward direction. In Fig. 4-31 (b) in the proposed control, the steady state of power output, dc side voltage is more stable than conventional control.

Fig. 4-32 shows the detail wave forms of DAB, including the current output, voltage output and power output. As depicted, under conventional control, significant oscillations occur in both the DAB current and power output, but in the proposed impedance control, the wave forms are more stable.

Experiment results verify that the impedance controller on the constant power inverter can alter the negative impedance, contributing the cascaded system better stability. The impedance control manages to reform the impedance interaction become more similar between different power flow directions.

4.5. CONCLUSION

In this chapter, the impedance based stability assessment is implemented to evaluate the stability of the cascaded interface converter.

The impedance of DAB converter and inverter in conventional control have been modelled, and the results show that under voltage control, the impedance of DAB converter presented to the dc link is the same between forward and reversed power flow. With constant power control, the impedance of inverter presented to the dc link is different from forward and reversed power flow, and in the forward power flow, inverter impedance presents negative impedance in the low frequency to the dc link, but when the power flow is reversed, the impedance to the dc link is resistive in the corresponding low frequency range. Therefore in the reversed power flow, the resistive impedance is more stable than the negative impedance in forward power flow.

So an important guide line can be offered to conventional cascaded converter, which is that system will be more stable if using the power controlled converter as the source, and dc link voltage maintaining converter as the load. Based on this issue, this chapter also presents an impedance control method on the constant power converter to create resistive impedance in the low frequency range to take the place of conventional negative impedance, and at the same time maintain the resistive impedance in reversed power flow, and then the interface converter will be more bidirectional stable.

CHAPTER 5. PROPORTIOANL CONTROL FOR CASCADED DC-AC INTERFACE CONVERTER

PI controllers are frequently implemented in a cascaded converter system to control the dc link voltage, because they can achieve zero steady state error by the high gain at low frequency. However the accurate tracking is at the expense of lifting the control system type number, which results the system more difficult to control. This chapter will firstly analyze the dc link voltage control issue in two stage cascaded converter, after that a coordinate dc link voltage control method is proposed, which only uses a proportional regulator for maintaining dc link voltage. This control method can: achieve zero steady state error on the dc link voltage; reduce the control system type number; improve the damping performance. Compared with the conventional PI control, the proposed control is totally symmetric, and it can have less impedance interaction between source converter and load converter. It can also be implemented in other general two stage cascaded converters, and suitable for both unidirectional and bidirectional applications.

5.1. CONTROLLER AND TYPES OF CONSTROL SYSTEMS

5.1.1. INTEGRAL CONTROLLER

In conventional proportional control, which does not possess the integrator $1/s$, steady state error or offset to the input reference will exist, and this problem can be solved by introducing an integrator into the controller, and then the whole controlled is named PI controller[81]. The transfer function of PI controller can be expressed as:

$$G_{PI}(s) = \frac{K_P s + K_i}{s} \tag{5.1}$$

For the integrator, the benefit is the removing of the offset and steady-state error, but it may also introduce undesirable factor to the systems, which is the oscillatory response of slowly decreasing amplitude, or even the unstable condition with increasing amplitude.

After eliminating steady state error, control system might suffer output error with other kinds of inputs. For instance, a system, with no steady-state error to a step input, may behave with steady-state error under a ramp input. Under a given type of

input, whether a control system will have steady-state error or not depends on the type of system open-loop transfer function.

Control systems type may be classified based their ability to track different kinds of input, such as the step input, ramp input, acceleration input, and so on. The magnitude of the steady state errors indicate the goodness of the control system.

For a unity feedback control system, its open loop transfer function is expressed as:

$$G_{open}(s) = \frac{K(T_a s+1)(T_b s+1)\cdots(T_s s+1)}{s^N(T_1 s+1)(T_2 s+1)\cdots(T_p s+1)} \tag{5.2}$$

The item s^N in the dominator indicates the multiplicity of the pole at the origin point. Based on the value of N, such as $N=0$, $N=1$, $N=2$, the control system will be correspondingly called type 0, type 1, type 2 system[82]. Attention is needed that it is different from the order of a system.

The higher the type number is, the more accuracy the system will be. On the other hand, higher type number aggravates more stability problems. So conventionally a compromise has to be made between the control accuracy and the stability. Therefore type 0, type 1 and type 2 control systems are widely used in practical application, and type 3 or higher type control system are rarely seen, because they are difficult to maintain stable.

5.2. SYSTEM TYPE IN CASCADED CONVERTER

For the cascaded interface converter, conventional control methods use one sub converter to maintain the dc link voltage, and the other to control the power flow. For instance cascaded DAB with inverter in Fig. 5-1, DAB converter controls the dc link voltage and inverter regulates the power output. The dc link voltage control patch can be obtained from Fig. 5-1, and Fig. 5-2 shows the block diagram of dc link voltage control scheme. As shown, a PI controller is used to eliminate the steady state error of dc link voltage[83] and improving the current tracking performance, and $G_i(s)$ is the open loop transfer function of the current loop. Therefore the open loop transfer funciton of the dc link voltage control is written as (5.3), where $G_{V-open}(s)$ is the open loop transfer function of the votlage loop, and K_{VP} K_{Vi} are respectively the proportional and integral parameter inthe PI controller.

$$G_{V-open}(s) = \frac{G_{i-open}(s)(K_{VP}s + K_{Vi})}{s^2 C(1+G_{i-open}(s))} \tag{5.3}$$
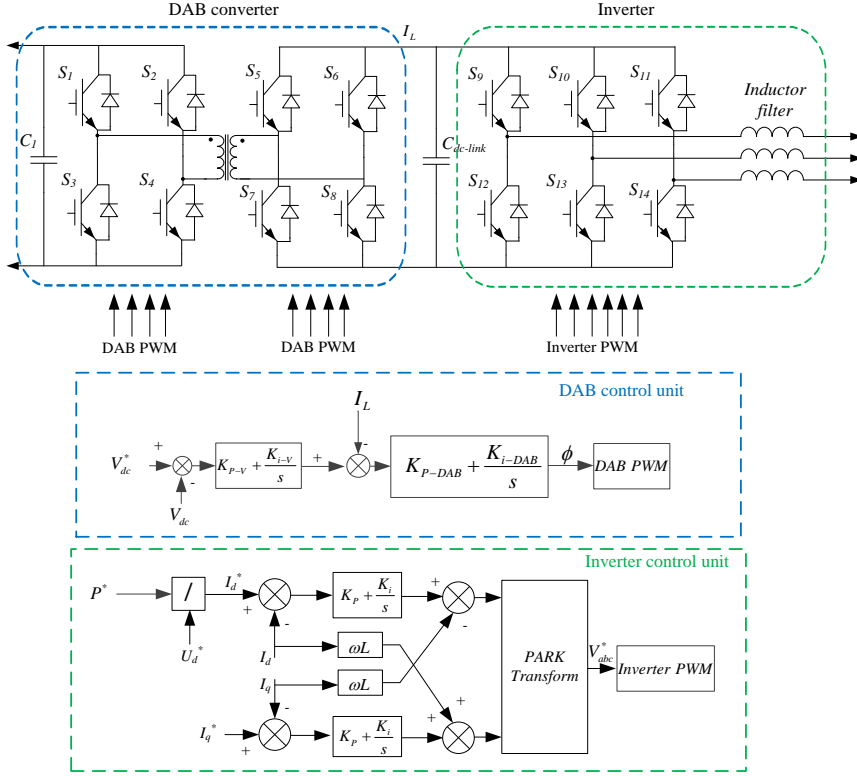
Fig. 5-1 Control scheme of cascaded DAB with inverter
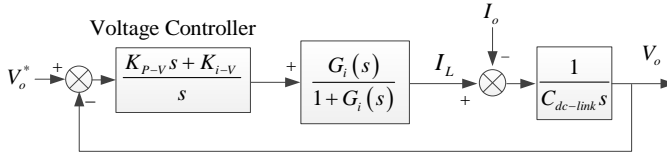
Fig. 5-2 Block diagram of dc link voltage control

From (5.3), it can be observed that in conventional control, dc link voltage control system is a typical type 2 control system, resulted from the existance of dc capacitor and the PI ocntroller. When eliminating the steady-state error on the dc link voltage, the PI controller also introduces more oscillary factor the the dc link voltage, and the system becomes more difficult to control.

For the grid interface converter, the staiblity and reliability is extremely important[84], because it is the foundation for the system operations[85], and the response time of power sytem is much slower than the power electronic based

converter[86]. Additionaly the dc link votlage reference normally is an fixed value, so it is unnecessary to sacrifice the stability to design the dc link votlage control to be type 2 control system. Therefore if the control system type number can be reduced from type 2 to type 1, then the stability of the grid interface converter will be greatly improved, which is substantially benefit for the grid interface covnerter.

The next part, a type number reduced control method will be proposed.

5.3. SYSTEM TYPE REDUCED CONTROL FOR CASCADED CONVERTER

Conventional type 2 control system can maintain the dc link voltage on the reference value, at the expense of raising the system type number. So it would be challenging and great benefit to formulate an alternative control method which will not lift system type model, at the same time remains the zero steady state error voltage tracking.

Therefore this chapter proposes a coordinated control scheme implementing only the proportional controller for controlling the dc link voltage. Accurate voltage tracking is still achieved, and this is realized without increasing the control system type, which is named as the coordinated proportional control. The proposed control designs the scheme based on the principle of balancing power flow at the dc link of two stages cascaded converters, and this method also works in other two stages cascaded systems.

5.3.1. PASSIVE INTEGRATORS

Passive integrators are widely used in conventional analog control circuit [87], and op-amp circuit [88]. As shown in Fig. 5-3, passive integrator refers to the circuit of four-terminal network consisting of two passive elements, where capacitor is necessary. It is also a typical first-order low-pass filter. This circuit can realize the integral calculation. The voltage on the capacitor can be written as:

$$V_o = \int (I_{in} - I_o)dt \qquad (5.4)$$
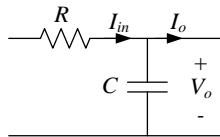
Fig. 5-3 Passive integrator circuit

There is also dc link capacitor in the cascaded converter system. So the proposed control method will utilize the dc link capacitor to reduce the control system type number.

5.3.2. OPERATING PRINCIPLES

Coordinated proportional control employs both the sub converters, DAB and inverter, to regulate the dc link voltage. It is different from the conventional control discussed previously, which only one sub converter regulates the dc link voltage by promoting power to dc link when the voltage drops, and exacting power when then voltage raises. Compared with DAB converter, for dc link voltage regulation, inverter control action is reversed, because inverter raises the dc link voltage by exacting less power from the dc link, and reduce the dc link voltage by promoting power output to utility grid. The difference in power output between DAB and inverter will be integrated on the dc link capacitor to vary the dc link voltage level.

Fig. 5-3 shows the block diagram of the coordinated proportional control. Compared with Fig. 5-1, the proposed control uses the same inner power loop structure, and the major difference is the dc link voltage control unit. The coordinated proportional control only uses a simple proportional controller, instead of conventional PI controller. The output of this controller is fed to both the DAB converter and inverter power loops, differing from that in Fig. 5-1, solely to the DAB converter. Substantially, providing the controller output ΔP to both sub-converters can improve the ride-through ability when one sub-converter fails. For instance, in the failure of DAB converter, inverter is still going to regulate the dc
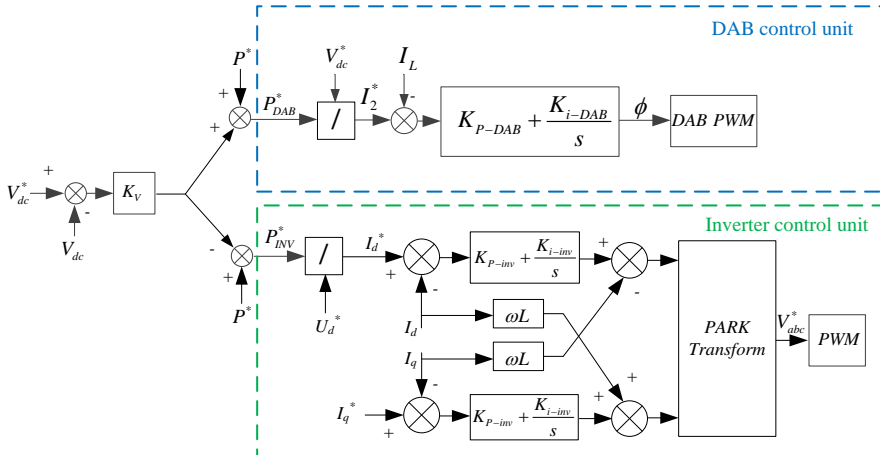
Fig. 5-3 Coordinated-proportional control scheme for cascaded converter

link voltage, but not the conventional schemes only rely on DAB converter for dc link voltage regulation. The compromise expected by the proposed control under the fault condition will be a non-zero dc link voltage error, because the proportional voltage controller at that time will behave as normal proportional control with steady state error. But the error does not exist under normal operating conditions.

At the same time DAB and inverter are both responsible for the power flow control, so the power reference (P^*) is given to both of them. The output of voltage controller is positively fed to DAB converter power reference and negatively fed to inverter power reference. So the power references for DAB and inverter can be expressed as:

$$P_{DAB}^* = P^* + \Delta P \tag{5.5}$$

$$P_{INV}^* = P^* - \Delta P \tag{5.6}$$

Where ΔP is the output of the proportional voltage controller, expressed as:

$$\Delta P = K_V \left(V_{dc}^* - V_{dc} \right) \tag{5.7}$$

So if the dc link voltage has offset from reference value, the proportional controller will generate power variations to DAB and inverter power reference. Therefore power output difference between DAB and inverter will be generated, and this power difference will be integrated on the dc link capacitor. According to the conservation law of energy, the relationship between dc link voltage and power difference can be expressed as:

$$\Delta V_{dc}^2 = 4 \frac{1}{Cs} \Delta P \tag{5.8}$$

Here ΔV_{dc}^2 is the offset between V_{dc0}^2 and V_{dc}^2. The voltage level of dc link is determined by the energy stored on the dc link capacitor, and the stored energy is the integration of the power difference between DAB and inverter.

Although there is no integrator in the control unit, but in the proposed control scheme, the dc link capacitor is the integrator for the dc link voltage, therefore in the proposed control strategy, the passive integrator in the main circuit is combined with the control unit. In normal steady state, ΔP is zero for that the interface converter only transfers power, not consumes. So power coming from the DAB converter has to be completely delivered by the inverter to the grid. According to above equations, ΔV_{dc}^2 and hence ΔV_{dc} should be zero even only a simple proportional controller K_P is used here.

5.3.3. CONTROL SYSTEM TYPE ANLYSIS

In Fig. 5-3, in the proposed control, proportional controller takes the place of conventional PI controller, and then dc link voltage control block diagram can be obtained, shown in Fig. 5-4. To obtain the linear model of dc link voltage control, the linearized energy model is built here to evaluate the dc link voltage control, so the terms of V_{dc}^2 is used here. $G_{DAB}(s)$ and $G_{INV}(s)$ are respectively the closed power control loop transfer functon of DAB and inverter. Based on Fig. 5-4, open-loop transfer function of the dc link voltage control is written as:

$$G_{V_{dc}^2}(s) = K_V \left[G_{DAB}(s) + G_{INV}(s) \right] \frac{2}{Cs} \tag{5.9}$$

It can be observed that the proposed control is a typical type 1 control system. Fig. 5-5 shows the bode plots of dc link voltage control, including the conventional control and the proposed coordinate proportional control.
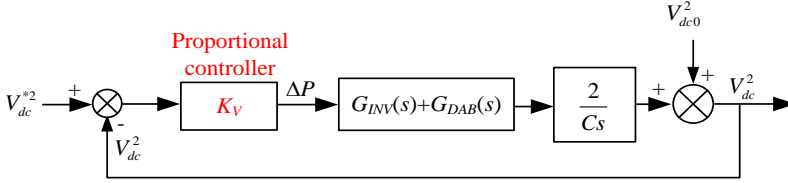
Fig. 5-4 *Energy-based coordinated-proportional control block diagram for cascaded converter*
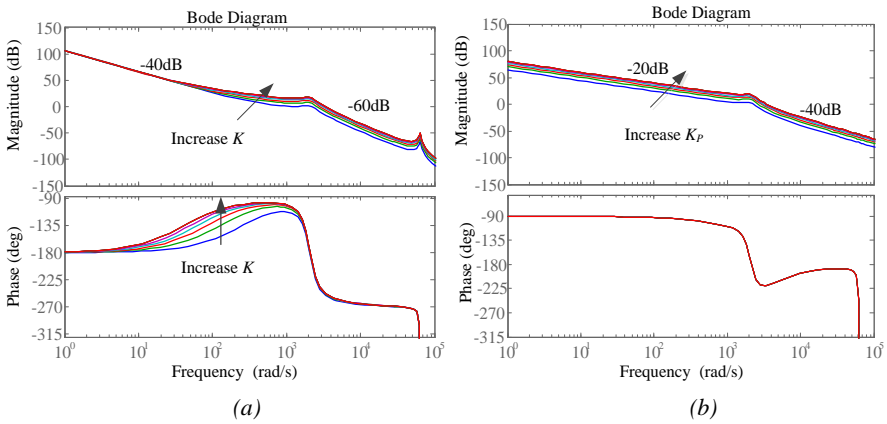
Fig. 5-5 *Open-loop Bode diagrams plotted with (a) conventional and (b) proposed DC-link voltage control*

As depicted in Fig. 5-5 (a), in conventional control, the phase-shift is $-180°$ at low frequency, indicating the control system is typical type 2 system. Fig. 5-5 (b) is the proposed coordinate control, the phase shift is $-90°$ in the low frequency range. Therefore dc link voltage in the proposed control scheme behaves as a typical type 1 system. This reduction of control system type number in the proposed control is substantially created by the absence of the extra pole at the origin point, which is introduced by the integral parameter of PI controller in conventional control.

5.3.4. DC-LINK VOLTAGE OSCILLATION UNDER POWER REFERENCE VARIATION

For the dc link voltage control, the reference value (V_{dc}^*) determines the steady state level, but it will also be influenced by the power reference P^* dynamically. Therefore this part will analysis the relationship between power reference variations and the dc link voltage.

The block diagrams of conventional control and the proposed control are redrawn in Fig. 5-6, focusing on the power reference interference effect on the dc link voltage. P^* is rearranged as the input, and V_{dc}^2 located on the right terminal as the output. Here the system performance is analyzed through the energy model [89], so V_{dc}^2 is used.

(a) Conventional

(b) Proposed schemes
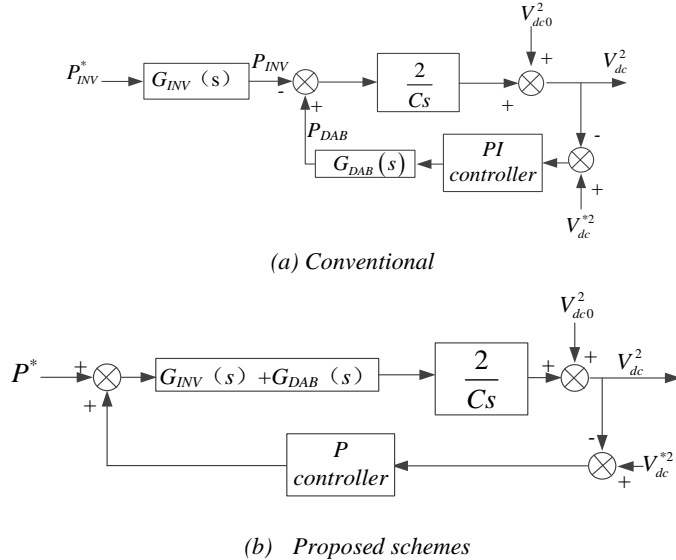
Fig. 5-6 Energy-based block diagrams with P^* as input and V_{dc}^2 as output.
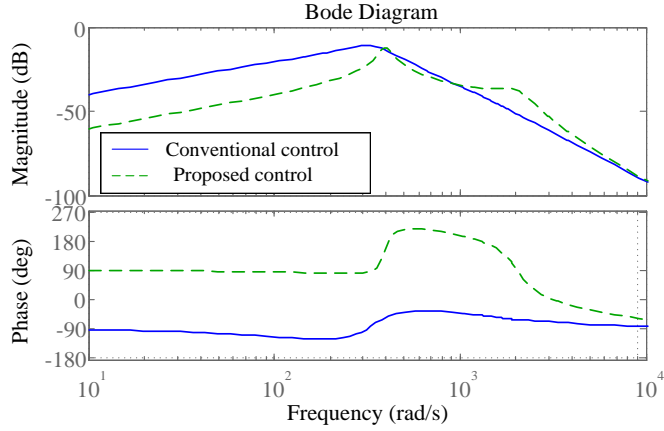
Fig. 5-7 Bode diagrams plotted for Fig 5-5 (a) and (b).

Based on Fig. 5-6, bode diagrams can be plotted, as shown in Fig. 5-7, and the bode plots will show how the power reference P^* affects the dynamic oscillation of V_{dc}^2. In the bode plots, a higher attenuation represents a smaller oscillation that mutative power reference will caused on V_{dc}^2. It can be observed that the dash line of the proposed control manages to attenuate the interference better. So under power reference variations, the proposed control can maintain dc link voltage with smaller oscillations than conventional control.

5.3.5. DC LINK VOLTAGE DAMPING PERFORMANCE

The damping performance of dc link voltage can be evaluated through the root loci [90], and the root loci of conventional and the proposed control scheme can be obtained from the control block diagram in Fig. 5-6. High order smaller time constant is omitted in case of complicating the root loci. The root loci of conventional control and the proposed control are respectively shown in Fig. 5-8 and Fig. 5-9. As shown, both the root loci of conventional control and the proposed control contain two parts, named part 1 and part 2. Part 1 in Fig. 5-8, which is the conventional control, locates closer to the vertical axis than the part 1 in the proposed control, which means that the proposed control can damped the oscillation more effectively. Part 2 in the proposed control locates along the real axis on the left half plane, while the corresponding part 2 in conventional control contains the components of vertical axis, so it means that conventional control will oscillatory, but the proposed one will not.

Therefore, the proposed control provides better damping performance than the conventional scheme.
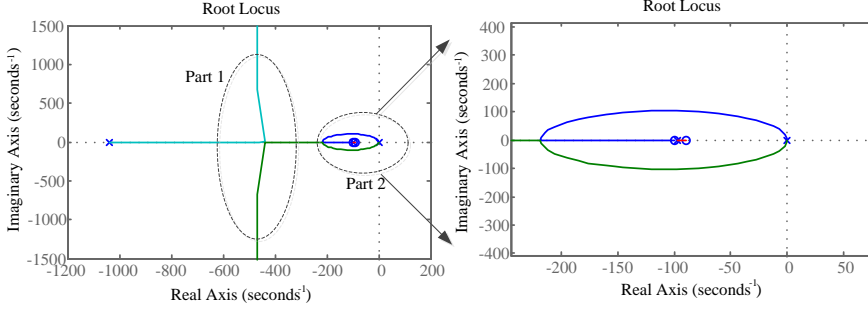
Fig. 5-8 Root loci obtained with conventional DC-link voltage control.
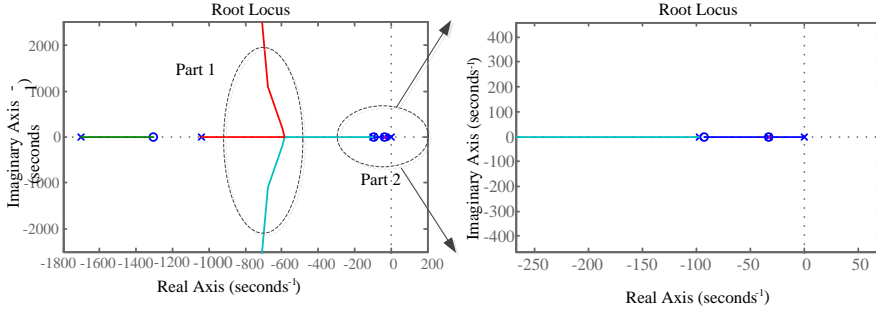
Fig. 5-9 Root loci obtained with proposed DC-link voltage control.

5.3.6. DESIGN OF PROPORTIONAL GAIN

In the proposed coordinate proportional control, the dc link voltage control block diagram is shown in Fig. 5-10 (a), and then tuning of the proportional gain can be performed according to this block diagram. In Fig. 5-10 (a), the power reference P^* behaves as a disturbance, therefore it can be ignored. $G_{DAB}(s)$ and $G_{INV}(s)$ are respectively the closed power loop transfer function, which can be obtained by the current loop block diagram, and they can be written as (5.9) and (5.10) which are obtained by the block diagram in Fig. 3-5 and Fig. 4-3. Then the proportional controller can be designed based on the stability requirement of phase margin and magnitude margin.

$$G_{DAB}(s) = \frac{G(K_{iP}s + K_{ii})}{Ts^2 + (1 + K_{iP}G)s + GK_{ii}}$$ (5.10)

$$G_{INV}(s) = \frac{V_{dc}K_{P-inv}s + V_{dc}K_{i-inv}}{V_{dc}(K_{P-inv}s + K_{i-inv}) + 2K_{PWM}(Ls^2 + s + rs)}$$ (5.11)
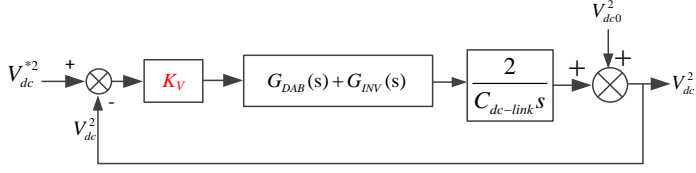
(a) Block diagram
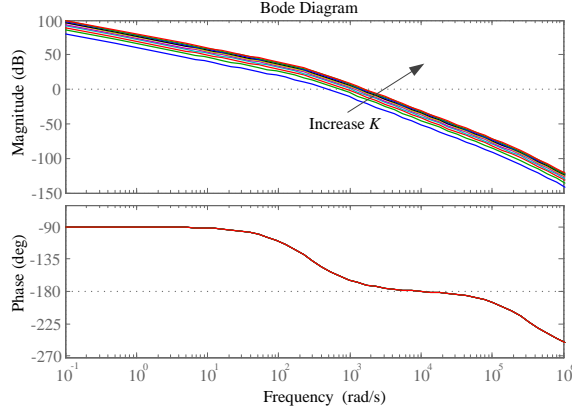
(c) Bode diagram

Fig. 5-10 Illustration of proposed DC-link voltage control with increasing K

Fig. 5-10 shows the bode plots of the dc link voltage control with the variation of this controller gain. It can be seen that the larger the proportional controller is, the wider the control bandwidth is. At the same time, the phase margin reduces with the increasing of this controller gain.

5.4. SIMULATION AND EXPERIMENT VERIFICATION

In the simulation and experiment, the proposed control is compared with conventional control. The same proportional dc link voltage controller gain is used for both control schemes, where same power controllers in DAB and inverter are applied. Simulation and experiment parameters are shown in the appendix.

5.4.1. SIMULATION RESULTS

The first simulation scenario is the step-changing power reference P^*, between 2kW and 7kW, and the period is 0.5 s. Fig. 5-11 and Fig. 5-12 shows the simulation results of conventional control and the coordinate proportional control. The other simulation scenario is that the dc link voltage under repeated step reference V_{dc}^*, stepping between 800 V and 900 V every 0.5 s.
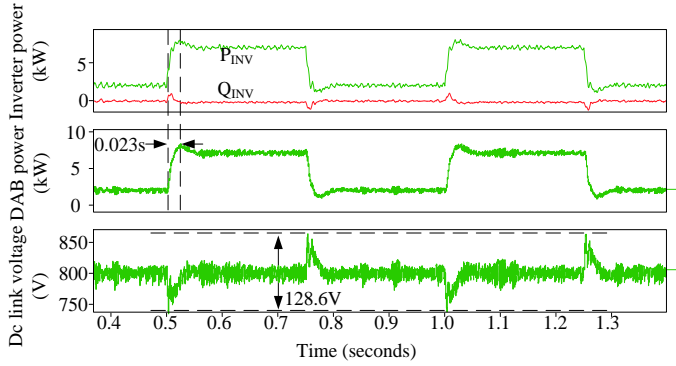
Fig. 5-11 Simulation results of conventional control with stepping power reference
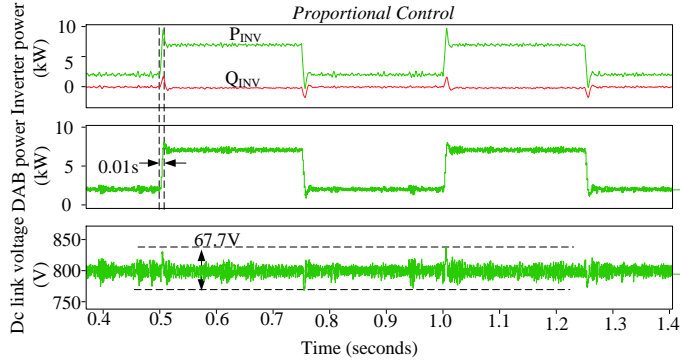
Fig. 5-12 Simulation results of coordinate proportional control stepping power reference.

Fig. 5-11 shows the simulation results of conventional control, where a 128.6 V peak to peak oscillation on the dc link voltage is observed. While in the coordinate proportional control scheme, the corresponding peak-to-peak oscillation is reduced to 67.7V in Fig. 5-12. Therefore the proposed control can effectively damp the interference triggered by power reference variations.

Fig. 5-13 shows the performance of conventional control. As shown, the dc link voltage has a typical second-order overshoot, and oscillation can also be observed.

Fig. 5-14 shows the waveforms under the coordinate proportional control. In the proposed control, the features of type 2 system can not be seen, such as overshoot and oscillations. The coordinate proportional control is a dynamically faster and more stable type 1 system. In the proposed control, the responsibility of dc link voltage control is shared between DAB converter and inverter, and this leads to a smaller power variation on DAB converter, because the extra power variation is imposed on the inverter. But in conventional control, inverter output power will not experience power variation like Fig. 5-13. However, in conventional control, the
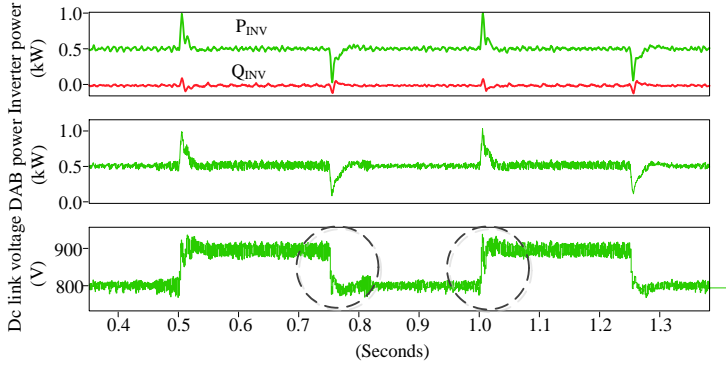
Fig. 5-13 Simulation results of conventional control with stepping dc link voltage reference.
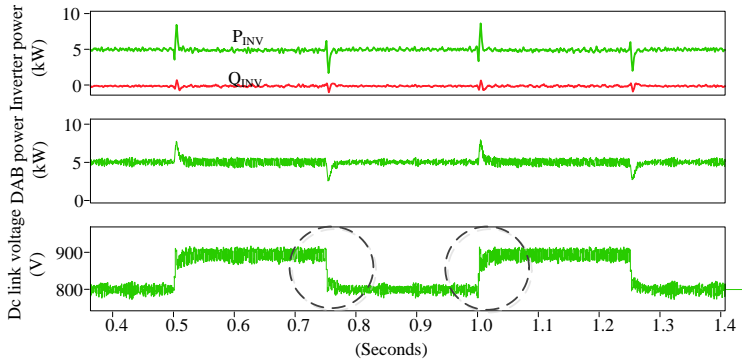
Fig. 5-14 Simulation results of coordinate proportional control with stepping dc link voltage reference

peak to peak oscillation in DAB converter is more than 4 kW, so DAB bear all the stress of dc link voltage regulation, and this generally should be discouraged. So in terms of spreading stresses between the sub-converters, the proposed scheme is more optimized than conventional control scheme.

5.4.2. EXPERIMENTAL RESULTS

Fig. 5-15 shows experiment waveforms of dc link voltage (V_{dc}), DAB output power (P_{DAB}) and current (I_{DAB}), where power reference P^* stepping between 0 and 800 W every 0.5 s. As shown, in conventional control, the peak to peak voltage oscillation is 32 V, with the rising time of 0.026 s. Under the same condition, in the proposed control, oscillations and rising time are immediately reduced to 21 V and 0.007 s, which effectively demonstrate the improvement of the coordinate proportional control.

Conventional Control   Proportional Control
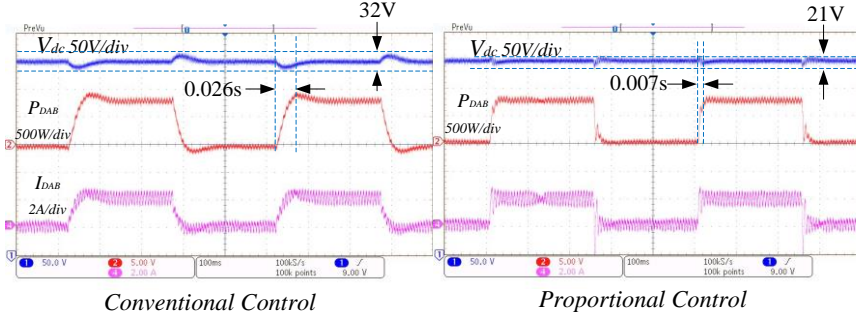
Fig. 5-15 Experimental dc link voltage, DAB power and output current under stepping power reference.

Conventional Control   Proportional Control
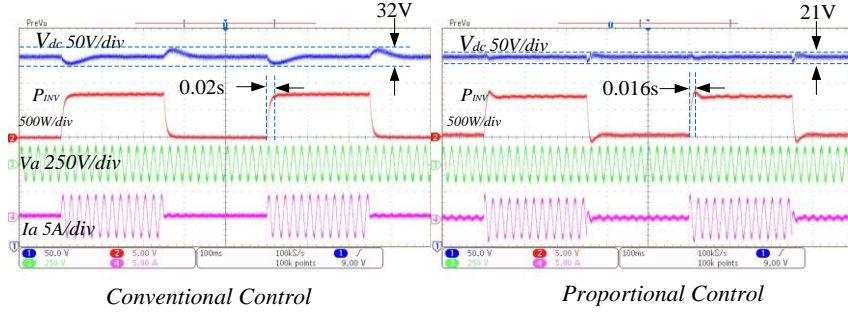
Fig. 5-16 Experimental DC-link voltage, inverter power and output current under P^* stepping.

Fig. 5-16 shows the detail waveforms of dc link voltage (V_{dc}), inverter output voltage and current in phase (V_a, i_a). Similar with before, the power output rising time of the coordinate proportional control is 0.016 s, while conventional control costs 0.02 s. So in the proposed control, the dynamic performance of inverter is also improved.

The second experimental set is performed with stepping dc link voltage, where the reference V_{dc}^* changing between 362.5 V and 437.5 V every 0.5 s.

Fig. 5-17 shows the experimental waveforms, in which the control scheme transfers from the proposed one to conventional one after the dash line.

Clearly shown in Fig. 5-17(a) and (b), under the proposed scheme, response speed of dc link voltage is faster. And also it can be seen that the proposed control is typical type 1 control system. In Fig. 5-17(b), when the proposed control is activated, the inverter power and current output engage disturbed component, which

(a).   *(b)*
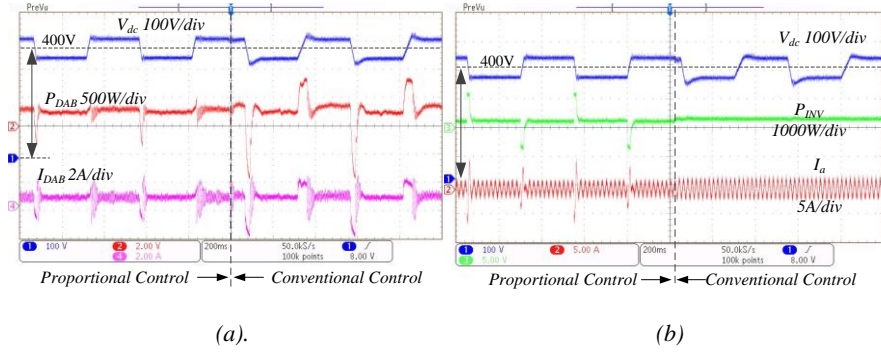
Fig. 5-17 Transition from proposed to conventional scheme with stepping dc link voltage reference V_{dc}^*. (a)DC-link voltage, DAB power and output current (b) DC-link voltage, inverter power and output current

are anticipated since the inverter shares the responsibility of controlling dc link voltage with the DAB.

Therefore, the experiment successfully verified the optimized features of the coordinate proportional control for the interface converter between dc active distribution network and the grid

5.5. CONCLUSION

In this chapter, the definition of control system type is introduced, and the analysis of conventional control schemes with PI voltage regulator is presented. For stability improvement, a coordinate proportional control scheme is proposed in this chapter.

With simply a proportional voltage controller, the proposed control scheme manages to maintain the dc link voltage with zero steady state error. Therefore, compared with conventional control schemes with PI voltage controller, the control system type number is reduced. The proportional controller saves the pole introduced by PI controller in conventional control, thus controller tuning is greatly simplified, and the stability is substantially improved.

CHAPTER 6. FRONT TO END IMPEDANCE CONTROL IN CASCADED AC-DC CONVERTER

In cascaded system, impedance interaction plays an important role in terms of the system dynamics and stability. Different control schemes result in different impedance behavior, such as the constant power converter, voltage mode converter. This chapter analyses the impedance behavior of typical voltage source converter, constant power converter, and proposes a conception, named front to end impedance control, which is capable to modify the front source converter and end load converter to present resistive low frequency impedance to the dc link, which can substantially improve the cascaded system stability. Also the proposed control method can adjust the cascaded system more bidirectional stable.

6.1. IMPEDANCE BEHAVIOR IN DC-DC   VOLTAGE MODE CONVERTER

Voltage source represents a two terminal device that is capable to maintain fixed output voltage [91]. Ideal voltage mode converter is assumed to maintain the output voltage constant, and its output voltage is independent of the load resistance or the output current. A practical industrial voltage source is the voltage mode converter, which operates with a specified output voltage, and aims to maintain this voltage constant. However, a practical voltage source converter cannot be totally independent of output current. For analysis, real-world voltage sources can be modeled as a combination of an ideal voltage source and an impedance element, which is the output impedance.

For voltage source converter, capacitor filter is necessary to hold the output voltage. To achieve zero steady state error, proportional and integral (PI) controller will be generally used regulate the voltage output. Inside the voltage control loop, there is normally the current functioning structure, which can be represented as the current loop. These common structures can be observed in typical voltage converter, such as the converters shown in Fig. 6-1, buck converter, boost converter, buck boost converter, rectifier, and dual active bridges converter [92, 93, 94].

Therefore, the general block diagram for voltage source DC converter can be illustrated as Fig. 6-2. In Fig. 6-2，$G_{i-plant}(s)$ is the transfer function of current functioning loop; $G_V(s)$ is the voltage controller transfer function, V_o is the

(a)Buck converter

(b) Boost converter

(c)Buck-boost converter

(d) Rectifier

(d)   Dual active bridge converter

Fig. 6-1 Typical voltage source converter scheme

        ----   *Voltage controller*
        ----   *Capacitor filter*
        ----   *Current function structure*
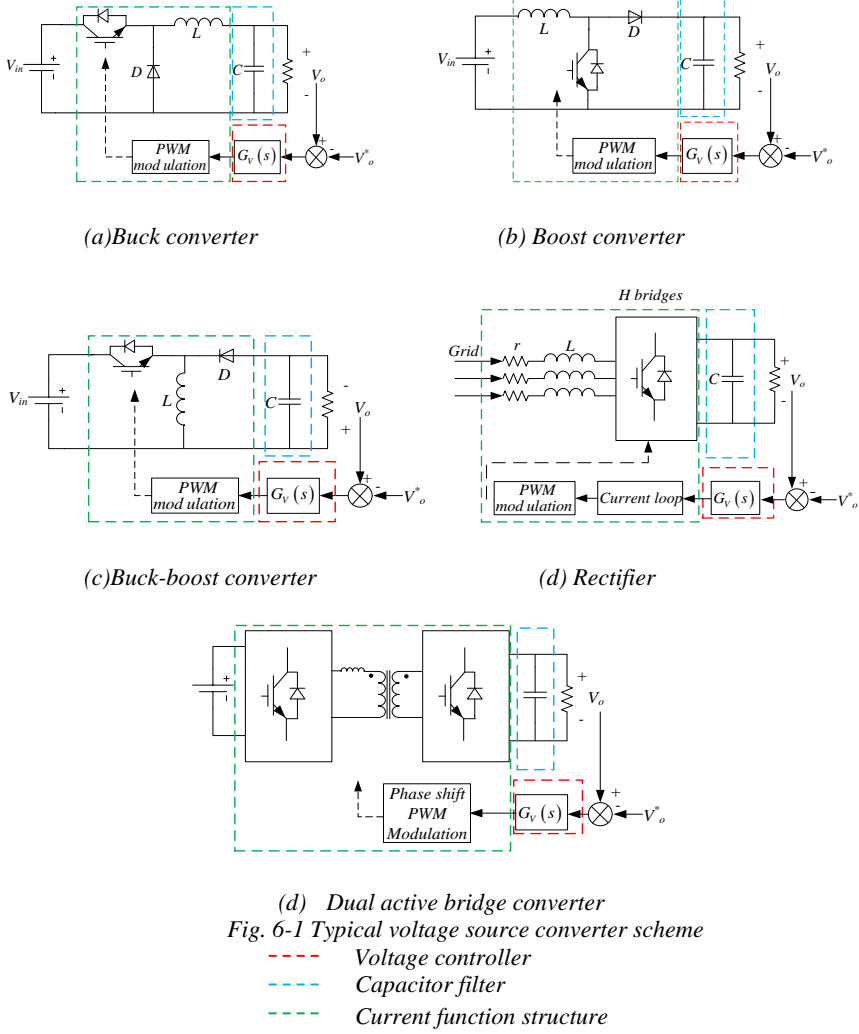
output dc voltage. The voltage output can be written as:

$$V_o(s) = V_o^* \frac{G_V(s)G_{i-plant}(s)}{Cs + G_V(s)G_{i-plant}(s)} - I_o \frac{1}{Cs + G_V(s)G_{i-plant}(s)} \tag{6.1}$$

And then the output impedance of PI controlled voltage source converter can be expressed as:

$$Z_o = \frac{1}{Cs + G_V(s)G_{i-plant}(s)} \tag{6.2}$$
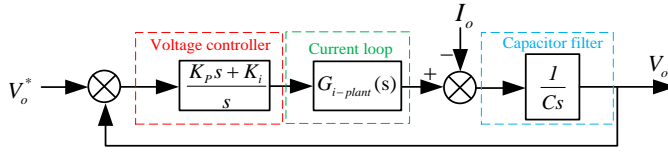
Fig. 6-2 Block diagram of DC/DC converter under voltage mode
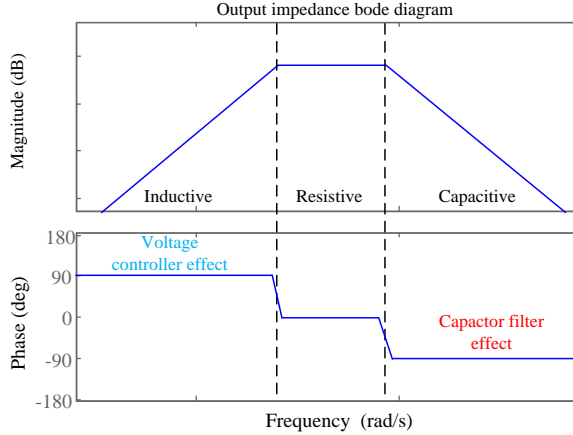
Fig. 6-3 Bode plots of impedance under voltage control

Normally, the inner current functioning loop is much faster than the outer voltage loop. For the analysis of the voltage loop performance, the inner current loop can be simplified as unit 1. Therefore the output impedance can be simplified as:

$$Z_V = \frac{1}{Cs + G_V(s)} \tag{6.3}$$

According to (6.3), the output impedance is greatly determined by the voltage controller $G_V(s)$ and the capacitor filter. Practically, PI controller is widely used in the voltage loop to eliminate steady state error. The transfer function of PI controller can be expressed as:

$$G_V(s) = \frac{K_P s + K_i}{s} \tag{6.4}$$

The bode plot of the output impedance is plotted in Fig. 6-3. As shown, the output impedance is generally inductive in the low frequency range, and capacitive in the high frequency range. The low frequency inductive feature is affected by the voltage controller, and the capacitive feature in high frequency is determined by the capacitor filter. This result is identical with references [95, 96, 97]. Therefore conclusion can be drawn that the voltage controller affects the output impedance of

low frequency range, and capacitor filter determines the high frequency range. The corner frequencies are related to the parameters and the filter capacitance value.

6.2. IMPEDANCE BEHAVIOR IN CURRENT AND POWER MODE CONVERTER

Current source refers to the device that can output or absorb a specified current. [98]. Ideal current source is assumed to maintain the terminal current constant, independent of the voltage cross it. A practical industrial current source is a current mode converter, operating with a specified current, and aims to maintain the output current constant. However, a practical current source converter cannot be totally independent of output voltage. For analysis, practical current source can be modeled as an ideal current source with parallel output impedance. When the current source absorbs power, this impedance is viewed as input impedance; while the current source delivers current, this impedance turns to the output impedance.

For the ideal current source converter, the impedance is assumed infinite. Actually, it is impossible to make the infinite characteristic. Moreover, in the power system, converter usually works in power mode, meaning that the current source is a voltage controlled current source.

In industry, a current source normally is an electric converter in current control. Therefore inductor filter in the power converter is necessary, and a current controller is implemented to regulate the output current [99, 100]. The output current is determined by the voltage difference between the two terminals of inductor filter, and the output of current controller is fed to a voltage functioning block, which is normally the modulation unit [101, 102]. These principles can be seen in Fig. 6-4 (a) and (b), the typical current source converter.

So when working as the load, the normal current source converter can be represented as Fig. 6-4. In Fig. 6-4, $G_i(s)$ is the current controller, $G_{V-plant}(s)$ is the functioning block between the output of current controller and the voltage in front of the inductor filter. For instance the current load converter, input current can be expressed as (6.5).

$$I_{in}(s) = V_{in} \frac{1}{Ls + G_i(s)G_{V-plant}(s)} + I^* \frac{G_i(s)G_{V-plant}(s)}{Ls + G_i(s)G_{V-plant}(s)} \tag{6.5}$$

Then the input impedance of current source converter is written as (6.6).

$$Z_{in}(s) = Ls + G_i(s)G_{V-plant} \tag{6.6}$$
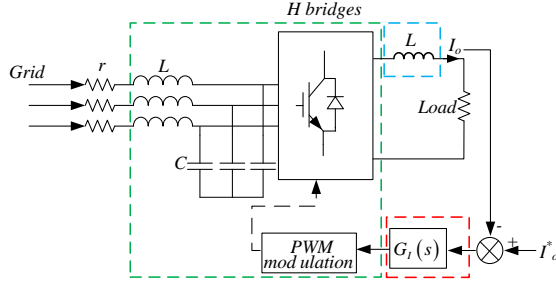
(a)   Current source rectifier
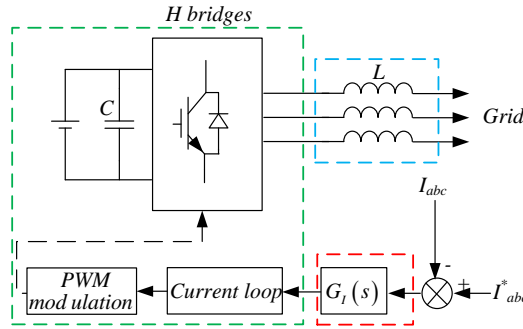
(b)   Current source inverter
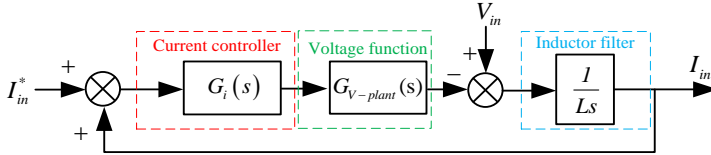
(c)   Block diagram of current source converter

Fig. 6-4 Current mode converter

- - - -   *Current controller*
- - - -   *Inductor filter*
- - - -   *Voltage function structure*

The input impedance of current mode converter is determined by the inductor filter (L) and the current controller $G_i(s)$. In the control loop, within control bandwidth $G_{V-plant}$ can be recognized as a proportional value.
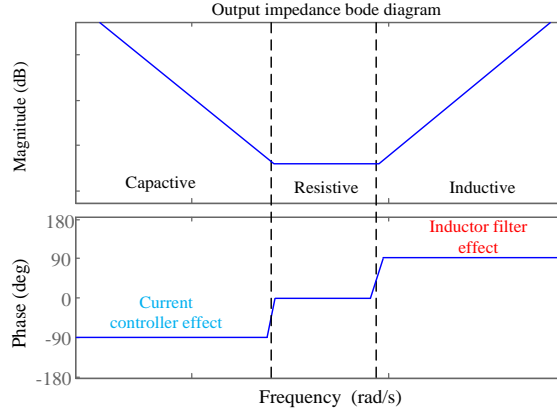
Fig. 6-5 Output impedance of current mode converter
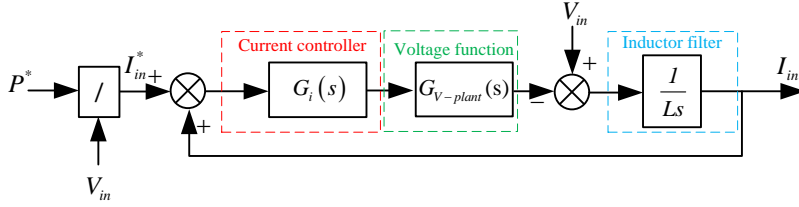
Fig. 6-6 Control block diagram of voltage controlled current source converter

Then the output impedance is:

$$Z_{in}(s) = \frac{Ls^2 + K_P s + K_i}{s} \tag{6.7}$$

Fig. 6-5 shows the bode plot of the current load converter. As shown, the output impedance of current load converter is capacitive in the low frequency part, and inductive in the high frequency part. This is because the PI current controller drives the low frequency impedance capacitive, and the inductor filter promotes the output impedance inductive in the high frequency part.

Fig. 6-6 shows the control block diagram of constant power load converter, and according to this, the input current can be expressed as:

$$I_{in}(s) = V_o \frac{1}{Ls + G_i(s)G_{V-plant}(s)} + \frac{P^*}{V_{in}} \frac{G_i(s)G_{V-plant}(s)}{Ls + G_i(s)G_{V-plant}(s)} \tag{6.8}$$
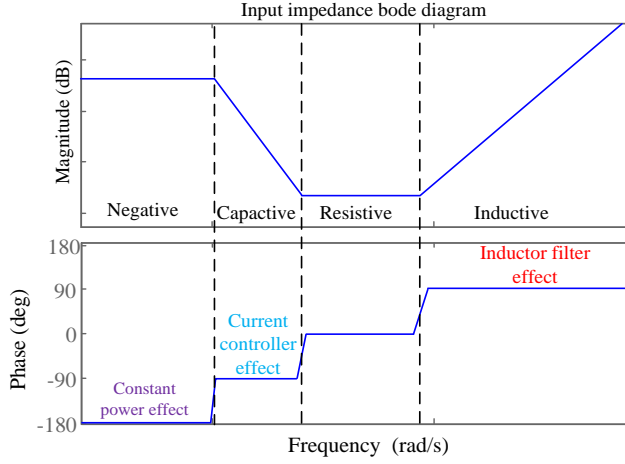
Fig. 6-7 Impedance bode plots of constant power converter input impedance

Also the voltage plant block can be recognized as unit 1 for simplified analysis. Then the input current can be expressed as:

$$I_{in}(s) = V_{in} \frac{1}{Ls + G_i(s)} + \frac{P^*}{V_{in}} \frac{G_i(s)}{Ls + G_i(s)} \tag{6.9}$$

Small signal can be obtained by:

$$I_{in}(s) + \Delta I_{in} = (V_{in} + \Delta V_{in}) \frac{1}{Ls + G_i(s)} + \frac{P^*}{V_{in} + \Delta V_{in}} \frac{G_i(s)}{Ls + G_i(s)} \tag{6.10}$$

Afterwards, the small signal of input impedance can be expressed as:

$$\frac{\Delta V_{in}}{\Delta I_{in}} = \frac{V_{in}^2 Ls + V_{in}^2 G_i(s)}{V_{in}^2 - P^* G_i(s)} \tag{6.11}$$

Fig. 6-7 shows the input impedance of the constant power converter. As shown, for constant power converter, the input impedance is -180° in the low frequency range, because of the constant power effect [103]; it goes to capacitive and inductive with the increasing of frequency. This spectrum indicates the impedance performance of the constant power converter. The -180° phase shift means that when the small

signal of input current will go against the small signal of input current. This is a destabilizing effect, explained as negative impedance instability [104].

6.3. INSTABILITY AND SOLUTIONS IN CASCADED CONVERTER

For the cascaded interface converter, conventional control methods use one sub converter to control the dc link voltage, and the other sub converter controls the load power. Regarding to the impedance interaction, the minor loop gain T_m can be written as:

$$T_m = \frac{|Z_o|\angle\theta_o}{|Z_{in}|\angle\theta_{in}} = |T_m|\angle\theta_T \tag{6.12}$$

Here the input and output impedance are written in the forms of magnitude and phase angle. If the source converter controls dc link voltage, it will be a voltage source converter, and load converter controls the fixed power, therefore it is constant power converter.

As previous analyzed, output impedance of voltage source converter is inductive in the low frequency part, where θ_o is 90°. The constant power converter is negative impedance in the low frequency range, where θ_{in} is -180°, so in the low frequency part, θ_T is 270°. In the high frequency part, θ_o is -90° and θ_I is 90°, then θ_T is -180°. Therefore θ_T ranges from 270° in the low frequency to -180° in the high frequency, which introduces significant phase shift to the overall system. If the load converter input impedance becomes small, which happens in high power occasion, or the source converter output impedance is large enough, meaning the source converter is slow and weak, then the instability phenomenon of T_m will appear[105].

6.3.1. RESISTIVE OUTPUT IMPEDANCE VS INDUCTIVE INPUT IMPEDANCE

As described in Chapter 4, for the CPL converter, when it works as the source, its output impedance can be obtained as Fig. 6-8.
The output current can be obtained as:

$$I_o(s) = V_o \frac{1}{Ls + G_i(s)G_{V-plant}(s)} - \frac{P^*}{V_o} \frac{G_i(s)G_{V-plant}(s)}{Ls + G_i(s)G_{V-plant}(s)} \tag{6.13}$$

The voltage function $G_{V-plant}(s)$ is recognized as a proportional value, and then the small signal modelling of current output can be obtained by:
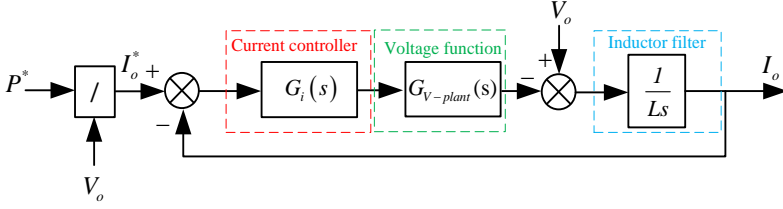
Fig. 6-8 Block diagram of constant power source converter
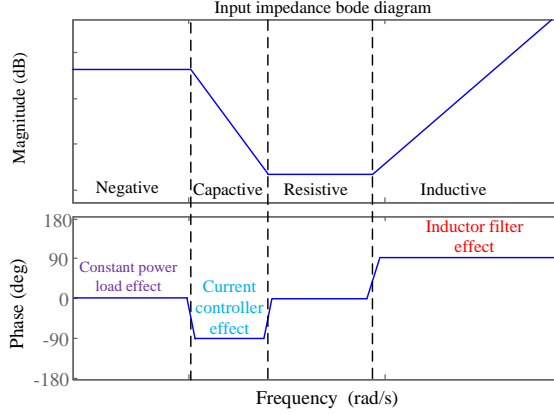
Fig. 6-9 Output impedance bode plots of constant power source converter

$$I_o(s) + \Delta I_o = \frac{P^*}{V_o + \Delta V_o} \frac{G_i(s)}{Ls + G_i(s)} - (V_o + \Delta V_o) \frac{1}{Ls + G_i(s)} \qquad (6.14)$$

Then the output impedance can be derived as:

$$Z_o = -\frac{\Delta V_o}{\Delta I_o} = \frac{V_o^2 Ls + V_o^2 G_i(s)}{P^* G_i(s) + V_o^2} \qquad (6.15)$$

The bode diagram of output impedance is shown in Fig. 6-9. As shown, when as the source, the negative impedance in the low frequency range is replaced by the resistive impedance.

If it is feasible to set the constant power converter as the source, and the voltage converter as the load, then the minor loop gain can be analyzed as:

$$T_m = \frac{|Z_{in}| \angle \theta_{in}}{|Z_o| \angle \theta_o} = |T_m| \angle \theta_T \tag{6.16}$$

In the low frequency range, $\theta_o = 0$, $\theta_{in} = 90°$, then θ_T is 90°. In the high frequency part, θ_o is 90°, and the voltage mode converter is capacitive, θ_{in} is -90°, therefore in the high frequency range, θ_T is -180°. In conclusion, θ_T ranges from 90° in low frequency to -180° in high frequency, much smaller than that condition in conventional control, from -270° to 180°. So setting the constant power converter at the source point can make the system more stable than deploying it as the load. However this can only be applied in unidirectional power flow, not suitable for bidirectional power flow, because the reversed power flow will bring back the instable negative impedance.

6.3.2. INDUCTIVE OUTPUT IMPEDANCE WITH RESISTIVE INPUT IMPEDANCE
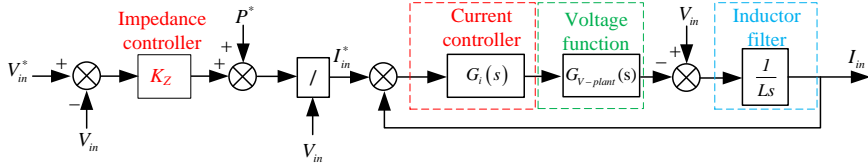
Fig. 6-10 Implementation of impedance controller on the constant load power converter

Another solution is to modify the negative impedance of constant power converter to resistive impedance through an impedance controller. The block diagram is shown in Fig. 6-10.

If the impedance controller is designed with a proportional value, then in the low frequency range, considering the small signal, input current can be expressed as:

$$I_{in}(s) + \Delta I_{in}(s) = (V_{in} + \Delta V_{in}) \frac{1}{Ls + G_i(s)} - \frac{(P^* - K_Z \Delta V_{in})}{V_{in} + \Delta V_{in}} \frac{G_i(s)}{Ls + G_i(s)} \tag{6.17}$$

Then small signal can be written as:

$$\Delta I_{in}(s) = \Delta V_{in} \left(\frac{1}{Ls + G_i(s)} - \frac{I_{in}^* - K}{V_{in}} \frac{G_i(s)}{Ls + G_i(s)} \right) \tag{6.18}$$

Therefore the input impedance can be expressed as:

$$Z_{in} = \frac{\Delta V_{in}}{\Delta I_{in}} = \frac{Ls + G_i(s)}{V_{in} - G_i(s)\left(I_{in}^* - K\right)} \tag{6.19}$$

If $K > I_{in}^*$, then $Z_{in} > 0$, meaning that the input impedance is resistive and the bode plot is shown in Fig. 6-11, where it is resistive in the low frequency and inductive in the high frequency. The impedance interaction minor loop gain is expressed as:

$$T_m = \frac{|Z_o|\angle\theta_o}{|Z_{in}|\angle\theta_{in}} = |T_m|\angle\theta_T \tag{6.20}$$

The two impedances are shown in Fig. 6-3 and Fig. 6-11, and then in the low frequency range, $\theta_o = 90°$, $\theta_{in} = 0$, so $\theta_T = 90°$. In the high frequency range, $\theta_o = -90°$, $\theta_{in} = 90°$, then $\theta_T = -180°$. Therefore θ_T ranges from $90°$ in the low frequency to -180° in the high frequency. Compared with conventional control, the phase shift variation is reduced, so the system is more stable.

But still, in the low frequency range, the impedance interaction also introduce 90 degree phase shift, which introduced negative effect on the system stability. This phase shift is introduced by the front source converter, so the front to end impedance control is proposed in this chapter.
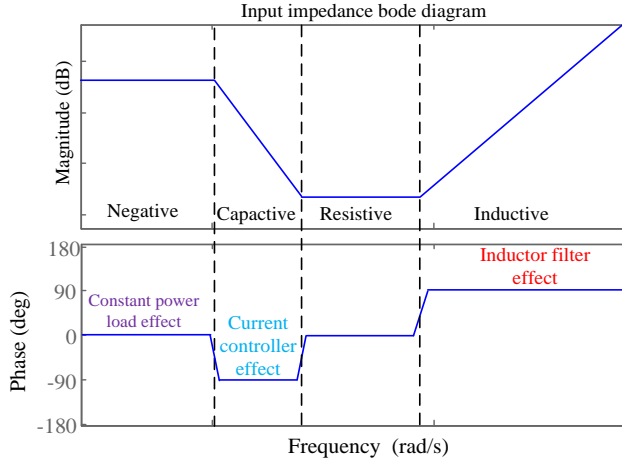
Fig. 6-11 Input impedance bode plots of constant power load converter with the impedance

6.4. FRONT TO END IMPEDANCE CONTROL

Conventional solutions only focus on the adjustment of single converter [106,107], but low frequency phase shift still exist. Therefore this chapter proposed the concept of front-to-end impedance control. The proposed concept aims to modify not only the impedance of end load converter, but also the front source converter. Both the impedance of sub converters, towards the dc link, behave as resistive impedance in the low frequency range, then the phase shift in low frequency becomes 0. At the same time, the reference power flow can also be guaranteed. The control scheme is shown in Fig. 6-12.

As shown Fig. 6-12, two impedance controllers are respectively implemented in the source and load sub system. In the source converter, conventional PI controller is replaced by a proportional impedance controller, and the power reference is shared between the load converter with the source converter. P^* is responsible for

controlling the transferred power, and the front-to-end impedance controllers regulate the intermediate dc link voltage. Therefore the constant power flow and rated dc link voltage still can be maintained. Even the impedance controllers are proportional, zero steady state error can still be achieved, because the front-to-end structure, which has be described in Chapter 5.

The front and end impedance controllers are designed with proportional value to make the front output impedance and end input impedance both resistive. For the load sub system, the end impedance controller K_{ZL} should be greater than the rated DC-link input current, as (4.29), because this can ensure the resistive impedance of load subsystem. The K_{ZL} is selected with 3-5 times of the rated DC-link input current, because over large values will greatly decrease the input impedance; for the
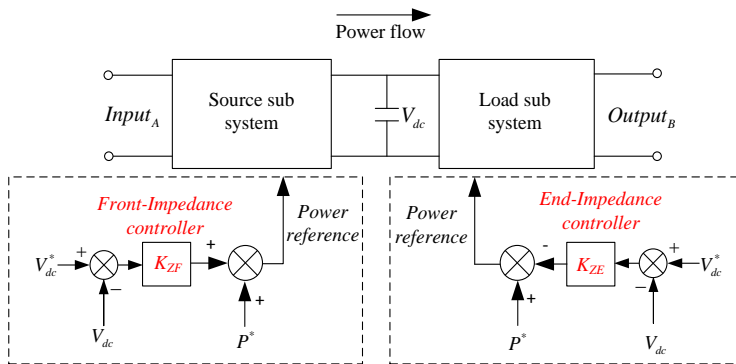
Fig. 6-12 Control scheme of front-to-end impedance controller

source sub system, the front impedance controller is designed with the maximum value within the stability area, because DAB output impedance is the smaller the better. Then the minor loop gain becomes:

$$T_m = \frac{|Z_o|\angle\theta_o}{|Z_{in}|\angle\theta_{in}} = |T_m|\angle\theta_T \qquad (6.21)$$

With resistive low frequency output and input impedance, $\theta_o = 0$ and $\theta_{in} = 0$, so the low frequency phase shift of minor loop gain (θ_T) in is 0. The filters remain the same, so θ_T in the high frequency part remains 180°.

The compared phase shift of minor loop gain θ_T are shown in the following table. As shown, the high frequency impedance phase shift is the same 180°, because they have the same output filter. In the low frequency range, conventional control introduces -270° phase shift, and it can be reduced to 90° or -90° in the adjustment method of single converter, but in the proposed front to end impedance control method, the low frequency phase shift is 0°, meaning that there is no phase shift. Therefore the system in the proposed control is more stable than previous conditions.

Table 6-1 Simulation Parameters for Bidirectional interface converter

Control method	Impedance feature	General phase shift of minor loop gain	
		Low frequency	High frequency
Conventioanl control	Inductive output impedance and Negative input impedance)	-270°	180°
Setting constant power converter as a source	Resistive output impedance and inductive input impedance	-90°	180°
Single impedance controller on the constant power converter	Inductive output impedance and Resistive input impedance	90°	180°
Coordinate front-to-end impedance control	Resistive output impedance and Resistive input impedance	0°	180°

6.5. DEMONSTRATION IN THE INTERFACE CONVERTER

6.5.1. ANALYSIS OF CASCADED DAB AND INVERTER
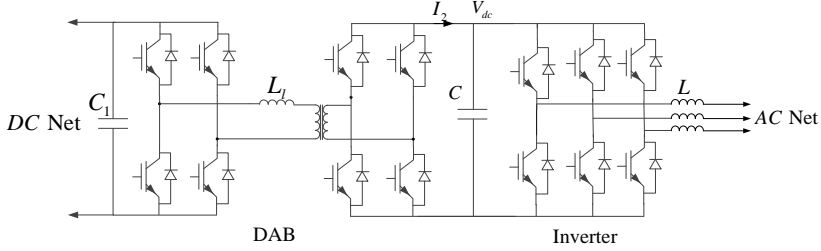
Fig. 6-13 Topology of the cascaded converters system

In this part, the front to end impedance control method will be demonstrated in the following topology, as shown in Fig. 6-13, interface converter between dc active distribution network and the power grid.

The compared control methods afore mentioned are shown in Fig. 6-14. Fig. 6-14 (a) shows the conventional control, in which DAB controls the DC-link voltage and inverter controls the power, so DAB low frequency output impedance is inductive, and inverter input impedance is negative. DAB output impedance and inverter input impedance has been modelled in Chapter 3.

(a)Conventional Control

DAB control DC-link voltage V_{dc}

Voltage Controller

Current Controller

V_{dc}^* + −

$G \cdot \dfrac{K_{P-V}s + K_{i-V}}{s}$

$\dfrac{K_{P-i}s + K_{i-i}}{s}$

φ

V_{dc}

Low pass filter ← I_2

Inverter controls power P^*

Impedance controller

V_{dc}^* + − K_Z −

P^* V_d I_d^*

PI Controller + D_d −

I_d ωL

I_q ωL

I_q^*

$Q^* = 0$ / PI Controller + D_q +

$-U_d$

DQ/abc PWM

(b) Single impedance controller implementation

DAB control unit

Front-Impedance controller

P^*

Current Controller

V_{dc}^* + − K_{Z-F} − + / I_L^* +

V_{dc} V_{dc}^* $\dfrac{K_{P-i}s + K_{i-i}}{s}$ D

Low pass filter ← I_L

Inverter control unit

V_{dc}^* + − K_{Z-E} −

End-impedance controller

V_{dc} P^* V_d I_d^*

PI Controller + D_d −

I_d ωL

I_q ωL

I_q^*

$Q^* = 0$ / PI Controller + D_q +

$-U_d$

DQ/abc PWM

(c) Coordinative front-to-end impedance control

Fig. 6-14 Control block diagram under different control methods

A simple way to set the constant power converter as the source converter is to change the power flow direction in conventional control, which is verified in Chapter 3. Relevant impedance modelling can also be checked in Chapter 3.

The coordinate front-to-end impedance control is shown in Fig. 6-14 (c). Previous PI controller in the voltage loop is replaced by the impedance controller, and power reference feed forward path is also introduced. The inverter input impedance is the same as in Fig. 6-14 (b). The front DAB impedance to the dc link can be obtained by:

$$Z_{DABo}^* = \frac{1}{Cs + K_{ZF}G_{DAB-I}} \tag{6.22}$$

Then the impedance minor loop gain can be obtained as:

$$T_{m-4} = \frac{Z_{DABo}^*}{Z_{INV-in}^*} \tag{6.23}$$

Viewed from the dc link voltage, the bode plots of DAB and inverter impedance in afore mentioned control methods are shown in Fig. 6-15.

Fig. 6-15 (a) shows the impedance of conventional control in forward power flow. As shown, inverter input impedance is negative in the low frequency range, and inductive in high frequency part; DAB output impedance is inductive in the low frequency range, and capacitive in the high frequency range. In reversed power flow, inverter output impedance is resistive in the low frequency range. The plotted curves match the predicted analysis well. Fig. 6-15 (b) shows the impedance bode plots with an impedance controller implemented on the inverter, and it shows that inverter input impedance is resistive in the low frequency range, and inductive in high frequency range, which is much different from that the conventional control in Fig. 6-15 (a).

Fig. 6-15(c) shows bode plots of the proposed coordinative front-to-end impedance control, where both the DAB and inverter present resistive impedance to the dc link voltage within the low frequency range, and the high frequency range impedances are determined by their filter, that is DAB capacitive and inverter inductive.
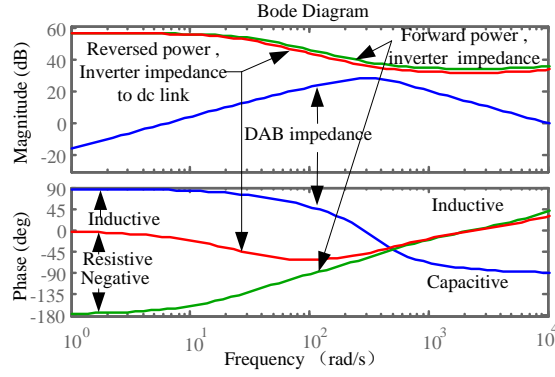
(a)Conventional control
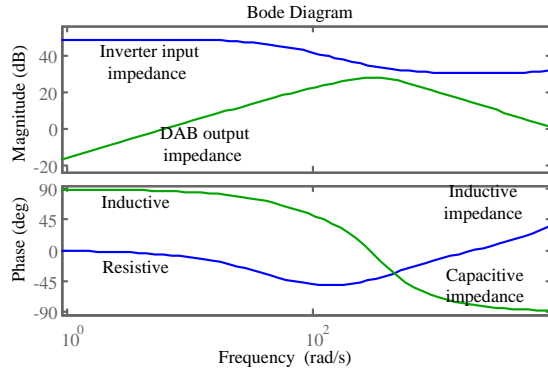
(b)Single impedance controller on the CPL converter
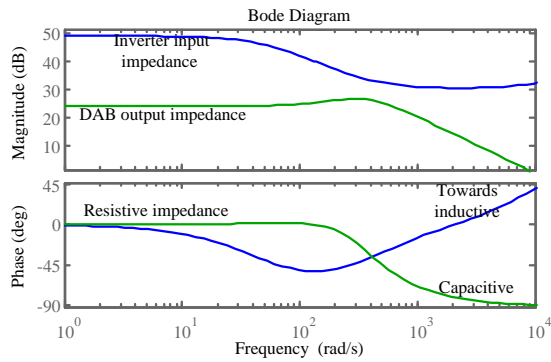
(d)   Coordinative front-to-end impedance control

Fig. 6-15 Bode plots of output and input impedance in different control methods

(a)Conventional control - forward power flow *(b) Conventional control - reverse power flow*

(c)Inverter with Impedance control *(d) Coordinate front-to-end impedance control*
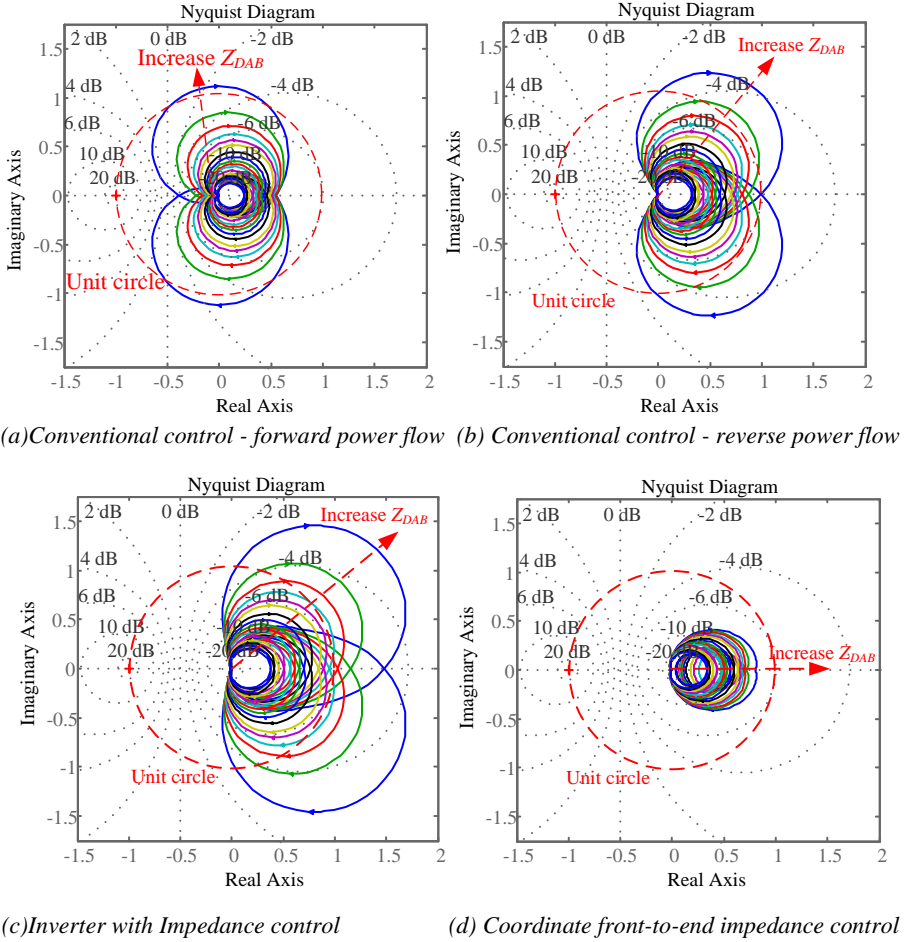
Fig. 6-16 Minor loop gain Nyquist plots with different control methods

Fig. 6-16 shows the Nyquist plots under different control methods, in which, DAB voltage controller gain in Fig. 6-14 (a), (b) and impedance controller in Fig. 6-14 (c) reduces from 1.2pu to 0.07pu, because this can increase the impedance of the DAB converter, meaning that the DAB converter becomes weaker, which will deteriorate the system stability, therefore the stability difference will be appear.

As shown in Fig. 6-16 (a), in forward power flow of conventional control, when increasing DAB output impedance, the Nyqusit plot of minor loop gain are approaching the unstable point (-1,0), indicating that the stability tends to be unstable.

In Fig.6-16 (b), when the power flow is reversed, the Nyquist plots still stay away from the unstable point (-1,0), meaning that under the same condition, the system is still stable in reversed power flow. So system stability in reversed power flow is more stable than that in forward power flow.

In Fig.6-16 (c), with the implementation of impedance controller on the inverter, it can be seen that the system also stay away from the unstable point (-1, 0). While in Fig.6-16 (d), in the coordinate front-to-end implementation control, the Nyqusit not only stay away from the unstable point, but also remain within the unit circle, meaning that the system is more stable than previous 3 control methods[108].

In the coordinate front-to-end impedance control, the impedance interaction is more decoupled, therefore the cascaded interface converter is more stable.

6.5.2. SIMULATION AND EXPERIMENT VERIFICATION

6.5.2.1 Simulation

Fig. 6-17 shows the measured impedances of DAB and inverter under the proposed coordinate front-to-end impedance control. As shown in Fig. 6-17 (a), the DAB output impedance is resistive in the low frequency range, and capacitive in the high frequency range. The measured results match the predicted curves well. In Fig. 6-17 (b), the inverter input impedance is also resistive in the low frequency, and goes to inductive in the high frequency. The measured results match the predicted results well.

In following simulation, the power reference is a periodic step-changing signal, between -5kW and 5kW. The DAB voltage controller and impedance controller are intentionally reduced to deteriorate the stability.

Fig. 6-18 shows the bidirectional simulation results of conventional control. As shown, in conventional control, with inductive output impedance and negative input impedance, there are significant oscillations in both DAB and inverter power outputs and the dc link voltage. But when the power flow is reversed, -5kW, with the resistive output impedance and inductive input impedance, the oscillations are much smaller, and system becomes stable quickly. So this can verify that under the same condition, with resistive output impedance and inductive impedance, system is more stable than that in the inductive output impedance with negative input impedance.

(a)   Front DAB output impedance

(b)End inverter input impedance
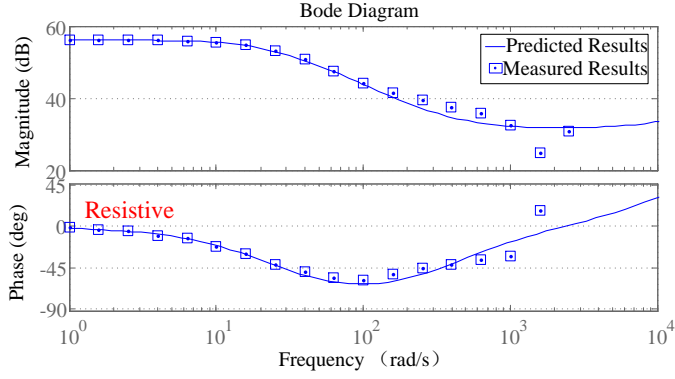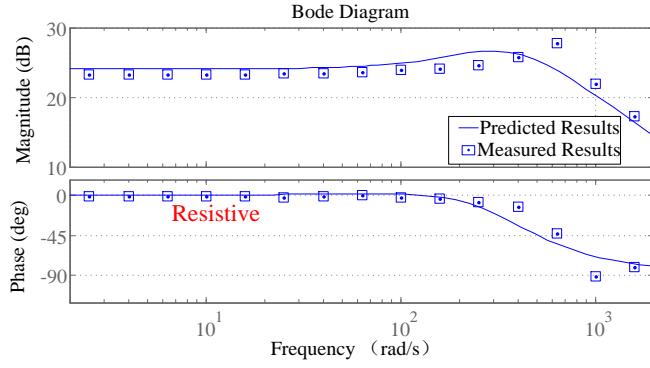
Fig. 6-17 Sub converter impedance with coordinate front-to-end impedance
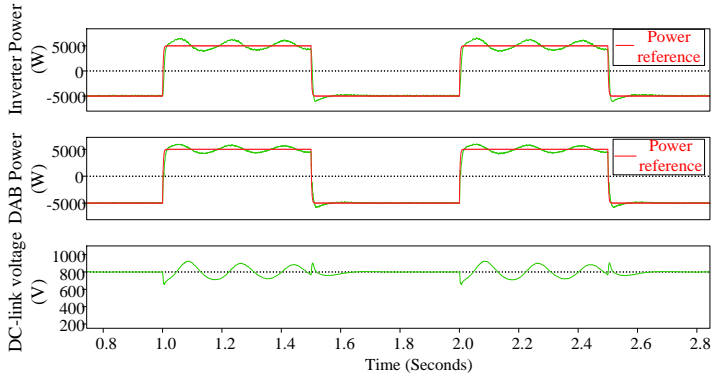
Fig. 6-18 Bidirectional simulation results of conventional control
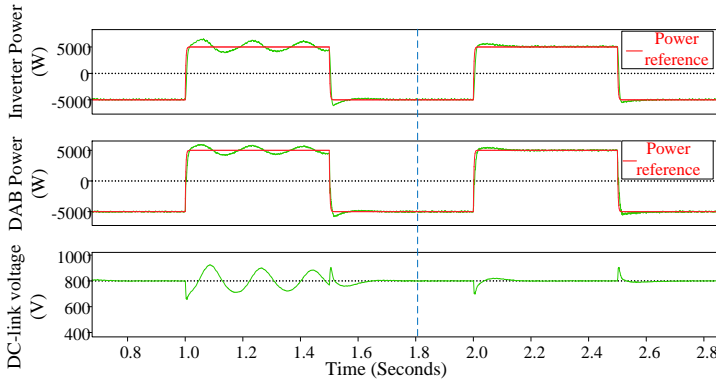
Fig. 6-19 Bidirectional simulation results of conventional control and single impedance controller

Fig. 6-19 shows the simulation results of the conventional control and the single impedance controller method. As shown, before 1.8s, the control is conventional control, and after 1.8s, single impedance control method is activated. With the implementation of impedance controller on inverter, inverter low frequency impedance is resistive to the dc link voltage. It can be seen that the adding of impedance controller make the oscillation much less than conventional control. It proves that with inductive output impedance and resistive input impedance, system stability is better than inductive output impedance with negative input impedance. And also the impedance control on the negative impedance converter can make the inverter present resistive low frequency impedance to dc link voltage, added that DAB impedance remains inductive and inverter impedance remains resistive in both forward and reversed power flow, so this control more suitable for bidirectional application than conventional control.

Fig. 6-20 shows the simulation results of single impedance control and the proposed front-to-end impedance control. The two control methods are tested under the same condition. The DAB voltage controller is a PI controller in conventional control and P controller in the proposed control, where the proportional parameters are the same. As shown, single impedance controller is used before 1.4s, and after 1.4s, the proposed coordinate front-to-end impedance control is activated. As shown, the proposed control can make the power output of DAB and inverter track the reference more quickly, and the dc link voltage is also more stable than single impedance controller method.

The simulation results show that: In conventional cascaded connection, the impedance combination of inductive source output impedance and negative load input impedance will introduce instability factor to the system. The method that changes the impedance combination to resistive output impedance with inductive input impedance or inductive output impedance with resistive input impedance can
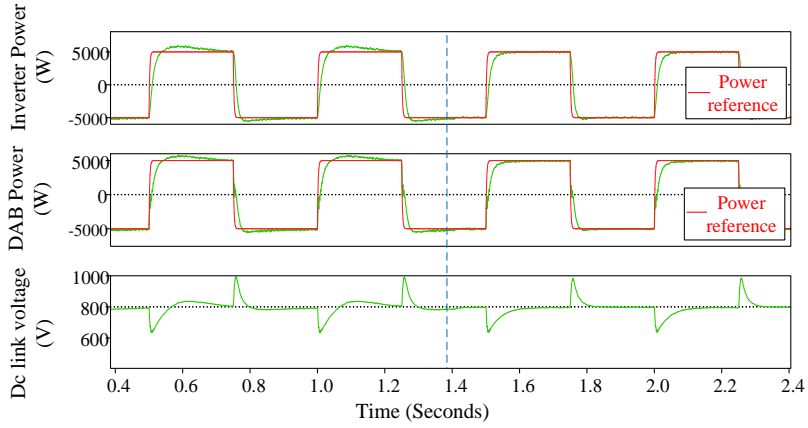
Fig. 6-20 Bidirectional simulation results of single and double impedance controller

improve the system stability. The proposed front-to-end impedance control can improve the system stability one step further, since the output impedance and input impedance are both resistive.

6.5.2.2 Experiment

In the experiment, the power reference wave is a periodic square waves stepping between 400W and -400W. In the experiment, the DAB voltage controllers and DAB impedance controllers (K_{Z-s}) are intentionally reduced to deteriorate the system stability. The experiment results are shown in following figures.

Fig. 6-21 shows the experimental results of conventional control. As shown, when the power output is 400W, the oscillations and dynamic performance is much worse than the reversed power flow, which means that with resistive output impedance
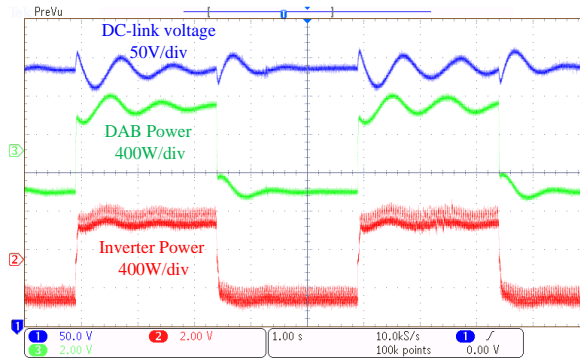
Fig. 6-21 Experiment results of conventional control
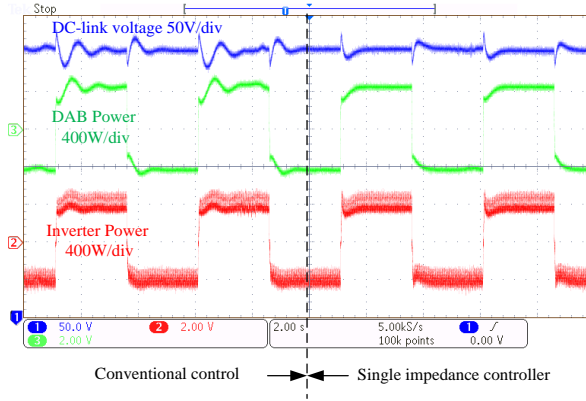
Fig. 6-22 Bidirectional of conventional control and single impedance controller
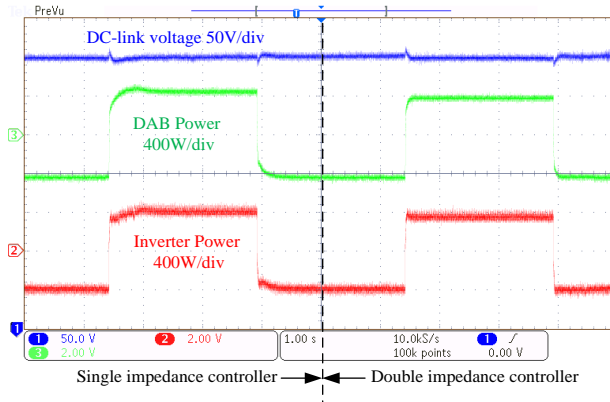
Fig. 6-23 Bidirectional control of single impedance controller and double impedance controller

and inductive input impedance, system will be more stable than that of inductive output impedance with negative input impedance.

Fig. 6-22 shows the experiment results of conventional control and single impedance controller method. As shown, with the implementation of single impedance controller on the inverter, oscillations in both forward power flow and reversed power flow is more damped than conventional control. The impedance controller changes the negative input impedance to resistive impedance, and this can make the system more stable.

Fig. 6-23 shows the comparing results between single impedance controller and the proposed front-to-end impedance controller. As shown, under the same condition,

in the proposed front-to-end impedance control, dynamics of DAB and inverter power output are much better than single impedance controller method, indicating.

that under the same condition, the proposed control is more stable than the single impedance controller method.

So conclusion can be drawn that, in the proposed front-to-end impedance control, the system is more stable than conventional control and single impedance controller method, because the source converter output impedance and load converter input impedance are both resistive in the low frequency range, which introduces minimum impedance phase shift to the cascaded system.

6.6. CONCLUSIONS

This chapter analyses the impedance interaction in cascaded converter systems, and it shows that using the constant power converter as the source can get rid of the low frequency negative impedance, which can make the system more stable, but it is only suitable for unidirectional power flow. An impedance controller can be implemented for the CPL converter, and it can change the negative impedance of CPL converter to resistive, which can greatly decouple the impedance interaction in both the power flow directions.

The front-to-end impedance control method is proposed, and it can drive the output impedance of source converter in low frequency part from inductive to resistive, as well as drive the input impedance of constant load converter from negative to resistive, thus the impedance interaction can be decoupled one step further. The conclusions have been analyzed with Nyquist plots, as well as bode plots. Simulation and experiment results are also offered to prove the correctness of the conclusion.

CHAPTER 7. CONCLUSIONS AND OUTLOOK

7.1. CONCLUSIONS

In this dissertation, control methods for the cascaded interface converter of dc active distribution network have been investigated and explored. This dissertation offers the following works to improve the performance of the interface converter:

- Active power and dc link voltage coordinative control. The coordinative control employs the inverter and DAB to share the responsibilities of dc link voltage control and power output regulation. It can reduce the dc link voltage fluctuations and provides more effectively damping with better stability. Therefore the required volume of dc link capacitors can be decreased, and the stress on the switching components can be reduced.

- The bidirectional impedance interactions in cascaded converter have been analyzed. Without changing control schemes, different power flow direction gives rise to different impedance interaction. Generally, the interaction is less stable when a voltage-controlled sub converter supports a power-controlled elementary converter. This sensitive interaction must be considered when designing control schemes for bidirectional applications of the cascaded converter. In unidirectional power flow application, the source converter and load converters should preferably be power- and voltage-controlled, respectively, since they give rise to a more stable and robust impedance interaction.

- The impedance controller can be implemented to cooperate the impedance of CPL converter to get rid of the low frequency negative impedance, improving the cascaded system stability. The implementation of impedance controller on constant power load converter can make the impedance interaction more similar between forward and reversed power flow, and gives the cascaded system more robust and stable feature. So in the occasion of constant power converter, the impedance control method can be considered to improve the system stability.

- A coordinated-proportional control scheme for cascaded converter has been proposed in this dissertation. Different from conventional scheme, DC-link voltage regulation only needs a proportional controller, but capable with zero steady-state error. Therefore overall system type is reduced, contributing with faster dynamic, more decoupling characteristic. Moreover, the proposed control helps to spread

oscillatory stresses between cascaded sub converters, hence avoiding the single point of failure associated with the conventional scheme.

- Setting the constant power converter as the source can get rid of the low frequency negative impedance, making the system more stable, but it is only suitable for unidirectional power flow. The impedance controller for the CPL converter can change the negative impedance of CPL converter to resistive, greatly decoupling the impedance interaction in both the power flow directions. But still there is space for improvement, so that the concept of coordinative front-to-end impedance control method is proposed in this dissertation, and it can drive the source converter low frequency output impedance from inductive to resistive, as well as drive the input impedance of constant load converter from negative to resistive, thus can decouple the impedance interaction one step further and contribute to a more stable cascaded system than before.

7.2. OUTLOOK

In this thesis cascaded interface converter control methods were discussed and evaluated. Further research would go on in two aspects: one is that, the individual control of a single converter would be investigated in a more detailed way to optimize the impedance behavior, being friendly to the utility grid, and the other would go to investigate the impedance stability in a multi converter system in the distribution system.

The following points for future research are presented:

- Effective modelling and connection analysis between the power flow character and the impedance stability of power electronic devices, and improvement methods for power electronic converters with flexible power processing ability.
- Implementation of the impedance theory. Flexibly and creatively apply it in the multi-terminal network system. Methods for characterizing the network impedance will be investigated for forecasting the performance of the network. Then accordingly control methods will be developed for improving the system performance. The active element in the network will be key considerations, such as the distributed generations, energy storage systems, and controllable loads.
- Creation of energy hub in distribution level of power network. The bidirectional multi terminal power conversion system, as the energy hub system. The internal stability representing the stability of the energy hub itself, and the external stability is to be friendly and supportive to the main utility grid. The capability of the energy hub will be investigated for the compensation of the vulnerable and inertia less character of the renewable

energy based generations. Generally, the energy hub is capable to parent and promote its connected green power based element, such as the PV systems, wind power, and storage system.

-

APPENDIX A:

Controller Parameters

Parameter	Value
DAB power loop, K_{P-DAB}	0.0001
DAB power loop, K_{i-DAB}	0.0105
DAB switching frequency	10 kHz
DAB control bandwidth	1884 rad/s
Inverter current loop, K_{P-inv}	20
Inverter current loop, K_{i-inv}	500
Inverter switching frequency	10 kHz
Inverter control bandwidth	1570 rad/s

Simulation Parameters

Parameter	Value
DAB input voltage	*400V*
Dc link voltage	*800V*
DAB leakage inductance	200uH
DAB switching frequency	10k Hz
Inverter inductor filter	3mH
AC grid voltage	*311V(phase)*
Inverter switching frequency	10 kHz

APPENDIX B:

Experiment Parameters

Parameter	Value
DC voltage (V_1)	130V
DC link voltage (V_2)	400V
Ratio for DAB Transformer	1:3
Transformer leakage inductor	200uH
Middle DC Capacitors	300uF
AC voltage (V_{grid})	150V
Inductor of LC filter	3mH
Inductor between Inverter and grid	3mH
Switching Frequency	10kHz

LITERATURE REFERENCE

[1]   From the website (2015), World Energy Needs and Nuclear Power[Online], Available:http://www.world-nuclear.org/info/Current-and-Future-Generation/World-Energy-Needs-and-Nuclear-Power/.

[2]   K. Gadi, "Cities VIII: Cities: Energy gluttons: A review of the energy demands and constraints that will be impressed upon our cities in future decades," Spectrum, IEEE, Volume:13 , Issue: 7, 1976.

[3]   L. Orr, Changing the World's Energy System, Stanford University Global Climate & Energy Project, 2005.

[4]   O. Ellabban, H. Abu-Rub, F. Blaabjerg, "Renewable energy resources: Current status, future prospects and their enabling technology." Renewable and Sustainable Energy Reviews, Vol.39, November (2014).

[5]   From the website: (25-Jun-2010), History of Solar Energy in California, [Online]. Available：http://www.gosolarcalifornia.ca.gov/about/gosolar/california.php

[6]   From the website(2015), APS NEWS: This month in Physics History [Online]. Available:http://www.aps.org/publications/apsnews/200904/physicshistory.cfm

[7]   F. M. Smits, "History of silicon solar cells." IEEE Transactions on Electron Devices, Volume:23 , Issue: 7, July. 1976.

[8]   From Wikipedia, Solar power in Spain [Online]. Available: https://en.wikipedia.org/wiki/Solar_power_in_Spain.

[9]   H. Yan, Z. Zhou, H. Lu, "Photovoltaic industry and market investigation." International Conference on Sustainable Power Generation and Supply SUPERGEN '09, Nanjing, 2009

[10]   A. Bruger, (2015), Report Confirms: 2015 is(Yet Another) Big Year for Solar[Online]; Available:http://www.triplepundit.com/2015/06/report-confirms-2015-yet-another-big-year-solar/.

[11]   J. S. Hill, (2015), Mercom Forecasts 2015 Global Solar Installations To Reach 57.4GW [Online], Available: http://cleantechnica.com/2015/06/17/mercom-forecasts-2015-global-solar-installations-reach-57-4-gw/.

[12]   T. J Price, "James Blyth - Britain's First Modern Wind Power Engineer." Wind Engineering, Vol: 29, NO. 3, May, 2005.

[13]   J. S. Hill, (2015) Global Wind Industry Grows 44% In 2014 [Online], Available: http://cleantechnica.com/2015/02/10/global-wind-industry-grows-44-2014/.

[14]   P. C. Loh, D. Li, Y. K. Chai, F. Blaabjerg, "Hybrid AC-DC Microgrids With Energy Storages and Progressive Energy Flow Tuning ," IEEE Transactions on Power Electroncis, vol. 28, no. 4, Apr, 2013.

[15]   J. M. Guerrero, J. Matas, L. G. D. Vicuna, M. Castilla, J. Miret. "Decentralized Control for Parallel Operation of Distributed Generation Inverter Using Resistive Output Impedance." IEEE Transactions on Industrial electronics, Vol.54, NO.2, April, 2007.

[16]   US. Department of Energy (2015), National Electric Transmission Congestion Studies [Online],Available:http://energy.gov/oe/services/electricity-policy-coordination-and -implementation /transmission-planning/national.

[17]   IEEE Application Guide for IEEE Std 1547(TM), IEEE Standard for Interconnecting Distributed Resources with Electric Power Systems. 1547.2-2008.

[18] V. F. Martins, C. L. Borges, "Active Distribution Network Integrated Planning Incorporating Distributed Generation and Load Response Uncertainties," IEEE Transactions on Power System, Vol. 26, NO. 4, Nov. 2011.

[19] F. Pilo, G. Celli, S. Mocci, G. G. Soma, "Active Distribution Network Evolution in Different Regulatory Environments," in proc. of 7th Mediterranean Conference and Exhibition on Power Generation, Transmission, Distribution and Energy Conversion. Agia Napa, 7-10 Nov, 2010.

[20] C. D. Adamo, S. Jupe, C. Abbey, "Global survey on planning and operation of active distribution networks—update of cigre C6.11 working group activities," in proc. of 20th International Conference and Exhibition on Electricity Distribution - Part .1, Prague, Czech Republic, 8-11 June. 2009.

[21] S. Shah, R. Hassan, J. Sun, "HVDC Transmission System Architectures and Control – A Review," in Proc. of 2013 IEEE 14th Workshop on Control and Modeling for Power Electronics (COMPEL), Salt Lake City, UT, 23-26 June 2013.

[22] C. Cho, J. Jeon, J. Kim, "Active Synchronizing Control of a Microgrid." IEEE Transactions on Power Electronics, Vol. 26, NO. 12, December 2011.

[23] T. Esram, P. L. Chapman, "Comparison of Photovoltaic Array Maximum Power Point Tracking Techniques." IEEE Trans on Energy Conversion, Vol. 22, NO. 2, June 2007.

[24] M. Meinhardt, G. Cramer, "Past, present and future of grid connected photovoltaic- and hybrid power-systems." in Proc. Of IEEE Power Engineering Society Summer Meeting, pp. 1283–1288. Seattle, WA, 16-20 July. 2000.

[25] C. Zhao, C. Guo, "Complete-Independent Control Strategy of Active and Reactive Power for VSC Based HVDC System." In proc. of Power & Energy Society General Meeting, Calgary, AB, 26-30 July 2009.

[26] R.H. Lasseter, "MicroGrids." in Proc. of Power Engineering Society Winter Meeting, 2002.

[27] 1547TM IEEE Standard for Interconnecting Distributed Resources with Electric Power Systems.

[28] T. Ackermann, G. Andersson, L. Soder, "Distributed generation: a definition." Electric Power Systems Research,Vol. 57, Issue 3, pp 195–204, April 2001.

[29] F. Blaabjerg, A. Consoli, J. Ferreira, J. D. V. Wyk, "The Future of Electronic Power Processing and Conversion," IEEE Transactions on Industry Application, Vol. 41, NO. 1, January/Februry 2005.

[30] D. Boroyevich, I. Cvetkovic, D. Dong, R. Burgos, F. Wang, F. Lee, "Future Electronic Power Distribution Systems-A contemplative view." in Proc. of 12th International Conference on Optimization of Electrical and Electronic Equipment (OPTIM 2010), Basov, 20-22 Ma 2005.

[31] D. Dong, F. Luo, X. Zhang, D. Boroyevich, P. Mattavelli, "Part One: High-Density Two-Stage Topology." IEEE Transactions on Power Electronics, Vol. 28, NO. 4, April 2013.

[32] D. Dong, F. Luo, X. Zhang, D. Boroyevich, P. Mattavelli, "Grid-Interface Bidirectional Converter for Residential DC Distribution Systems—Part 2: AC and DC Interface Design With Passive Components Minimization." IEEE Transactions on Power Electronics, Vol. 28, NO. 4, April 2013.

[33] L. Roggia, L. Schuch, J. E. Baggio, C. Rech, J. R. Pinheiro, "Integrated Full-Bridge-Forward DC–DC Converter for a Residential Microgrid Application," IEEE Transactions on Power Electronics, Vol. 28, NO. 4, APRIL 2013.

[34] H. Bai, C. Mi, "Eliminate Reactive Power and Increase System Efficiency of Isolated Bidirectional Dual-Active-Bridge DC–DC Converters Using Novel Dual-Phase-Shift Control," IEEE Transactions on Power Electronics, Vol. 23, NO. 6, November 2008.

[35] D. Segaran, D. G. Holmes, B. P. McGrath, "Enhanced Load Step Response for a Bidirectional DC–DC Converter," IEEE Transactions on Power Electronics, Vol. 28, No. 1, January 2013.

[36] F. Krisme, J. W. Kolar, "Efficiency-Optimized High-Current Dual Active Bridge Converter for Automotive Applications," IEEE Transactions on Power Electronics, Vol. 59, NO. 7, July 2012.

[37] H. Qin, J. W. Kimball, "Solid State Transformer Architecture Using AC-AC Dual Active Bridge Converter," IEEE Transactions early access.

[38] Y. Xue, Z. Xu, G. Tang, "Self-Start Control With Grouping Sequentially Pre-charge for the C-MMC-Based HVDC System." IEEE Trans on Power Delivery, Vol. 29, NO. 1, Feb 2014.

[39] H.Bai, C. Mi, "Eliminate Reactive Power and Increase System Efficiency of Isolated Bidirectional Dual-Active-Bridge DC–DC Converters Using Novel Dual-Phase-Shift Control." IEEE Trans on Power Electronics, Vol. 23, NO. 6, November 2008.

[40] A. K. Jain, R. Ayyanar, "PWM Control of Dual Active Bridge: Comprehensive Analysis and Experimental Verification." IEEE Transactions on Power Electronics, Vol. 26, NO. 4. April 2011.

[41] Y. Yang, "Bidirectional DC converter." Jiangsu Scientific Technology Press. 1st edition, 2004.

[42] G.G. Oggier, G.O. Garcia, A.R. Oliva, "Modulation strategy to operate the dual active bridge DC-DC converter under soft switching in the whole operating range." IEEE Transactions on Power Electronics, Vol.24, NO.4, pp 1228 – 1236, April 2011.

[43] H. Geng, D. Xu, B. Wu, G. Yang, "Active Islanding Detection for Inverter-Based Distributed Generation Systems With Power Control Interface." IEEE Transactions on Energy Conversion, Vol. 26, NO. 4, December 2011.

[44] R. W. Erickson, D. R. W. Maksimovic, "Fundamentals of Power Electronics." Second Edition. Springer Science+Business Media, 2001.

[45] X. Sun, Y. Tian, Z. Chen, "Adaptive decoupled power control method for inverter connected DG," I E T Renewable Power Generation, Vol. 8, pp. 171–182, Mar 2014.

[46] J. E. Garcia, S. Arnaltes, J.L. Rodriguez-Amenedo, "Direct power control of voltage source inverter with unbalanced grid voltages." IET Power Electronics. Vol. 1, NO. 3. 2008.

[47] H. Krishnamurthy, R. Ayyanar, "Stabitlity Analysis of Cascaded Converters for Bidirectional Power Flow Application", in proc. Of IEEE 30th International Telecommunications Energy Conference, INTELEC 2008. San Diego, CA 14-18 Sept, 2008.

[48] A. K. Jain, and R. Ayyanar, "PWM Control of Dual Active Bridge: Comprehensive Analysis and Experimental Verification." IEEE Transactions on Power Electronics, Vol. 26, NO. 4, April 2011

[49] D.Segaran, D. G. Holmes, "Enhanced load step response for a bidirectional DCDC converter. " IEEE Transactions on Power Electronics, Vol. 28, NO. 1, Jan 2013.

[50] L. Xue, Z. Shen, D. Boroyevich, P. Mattavelli, D. Diaz, "Dual Active Bridge-Based Battery Charger for Plug-in Hybrid Electric Vehicle with Charging Current Containing Low Frequency Ripple," IEEE Transactions on Power Electronics. Early access.

[51] H. Qin, J. W. Kimball, "Generalized Average Modeling of Dual Active Bridge DC-DC Converter", IEEE Transactions on Power Elelectronics, Vol. 27, NO. 44, pp. 2078-2084, April 2012.

[52] J. Shi, W. Gou, H. Yuan, T. Zhao, A. Q. Huang, "Research on Voltage and Power Balance Control for Cascaded Modular Solid-State Transformer." IEEE Transactions on Power Electronics, Vol. 26, NO. 4, April 2011.

[53] S. R. Sanders, J. M. Noworolski, X. Z. Liu, and G. C. Verghese, "Generalized averaging method for power conversion circuits." IEEE Transactions on Power Electron, Vol. 6, No. 2, pp. 251–259, April 1991.

[54] M. Monfared, S. Golestan, J. M. Guerrero, "Analysis, Design, and Experimental Verification of a Synchronous Reference Frame Voltage Control for Single-Phase Inverters", IEEE Transactions on Industrial Electronics, Vol. 61, NO. 1, January 2014.

[55] X. Sun, H. Gu, L. Wang, W. Yang, High Frequency Switching Inverters and Grid Connection and Parallel Connection Technology, Mechanic Press, 2011.

[56] H. M. Power, "General strategy for increasing type number of control systems." Electronics Letters, Vol. 9 , Issue: 26. December 1973.

[57] B. G. Gu, K. Nam. "A DC-link capacitor minimization method through direct capacitor current control." IEEE Transactions on Industry Applications, Vol. 42, NO. 2, Mar/Apr, 2006.

[58] X. Zhang, X.Ruan, H. Kim, C. K. Tse. "Adaptive active capacitor converter for improving stability of cascaded DC power supply system." IEEE Transactions on Power Electronics, Vol.28, NO. 4, Apr. 2013.

[59] F. C. Lee, D. Borojevic, "Impedance specification and impedance improvement for DC distributed power system." In proc. Of 30th Annual IEEE Power Electronics Specialists Conference. Vol. 2, pp. 889–894, Charleston. SC, 27 Jun-01 Jul 1999.

[60] H. Wang, F. Blaabjerg, "Reliability of capacitors for DC-link applications An overview." In proc. Of 2013 IEEE Energy Conversion Congress and Exposition, ECCE 2013, Vol. 50, Issue. 5, PP1866–1873, Denver, CO, 15-19 Sept. 2013

[61] Ahmadi, R; Ferdowsi, M," Controller design method for a cascaded converter system comprised of two DC-DC converters considering the effects of mutual interactions," Applied Power Electronics Conference and Exposition (APEC), 2012 ,5-9 Feb. pp:1838 – 1844.

[62] F. L. Luo, H. Ye, "Small signal analysis of energy factor and mathematical modeling for power dc-dc converters." IEEE Transactions on Power Electronics, Vol. 22, NO. 1, Jan. 2007.

[63] M. Chen, J. Sun, "Low-frequency input impedance modeling of boost single-phase PFC converters." IEEE Transactions on Power Electronics, Vol.22, NO. 4, July. 2007.

[64] J. M. Guerrero, L. G. De Vicuña, J. Matas, J. Miret, M. Castilla, "Output impedance design of parallel-connected UPS inverters." IEEE Transactions on Industrial Electroncis, Vol. 52, NO. 4, Aug. 2005.

[65] C. M. Wildrick, F. C. Lee, B. H. Cho, B. Choi, "A Method of Defining the Load Impedance Specification for A Stable Distributed Power System," IEEE Transactions on Power Electronics, Vol. 10, NO. 3, May. 1995

[66] J. Sun, "Impedance-based stability criterion for grid-connected inverters," IEEE Transactions on Power Electronics, Vol. 26, No. 11, pp. 3075–3078, Nov. 2011.

[67] F. C. LEE, Y. Yu, "Input-filter Design for Switching Regulators." IEEE Transactions on Aerospace and Electronic Systems, Sept. 1979.

[68] J. Wang, D. Howe, "A Power Shaping Stabilizing Control Strategy for DC Power Systems With Constant Power Loads," IEEE Transactions on Power Electronics, Vol. 23, No. 6, November.

[69] X. Feng, J. Liu, F. C. Lee, "Impedance specifications for stable DC distributed power system," IEEE Transactions on Power Electronics, vol.17 no. 2, March 2002.

[70] A. Riccobono, E. Santi, "Positive Feedforward Control of Three-Phase Voltage Source Inverter for DC Input Bus Stabilization With Experimental Validation," IEEE Transactions on Industry Applications, vol. 49, NO. 1, January/February 2013.

[71] A. Riccobono, E. Santi, "Comprehensive Review of Stability Criteria for DC Power Distribution Systems," IEEE Transactions on Industry Applications, vol. 50, NO. 5, September/October 2014.

[72] A. Emadi, A. Khaligh, C. H. Rivetta, G. A. Williamson, "Constant Power Loads and Negative Impedance Instability in Automotive Systems: Definition, Modeling, Stability, and Control of Power Electronic Converters and Motor Drives," IEEE Transaction on Vehicular Technology, vol. 55, NO. 4, July 2006.

[73] A. M. Rahimi, A. Emadi, "Active Damping in DC/DC Power Electronic Converters: A Novel Method to Overcome the Problems of Constant Power Loads." IEEE Transactions on Industrial Electronics, vol. 56, NO. 5, May 2009.

[74] A. Khaligh, "Realization of Parasitics in Stability of DC–DC Converters Loaded by Constant Power Loads in Advanced Multiconverter Automotive Systems." IEEE Transactions on Industrial Electronics, vol. 55, NO. 6, June2008.

[75] H. K. Krishnamurthy, R. Ayyanar, "Building Block Converter Module for Universal (AC-DC, DC-AC, DC-DC) Fully Modular Power Conversion Architecture." In Proc. of Power Electronics Specialists Conference, PESC 2007, pp: 483–489. Orlando, FL, 17-21 June 2007.

[76] A. Riccobono, E. Santi, "Positive Feedforward Control of Three-Phase Voltage Source Inverter for DC Input Bus Stabilization With Experimental Validation." IEEE Transactions on Industry Applications, Vol. 49, NO. 1, January/February 2013.

[77] J. Lee, G. Park, J. Choi, "Decoupling IPD controller design for three phase DC/AC inverter." In proc. of Power Quality and Supply Reliability Conference, 2008, pp: 73-78, Parnu, 27-29 Aug. 2008.

[78] B. N. Mobarakeh, F. M. Tabar, F. M. Sargos, "On-line identification of PMSM electrical parameters based on decoupling control," In proc. Of Thirty-Sixth IAS Annual Meeting, Chicago. USA, pp: 266-273, Sept. 30-Oct. 4, 2001.

[79] P. Liutanakul, A. B. Awan, S. Pierfederici, "Linear Stabilization of a DC Bus Supplying a Constant Power Load: A General Design Approach." IEEE Transactions on Power Electronics, Vol. 25, NO. 2, Febrary 2010.

[80] R. F. Hoskins, "Stability of negative-impedance convertors." Electronics Letters, Vol.2, NO. 9, September 1966.

[81] J. L. Hellerstein, Y. Diao, S. Parekh, D. M. Tilbury, "Feedback Control of Computing Systems." IEEE Press, 2004.

[82] K. Ogata, Modern Control Engineering, 5th Edition, Prentice Hall, 2010

[83] R. W. A. A. De Doncker, D. M. Divan, M. H. Kheraluwala, "A three-phase soft-switched high-power-density DC/DC converter for high-power applications," IEEE Transaction on Industrial Applications, Vol.27, NO. 1, pp. 63-73, Jan/Feb. 1991.

[84] J. Liu, X. Feng, F. C. Lee, D. Borojevich, "Stability margin monitoring for DC distributed power systems via\ncurrent/voltage perturbation." IEEE Transactions on Power Electronics, Vol. 18, NO.6, November. 2003.

[85]   M. J. Basler, R. C. Schaefer, "Understanding power-system stability." IEEE Transactions on Industry Applications, Vol44, NO. 2, April/March 2008.

[86]   "Distributed Generation—Educational Module". Virginia Tech. 2007. Retrieved July 2015

[87]   P. S. C. D. Roy, M. Sc, D. Phil, "Optimum passive integrators," IEE Proceedings G Electronic Circuits and Systems, Vol.130, NO. 5, Oct. 1983.

[88]   M. Reddy, "An insensitive active-RC filter for high Q and high frequencies." IEEE Transactions on Circuits and Systems, Vol. 23, NO. 7, July.1976.

[89]   J. Vazquez, P. Salmeron, "Active power filter control using neural network technologies." IEE Proceedings-Electric Power Applications, Vol.150, NO. 2, March 2005.

[90]   J. Hu, S. Member, Y. Huang, D. Wang, H. Yuan, "Modeling of Grid-Connected DFIG-Based Wind Turbines for DC-Link Voltage Stability Analysis." IEEE Transactions on Sustainable Energy, Vol. 6, Issue. 4, pp1325–1336. VOL. 6, October. 2015

[91]   From the website: https://en.wikipedia.org/wiki/Voltage_source

[92]   G. W. Wester, R. D. Middlebrook, "Low-Frequency Characterization of Switched dc-dc Converters." IEEE Transactions on Aerospace and Electronic Systems, Vol. AES-9, NO.3, May 1973.

[93]   B. Singh, B. N. Singh, A. Chandra, K. Al-Haddad, A. Pandey, D. P. Kothari, "A Review of Three-Phase Improved Power Quality AC–DC Converters." IEEE Transactions on Industrial Electronics, Vol.51, NO. 3, June 2004.

[94]   C. Mi, "Eliminate Reactive Power and Increase System Efficiency of Isolated Bidirectional Dual-Active-Bridge DC–DC Converters Using Novel Dual-Phase-Shift Control." IEEE Transactions on Power Electronics, Vol.23, NO. 6, November 2008.

[95]   L. Cao, K. Loo, Y. M. Lai, "Output-Impedance Shaping of Bidirectional DAB DC-DC Converter Using Double-Proportional-Integral Feedback for Near-Ripple-Free DC Bus Voltage Regulation in Renewable Energy Systems." IEEE Transactions on Power Electronics, Early access, 2015.

[96]   V. Šviković, J. a. Oliver, P. Alou, O. García, J. a. Cobos, "Synchronous Buck Converter With Output Impedance Correction Circuit." IEEE Transactions on Power Electronics, Vol.28, NO. 7, July 2013.

[97]   L. Cao, K. H. Loo, Y. M. Lai, "Systematic Derivation of a Family of Output-Impedance Shaping Methods for Power Converters — A Case Study Using Fuel Cell-Battery-Power Single-Phase Inverter System." Vol.30, NO. 10, October 2015.

[98]   From the website: https://en.wikipedia.org/wiki/Current_source

[99]   H. Nikkhajoei, "A current source matrix converter for high-power applications." In proc. of IEEE Annual Power Electronics Specialists Conference, Orlando, FL, 17-21 June 2007.

[100]   V. Monteiro, J. G. Pinto, B. Exposto, J. L. Afonso, "Comprehensive Comparison of a Current-Source and a Voltage-Source Converter for Three-Phase EV Fast Battery Chargers," in proc. Of 2015 9th International Conference on Compatibility and Power Electronics (CPE), Costa da Caparica, 24-26 June 2015.

[101]   M. P. Kazmierkowski, L. Malesani, "Current control techniques for three-phase voltage-source PWM converters: A survey." IEEE Transactions on Industry Electronic, Vol.45, NO.5, October 1998.

[102]   S. Buso, L. Malesani, P. Mattavelli, "Comparison of current control techniques for active filter\napplications." IEEE Transactions on Industrial Electronics, Vol.45 NO.5, October 1998.

[103] C. Rivetta, G. A. Williamson, A. Emadi, "Constant Power Loads and Negative Impedance Instability in Sea and Undersea Vehicles: Statement of the Problem and Comprehensive Large-Signal Solution." IEEE Electric Ship Technologies Symposium, Philadelphia, PA, 27-27 July 2005.

[104] A. Khaligh, A. M. Rahimi, A. Emadi, "Negative impedance stabilizing pulse adjustment control technique for DC/ DC converters operating in discontinuous conduction mode and driving constant power loads." IEEE Transactions on Vehicular Technology, Vol.56 NO.4, July 2007.

[105] F. Mura, C. Meyer, R. W. De Doncker. "Stability Analysis of High-Power DC Grids." IEEE Transactions on Industry Applications, Vol.46, NO.2, March/April 2010.

[106] A. Khaligh, "Realization of parasitics in stability of dc-dc converters loaded by constant power loads in advanced multiconverter automotive systems." IEEE Transactions on Industrial Electronics, Vol.55, NO.6, June 2008.

[107] A. M. Rahimi, A. Emadi, "An Analytical Investigation of DC/DC Power Electronic Converters With Constant Power Loads in Vehicular Power Systems." IEEE Transactions on Vehicular Technology, Vol.58, NO.6, July 2009.

[108] R. Turner, S. Walton, R. Duke, "A case study on the application of the Nyquist stability criterion as applied to interconnected loads and sources on grids." IEEE Transactions on Industrial Electronics, Vol.60, NO.7, July 2013.